UCLouvain

École polytechnique de Louvain

Stochastic Geometry-based Sleep Mode Strategies for Energy Efficient Cellular Networks

Author: **Martin Willame**
Supervisors: **Prof. Claude Oestges, Prof. Luc Vandendorpe**
Readers: **Prof. Jérome Louveaux, Charles Wiame**
Academic year 2020–2021
Master [120] in Electrical Engineering

Acknowledgments

I would like to thank several people who supported me and helped me during the writing of this thesis.

First, thank you to my supervisors Prof. Claude Oestges, Prof. Luc Vandendorpe, and Charles Wiame for their availability and their interest. They were able to pass on their knowledge and provide me advice throughout my years of study, and particularly during the research phase of my thesis, which results are presented in this work.

Then, I would like to thank Prof. Jérôme Louveaux for taking the time to read my work.

Next, a special thank to Dr. Olivier Eulaerts who took the time to proofread my work in detail and helped me improve the English of this thesis.

Finally, I would like to thank my family and my friends for encouraging me and supporting me throughout my studies and especially during this final year.

Abstract

With the growing demand in high data rate and mobile subscriptions triggered by the development of the 5^{th} generation of mobile networks, the power consumption of cellular networks is expected to increase. A growing interest towards greener wireless telecommunications has therefore been observed, with the view to cut down the carbon footprint of the whole sector. To this end, a potential solution is to introduce sleep modes strategies for the base stations. In this thesis, the benefit in terms of energy efficiency of activity based sleeping strategies is studied using stochastic geometry. A characterisation of the load, defining the activity of each base stations, is performed for different network configurations involving homogeneous and/or clustered distribution of users. Different features present in 5G network such as inhomogeneous networks, beamforming and millimeter wave transmission have been taken into account in the mathematical expressions developed herein to characterise the energy efficiency. The present work gives an overview of the impact of various network parameters on the energy efficiency and shows the benefit of load-dependent sleeping strategies. To sum up, this thesis provides a general framework to better understand the characteristics of greener 5G networks.

Avec la demande croissante de hauts débits de données et d'abonnements mobiles déclenchée par le développement de la $5^{ème}$ génération de réseaux mobiles, la consommation d'énergie des réseaux cellulaires devrait augmenter. On observe donc un intérêt croissant pour des télécommunications sans fil plus écologiques, dans le but de réduire l'empreinte carbone de l'ensemble du secteur. À cette fin, une solution potentielle consiste à introduire des stratégies de sommeil pour les stations de base. Dans cette thèse, l'avantage, en termes d'efficacité énergétique des stratégies de sommeil basées sur l'activité, est étudié en utilisant la géométrie stochastique. Une caractérisation de la charge, définissant l'activité de chaque station de base, est effectuée pour différentes configurations de réseau impliquant une distribution homogène et/ou à cluster des utilisateurs. Différentes caractéristiques présentes dans les réseaux 5G, telles que les réseaux inhomogènes, la formation de faisceaux et la transmission en ondes millimétriques, ont été prises en compte dans les expressions mathématiques développées pour caractériser l'efficacité énergétique. Le présent travail donne un aperçu de l'impact de divers paramètres du réseau sur l'efficacité énergétique et montre l'avantage des stratégies de sommeil basées sur la charge des stations de base. En résumé, cette thèse fournit un cadre général pour mieux comprendre les caractéristiques des réseaux 5G plus écologiques.

Contents

List of abbreviations

5G 5th generation mobile network

AKWCP Averaged K-tiers weighted coverage probability

AWGN Additive white Gaussian noise

BS Base station

ccdf Complementary cumulative distribution function

EE Energy efficiency

GREEN Globally resource optimized energy efficient network

HPPP Homogeneous poisson point process

i.i.d. Independently and identically distributed

IDFT Inverse discrete Fourier transform

LoS Line-of-sight

LT Laplace transform

MC Monte Carlo

MCP Matérn cluster process

MIMO Mutltiple-input multiple-output

mm-Wave Millimeter wave

NB Negative binomial

NS No sleeping

PCP Poisson cluster process

pdf Probability density function

PGFL Probability generating functional

pmf Probability mass function

PP Point process

PPP Poisson point process

QoS Quality of service

RS Random sleeping

SG Stochastic geometry

SINR Signal-to-interference-plus-noise ratio

SS Strategic sleeping

TCP Thomas cluster process

UE User equipment

WCP Weighted coverage probability

Chapter 1

Introduction

The *5th generation of mobile network* (5G) is being developed to meet the growing demand in data rate and mobile subscriptions, as observed on figure 1.1. This new generation promises a highly flexible and scalable network technology, providing an ultra-fast data rate for connecting everyone and everything, everywhere [1, 2]. To achieve this, 5G is being deployed commercially throughout the world with features such as inhomogeneous deployment of cells, massive *multiple-input multiple-output* (MIMO) to benefit from beamforming and *millimeter wave* (mm-Wave) transmission to boost the capacity.

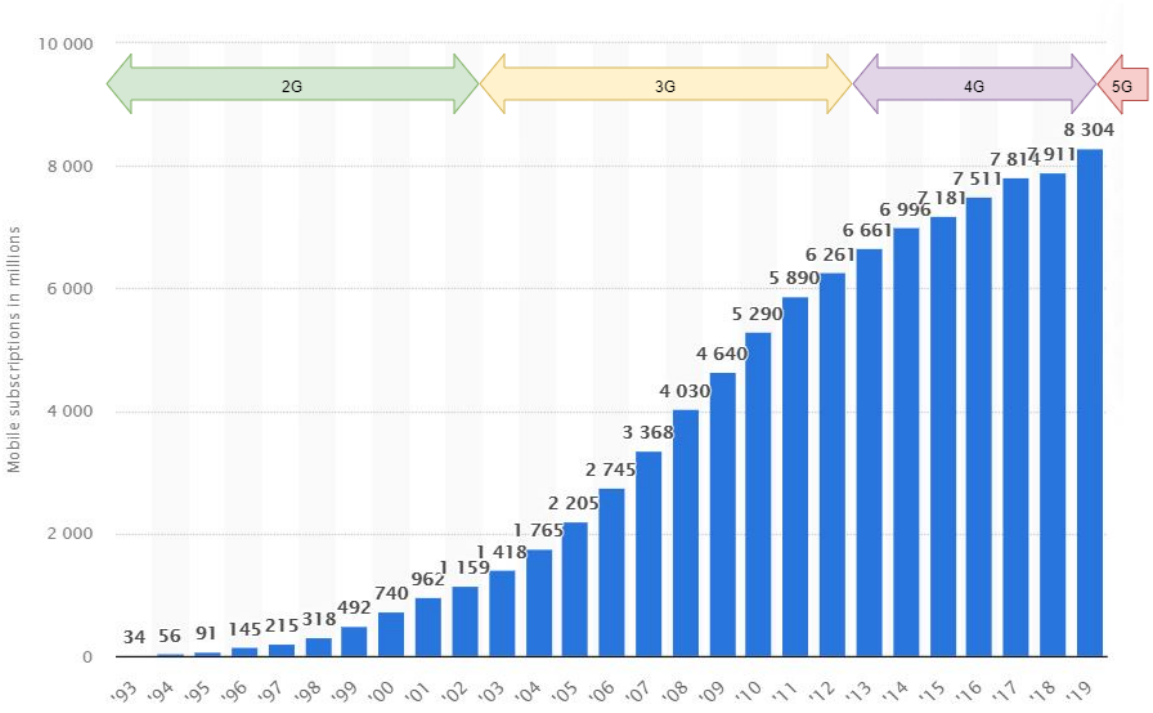

Figure 1.1: Evolution of the number of mobile cellular subscriptions worldwide from 1993 to 2019 [3].

The development of cellular technology has raised the energy consumption in mobile networks. This increased need in energy for telecommunications has lead to a growing carbon footprint of this sector, which has negative effects on the environment and human health. In order to address these aspects, a growing interest towards GREEN (*globally resource optimized energy efficient network*) communications has been observed. This field of research focuses on the impact of resource allocation to optimise the *energy efficiency* (EE) of cellular networks [4, 5].

The most energy-intensive resource in cellular mobile networks are *base stations* (BSs), consuming approximately 80% of the total network energy [6]. The increase in the number of small cell BSs resulting from the limited coverage distance of mm-Wave [7] is expected to further increase the energy consumption of the network. Therefore, most efforts to improve the EE in mobile radio networks focus on BSs [8]. An effective technique for this purpose is to introduce sleep mode for the BSs [9, 10]. Indeed, studies have shown that traffic demand is irregular in time and space in cellular networks, which opens up opportunities for energy savings by adapting the sleep mode of BSs to their corresponding load. [11].

In this thesis, the improvement on the EE provided by sleeping mode strategies is studied in different scenarios featuring various 5G characteristics. The average energetic performances of the network are evaluated using *Stochastic geometry* (SG) and *Monte-Carlo* (MC) simulations.

SG is a mathematical field that provides statistical tools to study the properties of random spatial patterns [12]. According to the studies in [13, 14], the location of BSs and *user equipments* (UEs) in different networks form random patterns. By abstracting their location by points in the Euclidean space, SG provides a general framework for analysing the average performances of the cellular network for metrics such as the coverage probability or the EE.

MC simulation is an empirical method to study the statistical behavior of a property by drawing a lot of samples and observing the said behavior [15]. Although it gives an overview of the performance of a network, it does not lead to closed-from expressions allowing to observe the impact of each network's parameters. Furthermore, it can be computationally expensive.

This thesis is structured as follows:

First, chapter 2 presents the fundamental theory of SG that is used for the mathematical developments in this thesis. The different metrics of interest for studying the performances of the network are also given.

Then, the impacts of different sleep control strategies on the EE are compared for homogeneous networks in chapter 3, using SG. The number of UEs served by each BS in this network configuration is also derived.

Next, in chapter 4, the benefit of the sleeping modes in mm-Wave networks featuring beamforming is studied. The performances of the network are compared with results of the analysis performed in chapter 3. Additionally, different distributions of UEs are considered to observe their impact on the load of each BS.

Finally, before some conclusions, chapter 5 provides a general framework for a multi-tiers inhomogeneous network, presenting the features of 5G networks. The analysis is performed for BSs whose locations are not independent of the UEs clusters. A new metric is also defined to analyse the benefit of the sleeping strategies in terms of EE. Moreover, a characterisation of the load in inhomogeneous network is presented.

Chapter 2

Fundamentals of stochastic geometry

This chapter outlines the fundamental theory of SG that is used for the mathematical developments of this thesis. First, the essential concepts of point processes are described. A focus is then made on a particularly useful type of point process. Next, the framework of Palm's theory is defined before stating the metrics studied throughout this thesis. Most of the definitions and theorems from this chapter can be found in [12, 16, 17, 18].

2.1 Point Process Theory Essentials

A ***point process*** (PP) $\Phi = \{\mathbf{X}_i : i \in \mathbb{N}\}$ is a random collection of points residing in a measure space, which is typically the Euclidean space $\mathbb{R}^n$. Each point $\mathbf{X}_i$ is a random variable abstracting the location of nodes. In the framework of wireless communication, these nodes are UEs or BSs and $\mathbf{X}_i$ describes the coordinates of the i^{th} node in $\mathbb{R}^2$. This way of describing a PP is called the **random set formalism**.

Another way to interpret the PP is to view it in terms of a **random counting measure**. It is defined as a function $\Psi(\cdot)$ that takes a subset $A \subset \mathbb{R}^n$ as input and returns the number of point of Φ within this area. By denoting the indicator function as $\mathbb{1}(\cdot)$, the random counting measure can be mathematically defined as follows:

$$\Psi : \mathbb{R}^n \to \mathbb{N} : A \to \sum_{\mathbf{X}_i \in \Phi} \mathbb{1}(\mathbf{X}_i \in A). \tag{2.1}$$

A **marked point process** is obtained when a random characteristic $m \in \mathbb{M}$, called a mark, is attributed to each point of a PP Φ called the ground process. $\mathbb{M}$ is the space in which the marks are defined. The combined marked PP on $\mathbb{R}^n \times \mathbb{M}$ is denoted $\hat{\Phi} = \{(\mathbf{X}_i, m_i)\}$. The marked PP is said to be independently marked if the marks of different points are independent. In this case the marks distribution is denoted M_x. If M_x does not depend on the location of the points then the marks are *independently and identically distributed* (i.i.d.). Such PP is referred to as a i.i.d. marked process.

2.1.1 Properties and Statistical quantities

Two important statistical measures of a PP can be define based on Ψ. First, the **void probability** of a PP is a deterministic function denoted $v(\cdot)$ that returns the probability of having no points of Φ within the area A:

$$v : \mathbb{R}^n \to [0, 1] : A \to \mathbb{P}(\Psi(A) = 0). \tag{2.2}$$

Secondly, the **intensity measure** Λ (also called **expectation measure**) of a PP is a deterministic function that returns the mean of the random counting measure within a subset $A \subset \mathbb{R}^n$

taken as input:

$$\Lambda : \mathbb{R}^n \to \mathbb{R} : A \to \mathbb{E}_\Psi\{\Psi(A)\}. \tag{2.3}$$

Another form for the intensity measure, based on a location-dependent **intensity function** $\lambda(\mathbf{x})$ ($\mathbf{x} \in \mathbb{R}^n$), is used in most applications. $\Lambda(\mathbf{x}) = \lambda(\mathbf{x})\mathbf{dx}$ can be interpreted as the infinitesimal probability to have a point from the PP within the infinitesimal region $\mathbf{dx}$ located at $\mathbf{x}$. Equation 2.4 follows from this interpretation:

$$\Lambda(A) = \int_A \lambda(\mathbf{x})\mathbf{dx}. \tag{2.4}$$

Two important properties for a PP are the **stationarity** and the **isotropy**. A process $\Phi = \{\mathbf{X}_i\}$ on $\mathbb{R}^n$ is said stationary if the translated process $\Phi_\mathbf{x} = \{\mathbf{X}_i + \mathbf{x}\}$ has the same distribution as Φ. A process $\Phi = \{\mathbf{X}_i\}$ on $\mathbb{R}^n$ has the isotropic property if its distribution is rotationally invariant. This property applies only for rotations about the origin of $\mathbb{R}^n$.

2.1.2 Useful theorems and functions

When a performance of interest is evaluated using SG, it often requires the evaluation of expectations applied on a sum or a product of random variables. When these operations involve all points of a PP, SG provides two main techniques that allows to transform the operation in an integral over the PP domain, namely Campbell's theorem and the *probability generating functional* (PGFL).

Campbell's theorem : This theorem transforms an expectation of a sum over all points of the PP into an integral over the PP domain. Let Φ be a PP in $\mathbb{R}^n$ and $f : \mathbb{R}^n \to \mathbb{R}$ be a measurable function, then:

$$\mathbb{E}\left\{\sum_{\mathbf{x}_i \in \Phi} f(\mathbf{x}_i)\right\} = \int_{\mathbb{R}^n} f(\mathbf{x})\Lambda(\mathbf{dx}). \tag{2.5}$$

In case of a PP in $\mathbb{R}^2$ with intensity $\lambda(\mathbf{x})$, 2.5 reduces to:

$$\mathbb{E}\left\{\sum_{\mathbf{x}_i \in \Phi} f(\mathbf{x}_i)\right\} = \int_{\mathbb{R}^2} f(\mathbf{x})\lambda(\mathbf{x})\mathbf{dx}. \tag{2.6}$$

PGFL : The PGFL transforms an expectation of a product over all points of the PP into an integral over the PP domain. Unlike Campbell's theorem, it has no explicit general expression since the analytical form depends on the type of PP considered. An implicit expression can be derived where $\mathcal{P}_\Phi(f)$ denotes the expression of the PGFL. Let Φ be a PP in $\mathbb{R}^n$ and $f : \mathbb{R}^n \to \mathbb{R}$ be a measurable function, then:

$$\mathcal{P}_\Phi(f) = \mathbb{E}\left\{\prod_{\mathbf{x}_i \in \Phi} f(\mathbf{x}_i)\right\}. \tag{2.7}$$

2.2 Poisson Point Process

Among the many different types of PP, the most popular one is the ***poisson point process*** (PPP), which is an appealing compromise between mathematical tractability and practicality.

2.2.1 Definition

The PPP is defined as a PP with intensity measure Λ such that:

- For every set $A \subset \mathbb{R}^n$, $\Psi(A)$ is a Poisson random variable defined with a mean $\Lambda(A)$.

$$\mathbb{P}(\Psi(A) = k) = \frac{(\Lambda(A))^k}{k!} \exp(-\Lambda(A)). \tag{2.8}$$

- For any sets A,$B \subset \mathbb{R}^n$ such that $A \cap B = \emptyset$, the random variables $\Psi(A)$ and $\Psi(B)$ are independent.

An important property of the PPP is that its PGFL is well defined. For a PPP Φ defined in $\mathbb{R}^n$, the PGFL is given by:

$$\mathcal{P}_\Phi(f) = \exp\left(-\int_{\mathbb{R}^n} (1 - f(\mathbf{x}))\Lambda(\mathbf{dx})\right). \tag{2.9}$$

2.2.2 Homogeneous Poisson Point Process

A particular type of PPP, called the ***homogeneous poisson point process*** (HPPP), is defined by fixing the intensity function $\lambda(\mathbf{x})$ of the PPP as a constant λ. An important property of a HPPP is that conditioned on the number of points in a subset $A \subset \mathbb{R}^n$, all the points are independently and uniformly distributed in A. In the case of a HPPP, the expression of the PGFL in equation 2.9 reduces to:

$$\mathcal{P}_\Phi(f) = \exp\left(-\lambda \int_{\mathbb{R}^n} (1 - f(\mathbf{x}))\right). \tag{2.10}$$

Figure 2.1 illustrates the differences between a HPPP and an inhomogeneous PPP. The steps to generate a HPPP in a MC simulation can be found in [19]. An inhomogeneous PPP can be generated from a HPPP following the methodology described in [12].

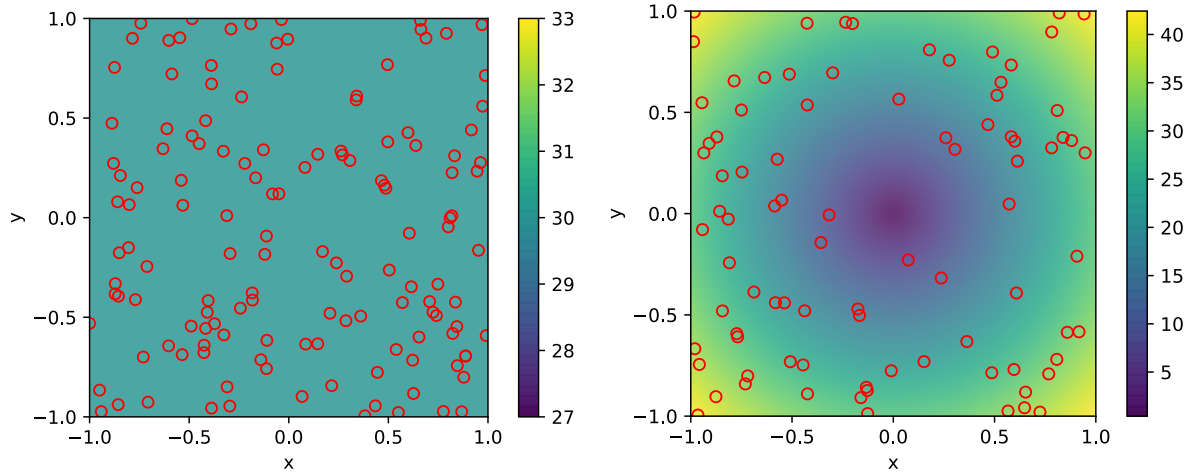

(a) HPPP with $\lambda(\mathbf{x}) = 30\ \forall \mathbf{x}$

(b) inhomogeneous PPP with $\lambda(\mathbf{x}) = 30\|\mathbf{x}\|$

Figure 2.1: Example of a HPPP and of an inhomogeneous PPP in $[-1, 1]^2$. The position of the points are given by the red circles and the colormap shows the value of the intensity function $\lambda(\mathbf{x})$.

2.2.3 Poisson Cluster Process

A general cluster process is generated by taking a parent PP and assigning a daughter PP to each of its points. The daughter PPs are then translated to the position of their corresponding parent point [18]. The cluster process is then formed by the union of all the points from all daughter PPs.
A ***Poisson cluster process*** (PCP) is a cluster process for which the parent PP is a PPP. The PCP $\Phi(\lambda_p, \overline{m}, f)$ can be defined as :

$$\Phi = \bigcup_{\mathbf{z}\in\Phi_p} \mathbf{z} + \Phi_d^{\mathbf{z}}, \tag{2.11}$$

where Φ_p is the parent PP with intensity λ_p. $\Phi_d^{\mathbf{z}}$ denotes the daughter PP corresponding to a cluster center $\mathbf{z} \in \Phi_p$ [20]. In this thesis, a constant intensity λ_p is considered. The random counting measure for each daughter PP is assumed to be given by independent Poisson random variables of parameter $\overline{m}$:

$$\Psi(\mathbb{R}^n) \sim \text{Poisson}(\overline{m}). \tag{2.12}$$

These assumptions correspond to a particular class of PCP called **Neyman-Scott cluster processes**[1]. The positions of the daughter points with respect to their cluster center $\mathbf{z}$ are i.i.d. random vectors $\mathbf{s} \in \Phi_d^{\mathbf{z}}$ where $\mathbf{s} \sim f(\mathbf{s})$. The function f is thus the *probability density function* (pdf) associated with the PCP. Using different functions f, two popular types of PCPs can be defined:

- **Thomas Cluster Process**: A PCP $\Phi(\lambda_p, \overline{m}, f)$ in $\mathbb{R}^n$ is called a *Thomas Cluster Process* (TCP) if the daughter points $\mathbf{s} \in \Phi_d^{\mathbf{z}}$ are distributed normally around $\mathbf{0}$ with a cluster variance σ^2. In $\mathbb{R}^2$, f can be expressed as:

$$f(\mathbf{s}) = \frac{1}{2\pi\sigma^2} \exp\left(-\frac{\|\mathbf{s}\|^2}{2\sigma^2}\right). \tag{2.13}$$

- **Matérn Cluster Process**: A PCP $\Phi(\lambda_p, \overline{m}, f)$ in $\mathbb{R}^n$ is called a *Matérn Cluster Process* (MCP) if the daughter points $\mathbf{s} \in \Phi_d^{\mathbf{z}}$ are distributed uniformly within a n-ball of radius r_m centered at the origin denoted $b(\mathbf{0}, r_m)$. In $\mathbb{R}^2$, the n-ball is simply a disc and f can be expressed as:

$$f(\mathbf{s}) = \frac{\|\mathbf{s}\|}{\pi r_m^2}, 0 < \|\mathbf{s}\| \leq r_m. \tag{2.14}$$

The PGFL for the TCP and the MCP can be defined with a general expression that depends on their respective density functions f [20]:

$$\mathcal{P}_\Phi(v) = \exp\left(-\lambda_p \int_{\mathbb{R}^n} \left[1 - \exp\left(\overline{m}\left[\int_{\mathbb{R}^n} v(\mathbf{x}+\mathbf{y}) f(\mathbf{y}) d\mathbf{y} - 1\right]\right)\right] d\mathbf{x}\right). \tag{2.15}$$

Figure 2.2 illustrates examples of a TCP and of a MCP. The steps to generate both PCPs in a MC simulation are given respectively in [21] for the TCP and in [22] for the MCP.

[1] Throughout this thesis, the Neyman-Scott process is referred to as PCP unless otherwise stated.

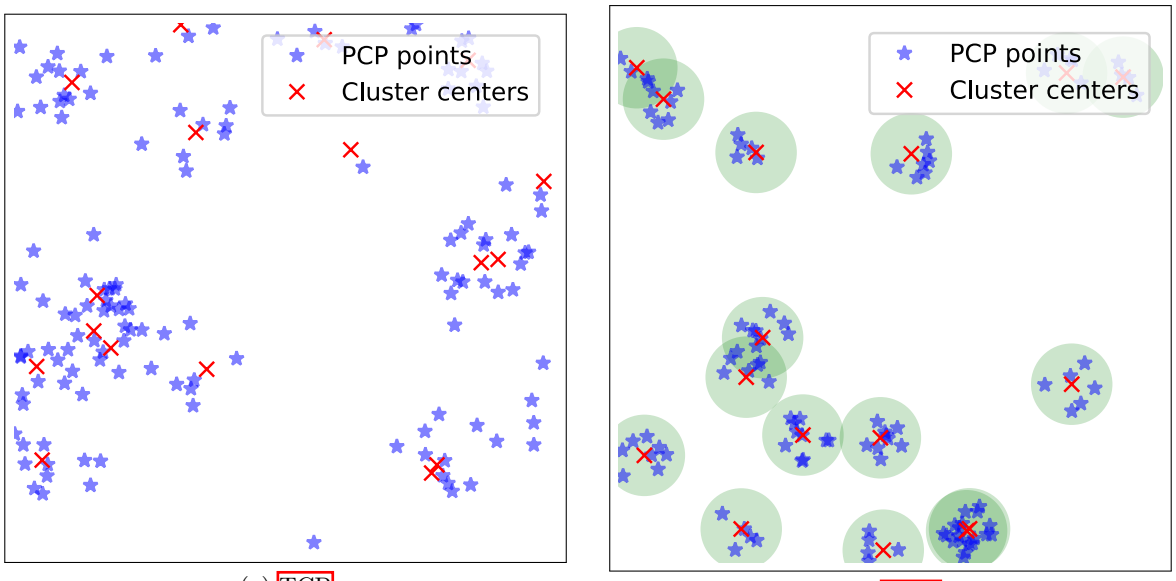

(a) TCP (b) MCP

Figure 2.2: Examples of a TCP and of a MCP

2.2.4 PPPs transformations

Two important operations on the PPPs are described in this section:

- **Independent thinning:** Let $g : \mathbb{R}^n \to [0, 1]$ be a thinning function and apply it to a PPP by deleting, with a probability $1 - g(\mathbf{x})$, each point $\mathbf{x}$ independently of all other points. This thinning procedure generates an inhomogeneous PPP with intensity function $\lambda g(\mathbf{x})$. This operation could also be applied to a marked PPP, in which case the input to the g function would be in $\mathbb{R}^n \times \mathbb{M}$.
- **Superposition:** The superposition operation consists in combining N independent PPPs with intensity functions $\lambda_i(\mathbf{x}), i \in \{1, 2, \ldots, N\}$. This operation creates a new PPP with $\lambda(\mathbf{x}) = \sum_{i=1}^{N} \lambda_i(\mathbf{x})$.

2.3 Palm theory

The Palm theory allows to study the conditioned distribution of a PP given that the PP contains a point at a certain location. The **Palm probability** is defined as the probability of a property E conditioned on the location of a point $\mathbf{x}$. It is equivalently denoted as follows:

$$\begin{aligned}\mathbb{P}(\Phi \text{ has property } E|\mathbf{x}) &= \mathbb{P}(\Phi \text{ has property } E|\mathbf{x} \in \Phi) \\ &= \mathbb{P}(\Phi \in E|\mathbf{x} \in \Phi) \\ &= \mathbb{P}^{\mathbf{x}}(E).\end{aligned}$$

This framework formalises the notion of the typical point of the process selected uniformly at random among all the points of the process. When SG is used to study the performances of a cellular network, the typical point is a randomly chosen UE equipment called the **typical UE**. Equation 2.16 shows that this UE can be considered to be located at the origin without loss of generality for a stationary process [18].

$$\mathbb{P}(\Phi \in E|\mathbf{x} \in \Phi) = \mathbb{P}(\Phi_{\mathbf{x}} \in E|\mathbf{0} \in \Phi) \tag{2.16}$$

The **reduced Palm distribution** is defined as the Palm probability $\mathbb{P}(\Phi \in E|\mathbf{x} \in \Phi)$ but without counting $\mathbf{x}$ has a point of Φ. This distribution can be useful when all transmitting

nodes of a wireless network form a PP and that one wants to assign one of the node as the transmitter and the others as interferers. The following notations are used equivalently to refer to the reduced Palm distribution:

$$\begin{aligned}\mathbb{P}(\Phi \setminus \{\mathbf{x}\} \text{ has property } E|\mathbf{x}) &= \mathbb{P}(\Phi \setminus \{\mathbf{x}\} \text{ has property } E|\mathbf{x} \in \Phi) \\ &= \mathbb{P}(\Phi \setminus \{\mathbf{x}\} \in E|\mathbf{x} \in \Phi) \\ &= \mathbb{P}^{!\mathbf{x}}(E).\end{aligned}$$

Theorem 1 (Slivnyak's Theorem)
The reduced Palm distribution of a PPP is equal to its original distribution. In particular:

$$\mathbb{P}^{!\mathbf{x}}(E) = \mathbb{P}(E). \tag{2.17}$$

A direct consequence of Slivnyak's Theorem is that points can be added or removed from a PPP without disturbing the distribution of the other points of the process.

2.4 SG Metrics

The SG framework is used to study the performances of wireless cellular networks by abstracting the position of BSs and of UEs as appropriate PPs. The metrics of interest for SG are described in this section. These metrics can be seen as properties of a PP, as it was mentioned in the section 2.3 about Palm theory.

The **success probability** is used to assess the *quality of service* (QoS) experienced by the typical UE when it is served by a BS located at $\mathbf{x}$:

$$\mathbb{P}_{suc}(\tau, \mathbf{x}) = \mathbb{P}(\text{SINR}(\mathbf{x}) > \tau), \tag{2.18}$$

where SINR is the *signal-to-interference-plus-noise ratio* and τ is a desired QoS threshold. The expression for the SINR depends on the system model considered for the network.

The **coverage probability** is obtained by taking the average of this success probability over the distance to the serving BS:

$$\mathbb{P}_{cov}(\tau) = \mathbb{E}_{\|\mathbf{x}\|}\left[\mathbb{P}(\text{SINR}(\mathbf{x}) > \tau)\right]. \tag{2.19}$$

Finally, the EE is defined as the ratio between the BS throughput $\mathcal{T} = \mathbb{P}_{cov}(\tau)\log_2(1+\tau)$ and the BS power consumption P_{tot}:

$$\text{EE} = \frac{\mathcal{T}}{P_{\text{tot}}} = \frac{\mathbb{P}_{cov}(\tau)\log_2(1+\tau)}{P_{\text{tot}}}. \tag{2.20}$$

Note that the EE is given in $\left[\frac{\text{bits}}{\text{Hz Joule}}\right]$. By multiplying this expression by the bandwidth, the EE can be expressed in bits per Joule.

Chapter 3

Sleep Control Strategies in Homogeneous Networks

In this chapter, the coverage probability and the energy efficiency are derived for a homogeneous network in which different sleep mode strategies are used. The system model and the different types of strategies are first defined before deriving the corresponding mathematical expressions. Numerous simulations are then performed in order to confirm the accuracy of the analytical expressions and to compare the performances of each strategy.

The goal of this chapter is to extend the results given in [23] using a realistic model for the activity in each cell. This activity on which the sleep mode strategies are based depends on the number of UEs served by each BS. This modelling is based on the work done in [24].

3.1 System model

A homogeneous cellular network is considered in this chapter. In such network, the positions of the UEs and of the BSs are both given by an independent HPPP in the Euclidean plane. The HPPPs associated to the UEs and the BSs are denoted respectively Φ_U with a constant intensity λ_U and Φ_B with a constant intensity λ_B. As explained in section 2.3, the analysis is performed in all generality for a typical UE located at the origin. A universal frequency reuse among all the BSs is assumed. Therefore, all BSs are interfering with each other and they all transmit with the same power P_t. All BSs are in open access which means that any UE is allowed to connect to any one of them. The UE association scheme discussed here is thus location-based. This means that each UE will be served by the closest BS.

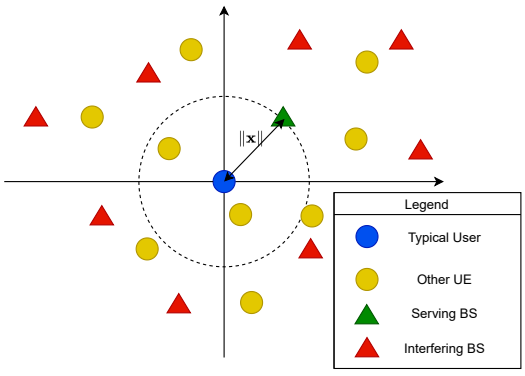

Figure 3.1: Topology of the network

Rayleigh fading and no shadowing are assumed for the channel model. The received power from each BS can thus be expressed as $P_t\ h_{\mathbf{x}}\|\mathbf{x}\|^{-\alpha}$, where $\alpha > 1$ is the path loss exponent and $h_{\mathbf{x}}$ is the Rayleigh channel coefficient which is a i.i.d. exponential random variable of parameter $\lambda = 1$ ($h_x \sim Exp(1)$). This coefficient can thus be denoted as a variable h for which the pdf is given by:

$$f_h(x;\lambda) = \begin{cases} \lambda e^{-\lambda x} & \text{if } x \geq 0, \\ 0 & \text{if } x < 0. \end{cases} \tag{3.1}$$

Notice that the path loss model yields to a power amplification when $\|\mathbf{x}\| \leq 1$. A circular excluding region of radius $R_{\min}$ around each BS is considered to address this problem. There is thus no UE in this excluding region.
For the downlink transmission from a BS located at $\mathbf{x}$ to a UE located at the origin, the expression of the SINR is given by:

$$\mathrm{SINR}(\mathbf{x}) = \frac{P_t\ h\ \|\mathbf{x}\|^{-\alpha}}{\sigma^2 + \sum_{\mathbf{y}\in\Phi_{\mathrm{B}}(\mathbf{x})} P_t\ h\ \|\mathbf{y}\|^{-\alpha}} = \frac{P_t\ h\ \|\mathbf{x}\|^{-\alpha}}{\sigma^2 + \mathcal{I}}. \tag{3.2}$$

In this expression, σ^2 is the variance of the *additive white Gaussian noise* (AWGN), $\Phi_{\mathrm{B}}(\mathbf{x})$ is the set of nodes interfering with $\mathbf{x}$ and $\mathcal{I} = \sum_{\mathbf{y}\in\Phi_{\mathrm{B}}(\mathbf{x})} P_t\ h\ \|\mathbf{y}\|^{-\alpha}$ is the interference term. Note that $\Phi_{\mathrm{B}}(\mathbf{x}) = \Phi_{\mathrm{B}} \setminus \{\mathbf{x}\}$ since universal frequency reuse is assumed.

The power consumption model considered is based on [11]. The total power consumption of a BS is given by:

$$P_{\mathrm{tot}} = \begin{cases} P_0 + \Delta_p P_t & \text{if the BS is active,} \\ P_{\mathrm{sleep}} & \text{if the BS is sleeping.} \end{cases} \tag{3.3}$$

In this model, P_0 is the static power consumption of the BS, Δ_p is the slope of the load dependent power consumption and P_{sleep} is the sleeping power consumption of the BS. Note that $P_0 > P_{\mathrm{sleep}}$ is assumed, which is a valid assumption for BSs with sleeping modes capabilities.

Two types of sleep mode strategies are studied, namely ***random sleeping*** (RS) and ***strategic sleeping*** (SS):

- **Random Sleeping:** For RS, the sleeping strategy is modelled as a Bernoulli trial. The BS is active with probability q and sleeps with probability $1 - q$. The average power consumption P_{RS} of a BS following this strategy is given by:

  $$P_{\mathrm{RS}} = q(P_0 + \Delta_p P_t) + (1-q)P_{\mathrm{sleep}}\ [\mathrm{W}]. \tag{3.4}$$

  Notice that a RS strategy with probability $q = 1$ can be interpreted as a ***no sleeping*** (NS) strategy.

- **Strategic sleeping:** For SS, the BSs are switched off when the activity within their Voronoï cell is low. While in [23] continuous values for the activity in $[0, 1]$ are assumed, this thesis is more general. This activity is modelled as a random variable $\mathcal{A}$ that can be discrete (e.g. if it models the load) or continuous (e.g. if it models the traffic demand) and can take values in $\mathbb{A} \subseteq \mathbb{R}$. Further developments are performed in all generality for a continuous variable. To adapt the expression for a discrete one with a certain *probability mass function* (pmf), the corresponding continuous pdf can be replaced by a sum of delta function as stated in equation 3.5, in which $\delta(\cdot)$ denotes the Dirac delta function.

  $$\mathrm{pdf}_{discrete}(x) = \sum_{n=-\infty}^{\infty} \mathrm{pmf}(n)\delta(n-x). \tag{3.5}$$

The SS is modelled as a function $s : \mathbb{A} \to [0,1] : a \to s(a)$. The input is the activity level of the BS while the output gives the probability that the BS is active. In other words, if the activity level of a BS is a, then it is active with probability $s(a)$ and it is sleeping with probability $1 - s(a)$. The average power consumption P_{SS} per BS is given by:

$$P_{\text{SS}} = \mathbb{E}\{s\}(P_0 + \Delta_p P_t) + (1 - \mathbb{E}\{s\})P_{\text{sleep}} \text{ [W]} \tag{3.6}$$

where $\mathbb{E}\{s\} \triangleq \mathbb{E}\{s(\mathcal{A})\} = \int_{\mathbb{A}} s(a) f_{\mathcal{A}}(a) da$ and $f_{\mathcal{A}}(a)$ is the pdf of the random activity. When strategic sleeping is applied, the activity can be seen as a random mark associated to each point of Φ_{B}. The BS can thus be modelled as a marked PP denoted as $\hat{\Phi}_{\text{B}}$ defined in $\mathbb{R}^2 \times \mathbb{A}$.

Notice that for both sleeping strategies, the set of interfering BSs $\Phi_{\text{B}}(\mathbf{x})$ considered in the interference term $\mathcal{I}$ must be thinned accordingly.

3.2 Analytical results

This section is subdivided in three parts. In the first part, some useful lemmas for studying the coverage probability are stated. In the second, the expression of the coverage probability is derived for different sleeping strategies without explicitly defining the activity $\mathcal{A}$. In the third part, a model is developed for this activity based on [24].

3.2.1 Important Lemmas

First, a general expression for the coverage probability is given recalling that the *Laplace transform* (LT) of a random variable X is defined as $\mathcal{L}_X(s) = \mathbb{E}_X[\exp(-sX)]$.

Lemma 1
The coverage probability of a BS under the assumption of Rayleigh fading is given by:

$$\mathbb{P}_{cov}(\tau) = \int_{R_{min}}^{\infty} \mathcal{L}_N\left(\frac{r^\alpha \tau}{P_t}\right) \mathcal{L}_{\mathcal{I}}\left(\frac{r^\alpha \tau}{P_t}; \lambda_{\mathcal{I}}\right) f_R(r; \lambda_R) dr. \tag{3.7}$$

- $\mathcal{L}_N(s) = \exp\left(-s\sigma^2\right)$ *is the LT of the constant noise power*[a].
- $\mathcal{L}_{\mathcal{I}}$ *is the LT of the interference term* $\mathcal{I}$. $\lambda_{\mathcal{I}}$ *is the intensity of the interfering BSs HPPP.*
- f_R *is the pdf of the distance to the serving BS.* λ_R *is the intensity of the HPPP of BSs.*

[a] The constant variable σ^2 can be seen as a random variable with $\text{pdf}(x) = \delta(\sigma^2 - x)$. This allows the use of the LT definition for constant variables

To use Lemma 1, the distribution of the distance between the typical UE and the closest awake BS must be derived. For notation convenience, the points of the BSs PP $\Phi_{\text{B}} = \{\mathbf{X}_i : i \in \mathbb{N}\}$ are ordered with respect to their distance to the origin such that $\|\mathbf{X}_i\| \leq \|\mathbf{X}_j\|$ for $i < j$.

Lemma 2
Assuming that the BSs are distributed as a HPPP of intensity λ_R*, the pdf of the distance between the typical UE and the* i^{th} *closest BS is given by:*

$$f_{R_i}(r_i; \lambda_R) = \frac{2(\pi\lambda_R)^i}{(i-1)!} r_i (r_i^2 - R_{min}^2)^{i-1} \exp\left(-\pi\lambda_R(r_i^2 - R_{min}^2)\right), \quad r_i \geq R_{min}. \tag{3.8}$$

In the next lemma the expression of the LT of the interference is given.

Lemma 3
When Rayleigh fading and HPPP distributed interfering BSs of intensity $\lambda_{\mathcal{I}}$ are assumed, the LT of the interference term is given by:

$$\mathcal{L}_{\mathcal{I}}\left(\frac{r^{\alpha}\tau}{P_t};\lambda_{\mathcal{I}}\right)=\exp\left(-\pi\lambda_{\mathcal{I}}\, r^2\rho(\tau,\alpha)\right) \tag{3.9}$$

with:

$$\rho(\tau,\alpha)=\tau^{2/\alpha}\int_{\tau^{-2/\alpha}}^{\infty}\frac{1}{1+u^{\alpha/2}}du. \tag{3.10}$$

3.2.2 Coverage probability

The RS strategy described in section 3.1 can be interpreted as an independent thinning operation applied on the BSs HPPP Φ_{B}. The thinning function is defined as $g(\mathbf{x})=q$. Since this function is not location dependent, the resulting BSs PP is a HPPP with intensity $q\lambda_{\mathrm{B}}$. Proposition 1 states the coverage probability when RS is applied.

Proposition 1
In homogeneous networks with RS, the coverage probability of the typical UE is given by:

$$\mathbb{P}_{cov}^{RS}(\tau)=2\pi q\lambda_B\int_{R_{min}}^{\infty} r\exp\left(\frac{-r^{\alpha}\tau\sigma^2}{P_t}\right)\exp\left(-\pi q\lambda_{\mathrm{B}}\left(r^2(1+\rho(\tau,\alpha))-R_{min}^2\right)\right)dr. \tag{3.11}$$

When the noise power is considered to be zero (i.e. $\sigma^2=0$), the expression for the coverage probability can be simplified.

Corollary 1
For $\sigma^2=0$, the expression of the coverage probability in Proposition 1 reduces to:

$$\mathbb{P}_{cov,\sigma^2=0}^{RS}(\tau)=\frac{\exp\left(-\pi q\lambda_{\mathrm{B}}R_{min}^2\rho(\tau,\alpha)\right)}{(1+\rho(\tau,\alpha))}. \tag{3.12}$$

The expressions for the coverage probability in Proposition 1 and Corollary 1 already allow to draw some interpretations before proceeding to numerical simulations in section 3.3.
Without noise, the coverage probability is independent of the transmit power P_t. This can be explained by the fact that in the absence of noise, the SINR is a signal-to-interference ratio. Indeed, in equation 3.2 the transmit power of the serving BS cancels out with the transmit power of the interfering BSs when $\sigma^2=0$. Moreover, when the excluding region is not considered (i.e. by setting $R_{\min}=0$), the coverage probability only depends on the path loss α and on the QoS threshold τ. In such situation, the coverage probability is independent of the random sleeping policy q and of the density of BSs λ_{B}. In the presence of noise (i.e. $\sigma^2>0$), the coverage probability is obtained using numerical integration.

To study the SS case, it is first shown that the coverage probability is not a relevant metric to express the benefit of this strategy compared to RS. Then a new, more appropriate metric called the ***weighted coverage probability*** (WCP) is proposed.

As stated in Proposition 1, the coverage probability in the case of RS can be computed considering that the awake BSs are distributed as a thinned HPPP of intensity $q\lambda_{\mathrm{B}}$ instead of λ_{B}. In this case, the typical UE is served by the closest BS of the thinned HPPP. An equivalent way to compute this would be to split the total probability into the one of the events in which the

UE connects to each BS of the HPPP Φ_B of intensity λ_{B}. The coverage probability can thus be expressed as follows:

$$\mathbb{P}_{cov}(\tau) = \sum_{i=1}^{\infty} \mathbb{P}_{cov}(\tau | N_{\mathrm{ord}} = i)\mathbb{P}(N_{\mathrm{ord}} = i). \tag{3.13}$$

N_{ord} denotes the index of the BS to which the typical UE is connected. $\mathbb{P}(N_{\mathrm{ord}} = i)$ is therefore the probability to be connected to the i^{th} closest BS. For RS, $\mathbb{P}(N_{\mathrm{ord}} = i) = q(1-q)^{i-1}$ since the UE would connect to the i^{th} BS if the $i-1$ closer BSs are sleeping and the i^{th} one is awake. $\mathbb{P}_{cov}(\tau | N_{\mathrm{ord}} = i)$ is given by Lemma 1 in which $f_R(r;\lambda_R) = f_{R_i}(r;\lambda_B)$ is given by Lemma 2.

In the SS case, the coverage probability can be developed as follows:

$$\begin{aligned}
\mathbb{P}_{cov}^{SS}(\tau) &= \int_{\mathbb{A}} \mathbb{P}_{cov}(\tau|a_1) f_{\mathcal{A}}(a_1) da_1 \\
&\overset{(a)}{=} \int_{\mathbb{A}} \sum_{i=1}^{\infty} \mathbb{P}_{cov}(\tau | N_{\mathrm{ord}} = i)\mathbb{P}(N_{\mathrm{ord}} = i|a_1) f_{\mathcal{A}}(a_1) da_1 \\
&\overset{(b)}{=} \int_{\mathbb{A}} \Big[s(a_1)\mathbb{P}_{cov}(\tau | N_{\mathrm{ord}} = 1) + (1 - s(a_1)) \\
&\quad \sum_{i=2}^{\infty} \mathbb{P}_{cov}(\tau | N_{\mathrm{ord}} = i)\mathbb{P}(N_{\mathrm{ord}} = i | N_{\mathrm{ord}} > 1) \Big] f_{\mathcal{A}}(a_1) da_1 \\
&= \mathbb{E}\{s\}\mathbb{P}_{cov}(\tau | N_{\mathrm{ord}} = 1) \\
&\quad + \sum_{i=2}^{\infty} (1 - \mathbb{E}\{s\})\mathbb{P}_{cov}(\tau | N_{\mathrm{ord}} = i)\mathbb{P}(N_{\mathrm{ord}} = i | N_{\mathrm{ord}} > 1) \\
&= \sum_{i=1}^{\infty} \mathbb{E}\{s\}(1 - \mathbb{E}\{s\})^{i-1} \mathbb{P}_{cov}(\tau | N_{\mathrm{ord}} = i).
\end{aligned}$$

(a) is from equation 3.13 and (b) is obtained by definition of the sleeping strategy. The closest BS is awake with probability $s(a_1)$.

Note from this last expression that by taking $q = \mathbb{E}\{s\}$, the coverage probability of the SS and of the RS are equivalent when the proportion of awake BSs is the same. With this metric, the same importance is given to locations where the number of UEs might be very small as to locations in which it is known that there is a large number of UEs. It would thus be interesting to use a metric that would weight the importance of each cell. This metric is the weighted coverage probability.

Definition 1 (WCP metric)
The weighted coverage probability metric is defined as:

$$\mathbb{P}_{WCP}(\tau) = \frac{1}{\mathbb{E}\{a\}} \int_{\mathbb{A}} a_1 \mathbb{P}_{cov}(\tau|a_1) f_{\mathcal{A}}(a_1) da_1 \tag{3.14}$$

where $\mathbb{E}\{a\} \triangleq \mathbb{E}\{\mathcal{A}\} = \int_{\mathbb{A}} a f_{\mathcal{A}}(a) da$.

From now on, the EE is computed by replacing the coverage probability by the WCP. In the two next propositions, the expressions of the WCP metric for RS and SS are stated.

Proposition 2
In homogeneous networks with random sleeping, the WCP of the typical UE is equivalent to the coverage probability given in Proposition 1.

Proposition 3
In homogeneous networks with strategic sleeping, the WCP of the typical UE is given by:

$$\begin{aligned}\mathbb{P}^{SS}_{\mathrm{WCP}}(\tau) =& \frac{\mathbb{E}\{as(a)\}}{\mathbb{E}\{a\}} \int_{R_{min}}^{\infty} \mathcal{L}_N\left(\frac{r^\alpha \tau}{P_t}\right) \mathcal{L}_{\mathcal{I}}\left(\frac{r^\alpha \tau}{P_t}; \mathbb{E}\{s\}\lambda_B\right) f_{R_1}(r;\lambda_B) dr \\ &+ \frac{(\mathbb{E}\{a\} - \mathbb{E}\{as(a)\})}{\mathbb{E}\{a\}} \sum_{i=2}^{\infty} \mathbb{E}\{s\}(1-\mathbb{E}\{s\})^{i-2} \int_{R_{min}}^{\infty} \mathcal{L}_N\left(\frac{r^\alpha \tau}{P_t}\right) \\ &\mathcal{L}_{\mathcal{I}}\left(\frac{r^\alpha \tau}{P_t}; \mathbb{E}\{s\}\lambda_B\right) f_{R_i}(r;\lambda_B) dr. \end{aligned} \tag{3.15}$$

When the noise power is considered to be zero (i.e. $\sigma^2 = 0$), the expression of the WCP for strategic sleeping can be simplified.

Corollary 2
For $\sigma^2 = 0$, the expression of the coverage probability in Proposition 3 reduces to:

$$\mathbb{P}^{SS}_{\mathrm{WCP},\sigma^2=0}(\tau) = \exp\left(-\pi \mathbb{E}\{s\}\lambda_B R_{min}^2 \rho(\tau,\alpha)\right) \frac{1 + (\rho(\tau,\alpha)\mathbb{E}\{as(a)\}/\mathbb{E}\{a\})}{(1+\mathbb{E}\{s\}\rho(\tau,\alpha))\,(1+\rho(\tau,\alpha))}. \tag{3.16}$$

Similarly to the analysis performed for the coverage probability of the RS strategy, one can draw some interpretations before performing numerical simulations in section 3.3.
As for RS, it can be observed that the WCP metric for SS is independent of the transmit power P_t when $\sigma^2 = 0$. When no excluding region is considered (i.e. $R_{\min} = 0$), the WCP metric is independent from the density of BSs λ_B. Unlike the RS case, the metric depends on the strategy used. When the noise power is not zero, the WCP metric is obtained using numerical integration.

3.2.3 Modelling of the load

As described in section 3.1, the activity of a cell can be defined in many different ways. In this thesis, the activity of a BS is modelled as the load of its Voronoï cell. The load is a non negative integer representing the number of UEs that the BS would serve if no sleeping strategy was used. The distribution of the activity for a typical BS located at the origin is stated in the next proposition.

Proposition 4
In homogeneous networks with nearest BS association, the activity, defined as the load of the Voronoï region, follows a negative binomial (NB) distribution (i.e. $\mathcal{A} \sim NB(c, p_s)$):

$$f_{\mathcal{A}}(a) = \frac{\Gamma(n+c)}{\Gamma(c)\Gamma(n+1)} p_s^a (1-p_s)^c, \quad a \in \mathbb{N} \tag{3.17}$$

where:

- $c = 3.575$ *is a constant linked to the size of the Voronoï region. [25]*
- $p_s = \frac{1}{1+c\lambda_B/\lambda_U}$ *is interpreted as the probability of success for the NB distribution.*
- $\Gamma(x)$ *is the gamma function.*

The activity is thus a non negative discrete random variable. To be able to compute the expectations $\mathbb{E}\{a\}, \mathbb{E}\{s(a)\}$ and $\mathbb{E}\{as(a)\}$, the SS function $s(a)$ is defined as follows:

$$s : \mathbb{N} \to [0,1] : a \to s(a) = \begin{cases} 1 & \text{if } a \geq \mu, \\ 0 & \text{if } a < \mu, \end{cases} \tag{3.18}$$

where μ is the SS threshold. Using Proposition 4 and the definition of the SS function, the expressions of the desired expectations are stated in Corollary 3

Corollary 3

For an activity $\mathcal{A} \sim NB(c, p_s)$, the expressions of the expectations needed to compute the WCP metric are given by:

$$\mathbb{E}\{a\} = \frac{p_s c}{1 - p_s}, \tag{3.19}$$

$$\mathbb{E}\{s(a)\} = 1 - \sum_{k=0}^{\lceil \mu - 1 \rceil} f_{\mathcal{A}}(k) = \bar{F}_{\mathcal{A}}(\lceil \mu - 1 \rceil), \tag{3.20}$$

$$\mathbb{E}\{as(a)\} = \mathbb{E}\{a\} - \sum_{k=0}^{\lceil \mu - 1 \rceil} k f_{\mathcal{A}}(k), \tag{3.21}$$

where $\bar{F}_{\mathcal{A}}(x)$ is the complementary cumulative distribution function (ccdf) of the activity.

For SS, the threshold μ can be chosen to reach a targeted ratio q_{SS} of awake BS. In most cases, $\mathbb{E}\{s\}$ will not be exactly equal to q_{SS} since the activity variable $\mathcal{A}$ is discrete. When q_{SS} is specified, μ is the biggest integer such that $\mathbb{E}\{s\} \geq q_{SS}$.

3.3 Numerical results

In this section, the analytical expressions obtained in section 3.2 are first compared to MC simulations in order to confirm their validity. Then, the influence of some parameters on the different metrics is studied based only on the analytical expressions. For each simulation, the default values from Tables 3.1,3.2 and 3.3 are used unless otherwise stated. The values for the power consumption parameters are from [11]. The MC parameters n and L are respectively the number of iterations and the length of the side of the simulation square.

Parameters	Values
$B[m^{-2}]$	10^{-4}
$U[m^{-2}]$	10^{-3}
α	4
q/q_{SS}	0.5
$\tau[dB]$	-10
$P_t[dB]$	13
σ^2	10^{-6}
$R_{min}[m]$	1

Table 3.1: Network parameters

Parameters	Values
$P_0[W]$	130
$P_{sleep}[W]$	75
Δ_p	4.7

Table 3.2: Power consumption parameters

Parameters	Values
n	5000
$L[m]$	5000

Table 3.3: MC simulation parameters

3.3.1 Validity of the expressions using MC simulations

Preliminary note: For each figure, the solid lines represent the result of the MC simulations while the stars represent the values obtained with the analytical expressions.

Figures 3.2a and 3.2b illustrate respectively the evolution of the coverage probability and of the WCP metric with respect to the noise variance σ^2. RS is applied for the coverage probability, while SS is used for the WCP metric. As seen in Proposition 2, the coverage probability is equivalent to the WCP metric for RS. The transmitting power is set to $1[W]$ to make the x-axis correspond to the inverse of the transmitted signal-to-noise ratio. For the tested sleeping probabilities and densities of BSs, the validity of the analytical expressions of Proposition 1 and 3 is verified. One can observe that for a given noise variance, both the coverage probability for RS and the WCP metric for SS increase with the density of awake BSs (respectively $q\lambda_B$ and $\mathbb{E}\{s\}\lambda_B$). When the noise level tends towards zero, the curves tend towards an upper bound which has approximately the same value for all tested parameters. For RS, this observation confirms the observations made on the analytical expression of the coverage probability without noise given in Corollary 1. For SS, it confirms the same observations made on the analytical expression of the WCP metric without noise given in Corollary 2. The slight difference between the expressions is given by the term $\exp\left(-\pi q\lambda_{\mathrm{B}}R_{\mathrm{min}}^2\rho(\tau,\alpha)\right)$ for RS and by the term $\exp\left(-\pi\mathbb{E}\{s\}\lambda_{\mathrm{B}}R_{\mathrm{min}}^2\rho(\tau,\alpha)\right)$ for SS. In both cases, these exponential terms are approximately equal to 1 with the considered parameters, which explains why the curves tend towards the same upper bound.

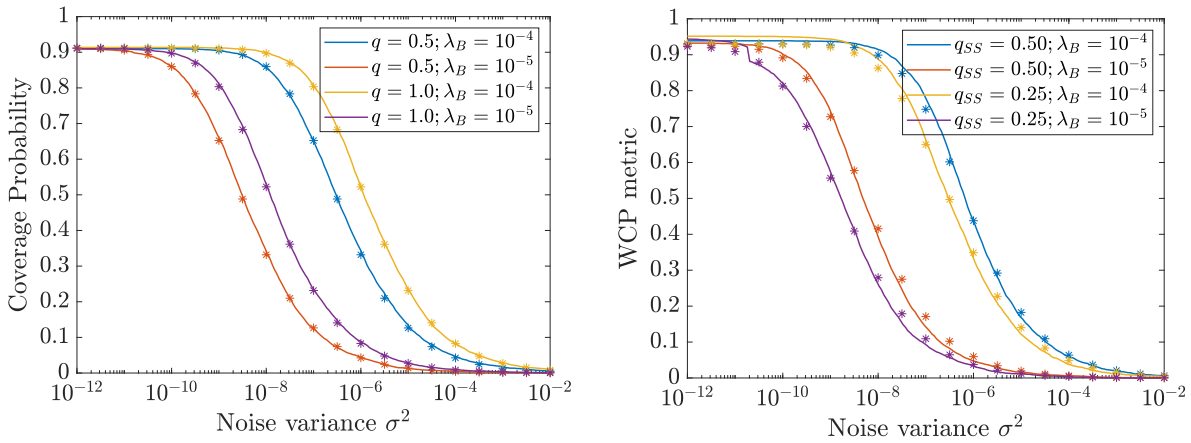

(a) Proposition 1

(b) Proposition 3

Figure 3.2: Comparison of analytical and numerical results for Propositions 1 and 3 with $P_t = 1[W]$

Figure 3.3 confirms the accuracy of the pmf of the load given in Proposition 4. Note that even if solid lines are used for the curves for the sake of readability, the plotted pmfs are discrete. One can also observe that the standard deviation of the pmf increases when the density of BSs decreases. As expected, the value of the most probable load increases when the density of BSs decreases since each BS must serve more UEs.

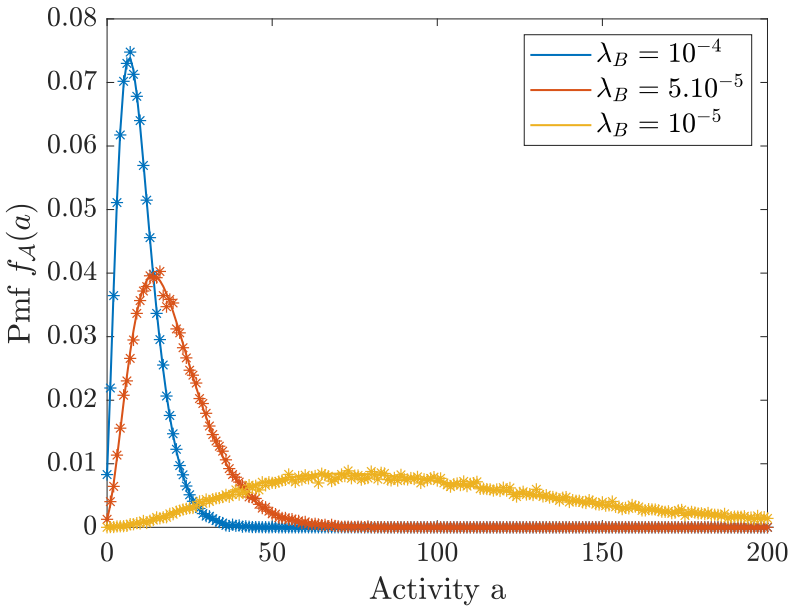

Figure 3.3: Comparison of analytical and numerical results for Proposition 4 for $n = 50000$.

Finally, figure 3.4 shows the evolution of the WCP metric without noise with respect to the QoS threshold. This can be interpreted as the upper bound of the metric for a given τ. The upper bound provided by SS is always higher than the one provided by RS. The validity of both expressions is confirmed with a better accuracy for the RS. The slight difference observed for the SS case can be explained by the model used for the activity. Figure 3.3 confirms the model for the typical BS, but it is not strictly correct to represent the activity of the nearest BS. Recall from section 2.3 that Palm theory allows to characterise the distribution of the activity of the

BSs in a network, by studying this distribution for a typical BS located at the origin. This distribution can then be generalised for any BS selected uniformly at random amoung all points of the PP Φ_B. When the WCP metric is studied for a typical UE at the origin, the distribution of interest for the load is the one of the closest BS to the origin. This is not a randomly chosen BS among all possible choice so Palm theory does not apply. The impact on the distribution for the first BS is further discussed in chapter 5 in which a more complicated but more precise model for the activity is studied. For now, an approximation is made by considering that the distribution of the typical BS can be applied to the closest BS to the typical UE. This approximation allows to obtain a simpler model with a good accuracy as observed on figures 3.2b and 3.4

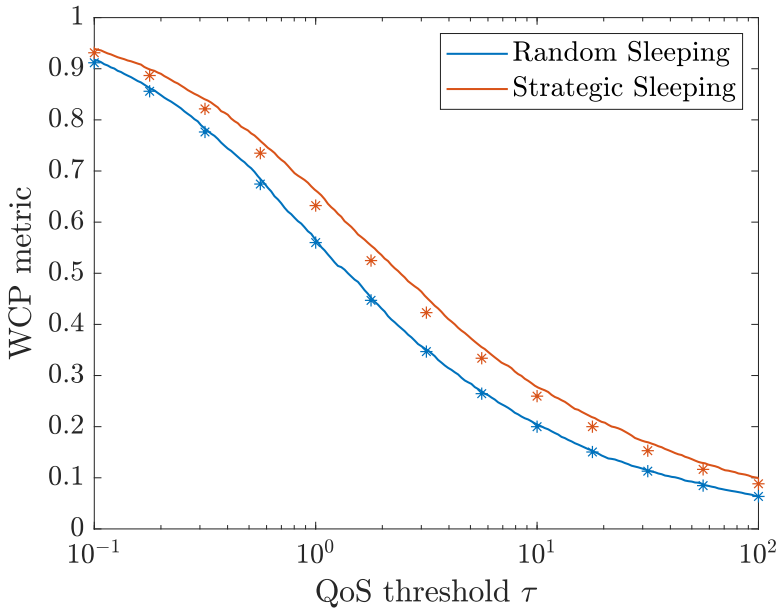

Figure 3.4: Comparison of analytical and numerical results for Corollary 1 and 2 with $\sigma^2 = 0$ and $P_t = 1[W]$.

3.3.2 SG based interpretations

In this subsection, the curves are obtained from the analytical expressions. Unlike previous subsection in which stars where used to represent the results of the analytical expressions, solid lines are used in this section unless otherwise stated.

On Figure 3.5, the two ways of computing the coverage probability with random sleeping are compared. One can observe that, as expected, both equations 3.11 and 3.13 lead to the same results.

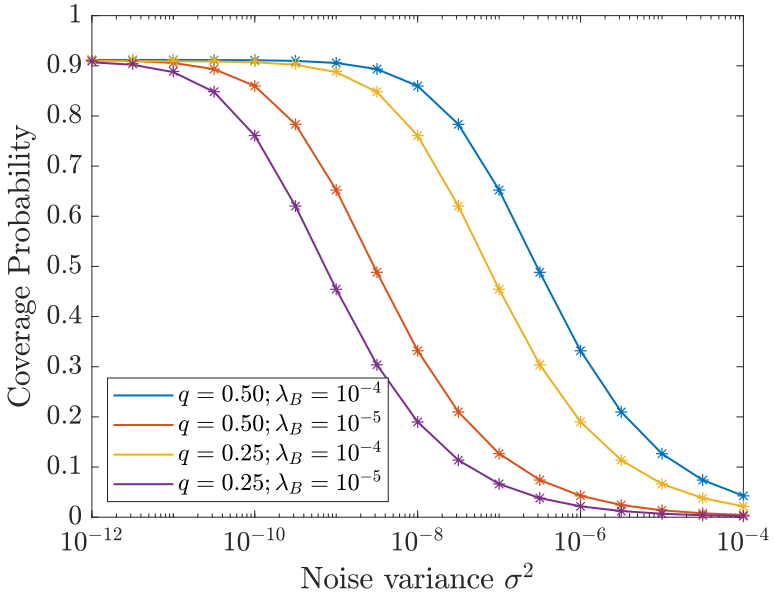

Figure 3.5: Comparison of equations 3.11 and 3.13 to compute the coverage probability. The stars represent the value obtained with 3.11 and the solid line represents the value obtained with 3.13.

Figures 3.6a and 3.6b illustrate the evolution of the EE with respect to the QoS threshold for two different levels of noise. For both levels, one can observe that SS outperforms RS and NS for the tested choices of q and q_{SS}. Another important observation is that the optimal choice of q and q_{SS} depends on the noise variance. This choice does not change for the considered interval of values of the QoS threshold τ. For $\sigma^2 = 10^{-4}$, the strategies with higher ratio of awake BSs result in the highest EE. For $\sigma^2 = 10^{-6}$, the strategies with smaller ratio of awake BSs result in the highest EE. Except for RS with $q = 0.25$ that is the worst strategy in both scenario.
There is thus an optimal choice $q_{SS,opt}$ for the ratio of awake BSs in SS. If $q_{SS} > q_{SS,opt}$, the power consumption increases faster than the WCP metric. In this situation, the increased power consumption does not lead to an increased coverage for the UEs. If $q_{SS} < q_{SS,opt}$, the WCP decreases faster than the power consumption. In this situation, the decreased power consumption does not lead to a sufficient coverage for the UEs. From the observations on Figure 3.6a and 3.6b, the optimal ratio of awake BSs increases with the noise variance.

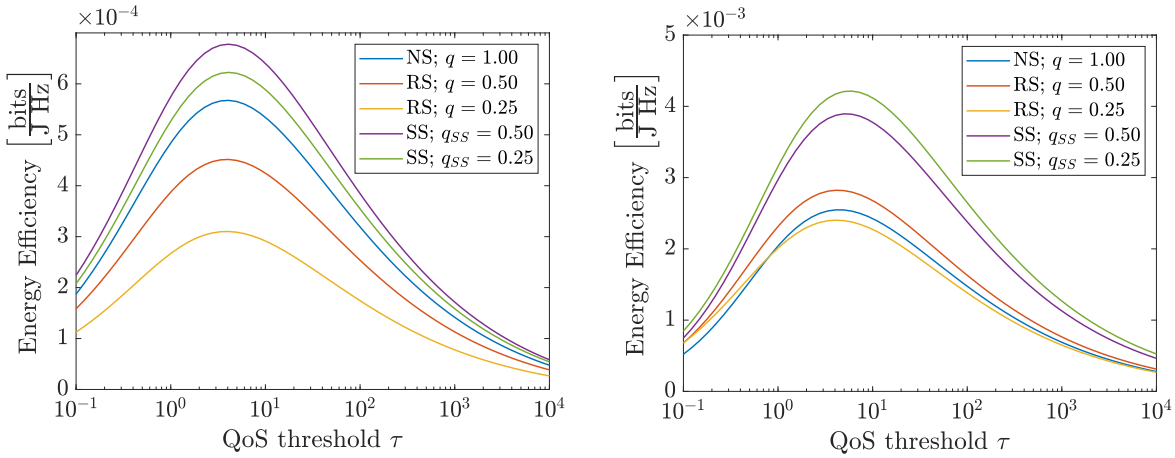

(a) $\sigma^2 = 10^{-4}$ (b) $\sigma^2 = 10^{-6}$

Figure 3.6: Energy efficiency for different sleeping strategies and levels of noise.

Figure 3.7 confirms the conclusion made on the basis of Figures 3.6a and 3.6b. For lower level of noise (e.g. $\sigma^2 = 10^{-8}$), the strategies with a low q_{SS} (here $q_{SS} = 0.1$) outperform the other strategies: the power consumption is decreased and the WCP metric is kept at a sufficiently high level. However, when the noise level increases, the WCP metric decreases faster for low values of q_{SS} than higher ones. This explains why, for $\sigma^2 = 10^{-6}$, the ratio providing the best performances is no longer $q_{SS} = 0.1$ but $q_{SS} = 0.25$. When the noise variance gets closer to 10^{-2}, the optimal strategy is the one with the highest ratio of awake BSs. However, the benefit for the EE obtained by choosing the optimal strategy gets smaller when the noise variance increases. For a high level of noise (i.e. $\sigma^2 = 10^{-2}$), the WCP metric is close to 0 for all strategies. In this case, the impact of the power consumption on the EE becomes insignificant.

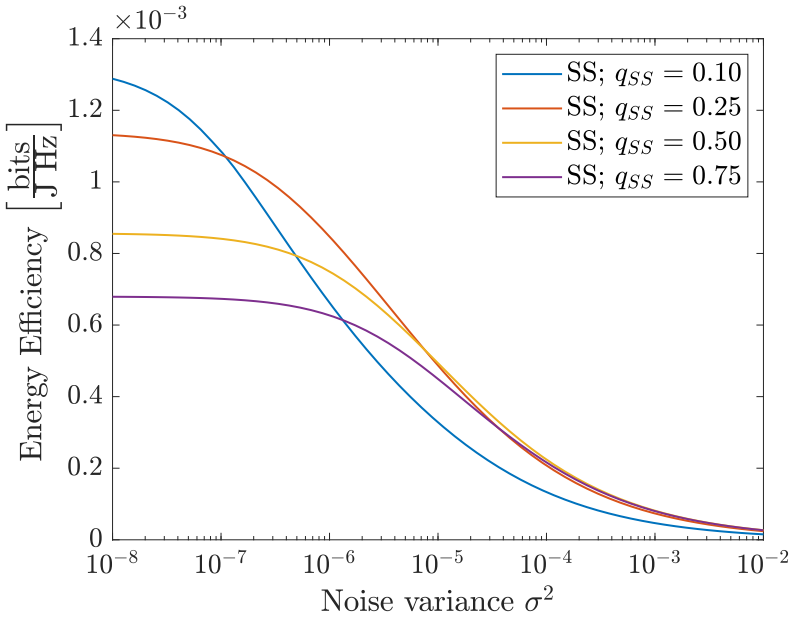

Figure 3.7: Comparison of the Energy Efficiency for different sleeping strategies.

Figures 3.8a and 3.8b illustrate the impact of the SS threshold μ. One can observe that the power consumption decreases before the WCP metric. This results in an increase of the EE. When the density of awake BSs tends towards zero, so does the WCP metric. However, the

power consumption stays to a non zero level because of the sleeping power consumption P_{sleep}. Hence, the EE tends to zero in this case. Between the situation in which all BSs are awake and the one in which they are all sleeping, there is thus an optimal choice of μ that maximises the EE. This optimal choice is different for networks with different density of BSs λ_B.
On Figure 3.8b, one can observe that there is only one local maximum for the EE, which is therefore also a global maximum. The optimal μ can be found with the algorithm 1, where $EE(\mu)$ denotes the value of the EE when the SS threshold is μ. The initial point is chosen as the rounded expectation of the activity. Then the algorithm compares the value of the EE for the initial point with the one obtained with the previous and the next integers. The initial point of the next iteration is the one providing the highest EE. The algorithm converges when the initial point provides the highest EE.

Algorithm 1: Find the optimal μ

Initialisation:
$\mu_0 = \text{round}(\mathbb{E}\{a\})$;
$\mu^* = \text{NaN}$;
while *isnan*(μ^*) **do**
  $\mu_{-1} = \max(0, \mu_0 - 1)$; $\mu_1 = \mu_0 + 1$;
  if $EE(\mu_1) > EE(\mu_0)$ **then**
    $\mu_0 = \mu_1$;
  else if $EE(\mu_{-1}) > EE(\mu_0)$ **then**
    $\mu_0 = \mu_{-1}$;
  else
    $\mu^* = \mu_0$;
  end
end
Result: μ^* is the optimal μ

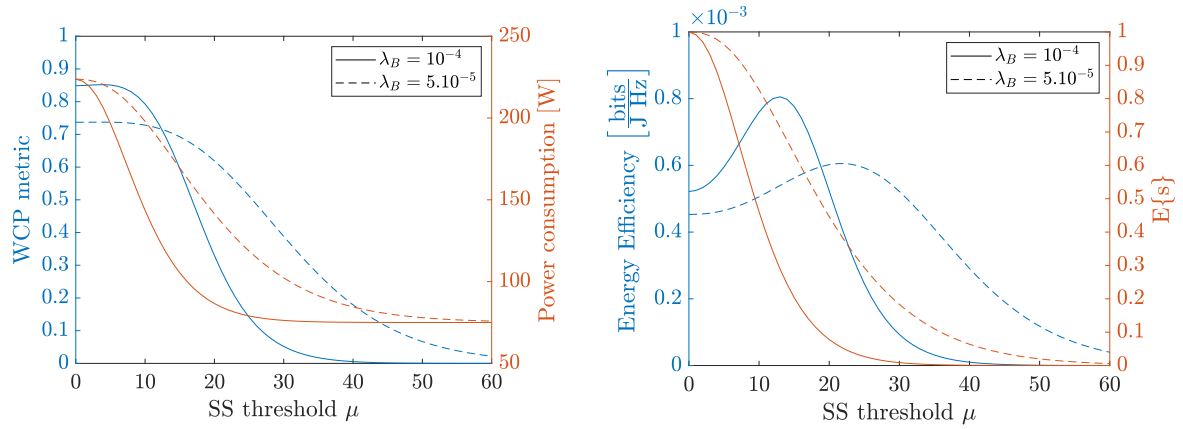

(a) (b)

Figure 3.8: Impact of μ on the WCP metric, the power consumption, the energy efficiency and the ratio of awake BSs for different density of BSs.

The heatmaps of Figures 3.9 and 3.10 show respectively the optimal EE and the corresponding $\mathbb{E}\{s\}$ for different density of BSs and UEs. One can observe that for a given density of UEs, the EE increases with the density of BSs. This could be counter intuitive since more BSs results in an increased power consumption. However one can observe that the corresponding proportion of awake BSs decreases when the density of BSs increases. This means that for a given density

of UEs, the network provider should increase the density of BSs to increase the EE. More BSs will be on sleep mode with a low power consumption while the BSs with a high load will provide a higher coverage probability.
Furthermore, for a given density of BSs, the energy efficiency increases when the density of UEs decreases. However, the impact of this parameter is less significant compared to the density of BSs. What is interesting to observe here is that when the density of UEs decreases, one could expect the optimal proportion of BSs awake to decrease as well. However the optimal $\mathbb{E}\{s\}$ appears to stay quite stable compared to the changes observed when the density of BSs changes. This can be explain by the HPPP distribution of the UEs over the network. Indeed, their locations being independent with each others, the UEs locations can be very spread. It means that whatever the density of UEs, the BSs must be spread over the whole network to be able to serve each UEs.
The conclusion is that the optimal μ mostly depend on the density of BSs, the impact of the density of UEs being very small.

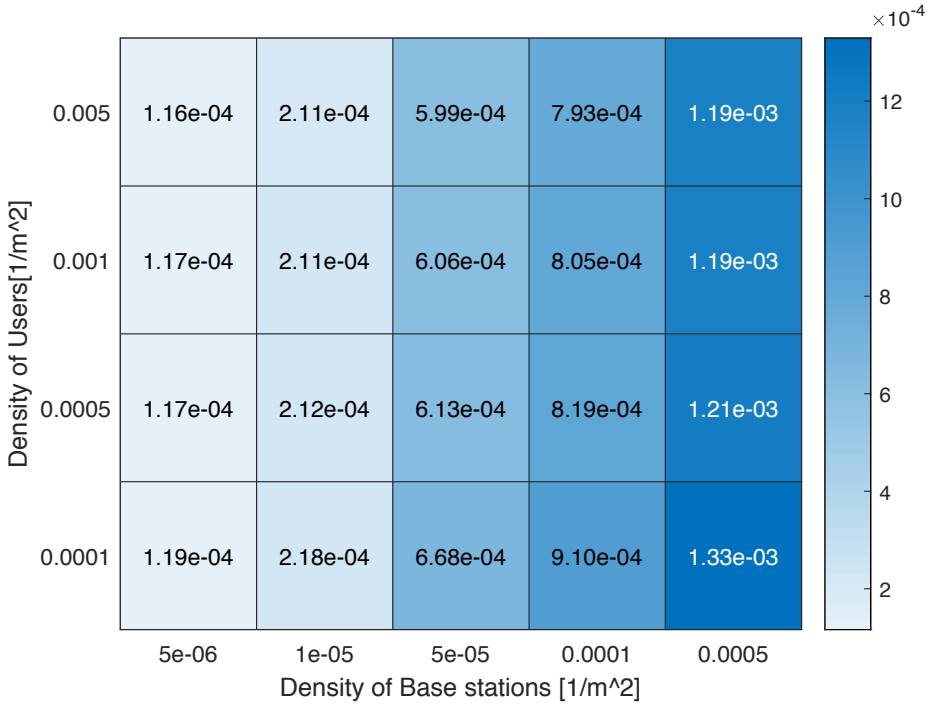

Figure 3.9: Comparison of the optimised EE for different densities of UEs and BSs. SS with the optimal μ is used in each case.

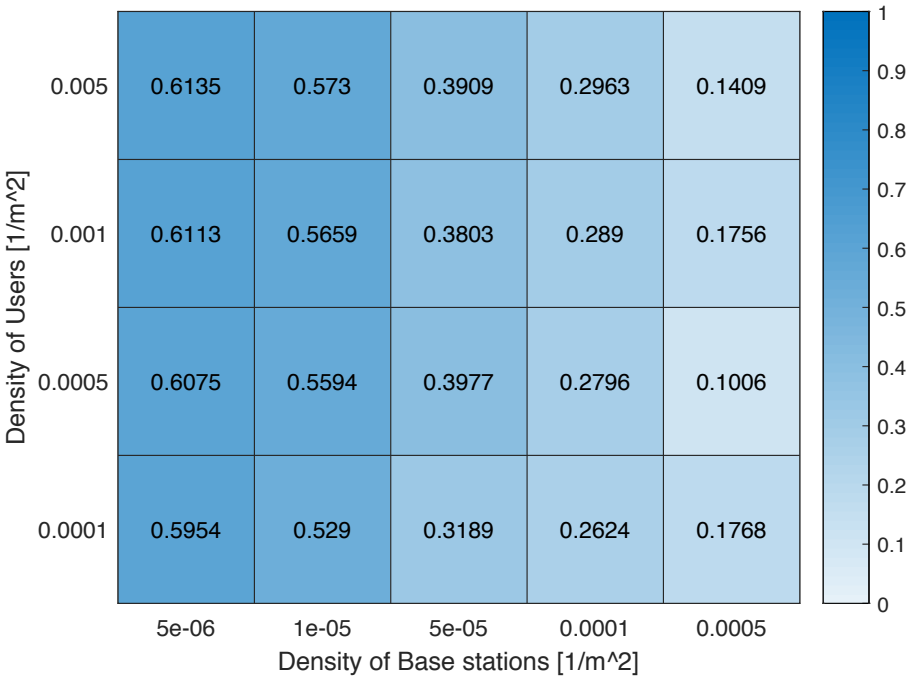

Figure 3.10: Corresponding ratio of awake BSs for the different densities of UEs and BSs when SS with the μ optimising the EE is used in each case.

Figure 3.11 compares the evolution of the EE with the noise variance for two strategies with the same density of awake BSs. For each values of the noise variance, the optimal $\mathbb{E}\{s\}$ is used for the SS strategy. The obtained EE is compared with the EE of a NS strategy for which the density of BSs is given by $\mathbb{E}\{s\}\lambda_B$. One can observe that the SS outperforms the NS for every level of noise. Despite the increased power consumption related to the sleeping BSs that are not used, the benefit obtained for the coverage probability is sufficient to provide a higher EE. The conclusion is that, for a network provider, it is interesting, according to the EE metric, to have a high density of BSs with a low proportion of awake BSs compared to a non sleeping strategy with an equivalent density of awake BSs.
Figure 3.11 also confirms that the optimal ratio of awake BSs increases with the noise variance (as observed in Figures 3.9 and 3.10).

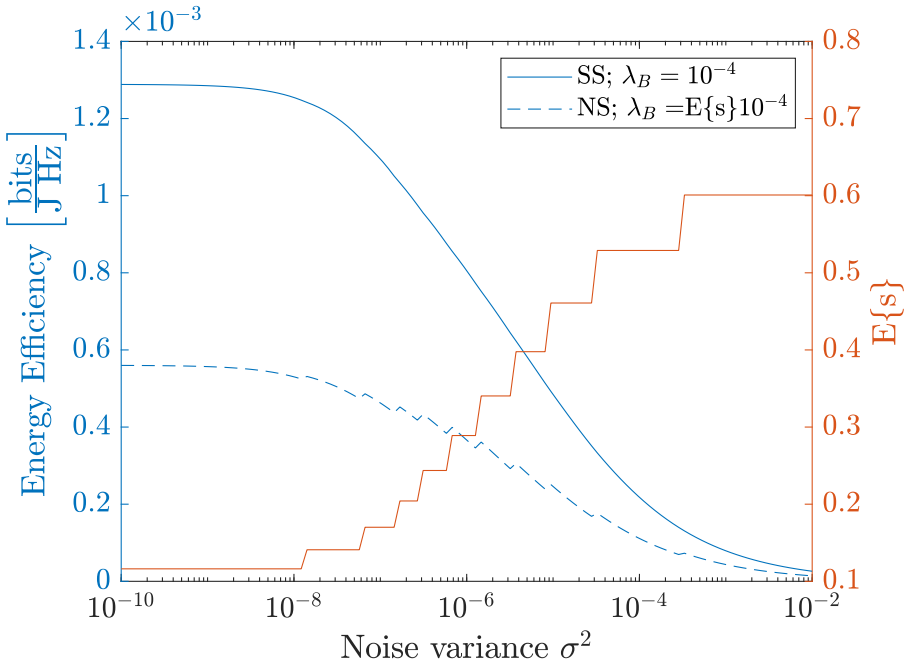

Figure 3.11: Comparison of the energy efficiency of an optimal strategic sleeping and a non sleeping strategy with the same ratio of awake BSs.

Chapter 4

Sleep Control Strategies in Millimeter Wave Networks with Clustered User Distribution

In this chapter, the benefit of SS is studied for mm-Wave networks. The analysis is carried out for two different types of UEs distribution, namely the HPPP and the PCP. Firstly, the system model of chapter 3 is adapted to match the features of mm-Wave network. The derived analytical expressions are then presented. Secondly, the validity of these expressions is assessed by MC simulations and an analysis is performed.

The main contribution of this chapter is to extend the coverage analysis performed in [26] for homogeneous networks. This extension consists in developing the WCP metric for homogeneous and clustered networks with sleeping strategies featuring mm-Wave transmissions. The modelling of the activity for the clustered UEs is based on [27].

4.1 System model

As described in the introduction of this chapter, two types of PP are studied to model the location of the UEs:

- **HPPP:** In this case, the PP is denoted $\Phi_{\mathrm{U}}^{\mathrm{H}}$ and has a constant intensity denoted λ_{U}.
- **PCP:** Here, the PP is denoted $\Phi_{\mathrm{U}}^{\mathrm{C}}$. The constant intensity of the parent PP is denoted λ_{U}^{p}. The other parameters are denoted as described in section 2.2.3, except for the cluster variance of the TCP which is denoted by σ_{U}^{2}.

The BSs locations are modelled as an independent HPPP Φ_{B} with a constant intensity λ_{B}. The main difference for the BSs, compare to the analysis made in chapter 3, is their ability to perform beamforming. The BSs are equipped with a directional uniform linear array of N_t antennas. The distance between the antennas is denoted d while the wavelength is denoted λ. Universal frequency reuse and constant transmit power P_t is still considered. The association scheme is therefore location-based. Note that P_t is considered to be the total power transmitted by the BSs. Hence, each antenna transmits with power $\frac{P_t}{N_t}$.

For the received signals, only *line-of-sight* (LoS) transmissions are considered since non-LoS transmissions have been shown to be negligible for mm-Wave in [28]. To focus the analysis on the LoS transmissions to a typical UE located at the origin, the LoS ball blockage model, introduced in [29], is used. The interfering BSs are located within an annulus of inner radius

r_0 and outer radius $R_{\max}$, r_0 being the distance to the serving BS and $R_{\max}$ being the LoS ball radius. Figure 4.1 illustrates the topology of the described network.

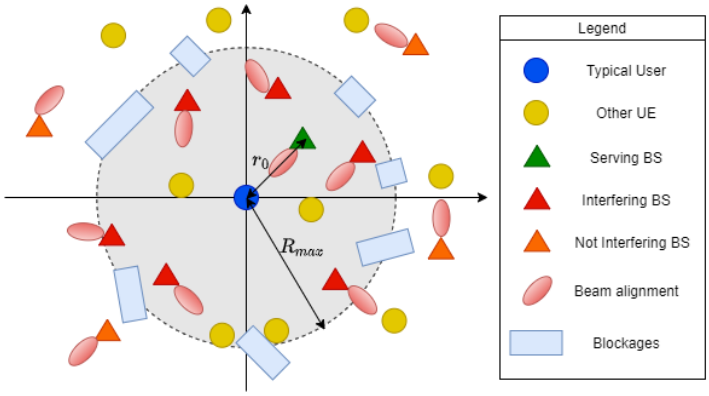

Figure 4.1: Topology of the network with beamforming and a LoS ball.

For a serving BS located at $\mathbf{x}_0$, the received signal for the typical UE is given by:

$$y = \sqrt{\beta} r_0^{-\frac{\alpha}{2}} \mathbf{h}_{\mathbf{x}_0} \mathbf{w}_{\mathbf{x}_0} \sqrt{\frac{P_t}{N_t}} s_{\mathbf{x}_0} + \sum_{\mathbf{x} \in \Phi_{\mathrm{B}}(\mathbf{x}_0)} \sqrt{\beta} \|\mathbf{x}\|^{-\frac{\alpha}{2}} \mathbf{h}_{\mathbf{x}} \mathbf{w}_{\mathbf{x}} \sqrt{\frac{P_t}{N_t}} s_{\mathbf{x}} + n_0, \tag{4.1}$$

where $\mathbf{h}_{\mathbf{x}}$ and $\mathbf{w}_{\mathbf{x}}$ are respectively the channel and beamforming vectors between a transmitter located at $\mathbf{x}$ and the typical UE, n_0 stands for the AWGN noise of variance σ^2, $s_{\mathbf{x}}$ denotes the transmitted signal, and β is the path loss intercept.

The effect of the channel is characterised by the **Saleh-Valenzuala model** [30]:

$$\mathbf{h}_{\mathbf{x}} = \sqrt{N_t} \rho_{\mathbf{x}} \mathbf{a}_t^H(\vartheta_{\mathbf{x}}), \tag{4.2}$$

where $\rho_{\mathbf{x}}$ is the complex small-scale fading gain and $\mathbf{a}_t^H(\vartheta_{\mathbf{x}})$ is the transmit array vector that can be written as:

$$\mathbf{a}_t(\theta_{\mathbf{x}}) = \frac{1}{\sqrt{N_t}} \left[1, \cdots, e^{j2\pi k \vartheta_{\mathbf{x}}}, \cdots, e^{j2\pi(N_t-1)\vartheta_{\mathbf{x}}}\right]^T, \tag{4.3}$$

where $\vartheta_{\mathbf{x}} = \frac{d}{\lambda} \cos \phi_{\mathbf{x}}$ is assumed to be uniformly distributed over $[-\frac{d}{\lambda}, \frac{d}{\lambda}]$, and in which $\phi_{\mathbf{x}}$ is the angle of departure from the BS to the served UE.

Rayleigh fading is not a valid assumption anymore due to the poor scattering environment for mm-Wave networks, as stated in [31]. In this chapter, **Nakagami-M fading** is therefore assumed for $|\rho_{\mathbf{x}}|$, as in [29].

To maximise the received power, the BS should align the beam in the direction of the UE (i.e. $\phi_{\mathbf{x}}$). The optimal beamforming vector is given by:

$$\mathbf{w}_{\mathbf{x}} = \mathbf{a}_t(\varphi_{\mathbf{x}}), \tag{4.4}$$

where $\varphi_{\mathbf{x}}$ is a variable depending on the direction of the beam. The beam is aligned if $\varphi_{\mathbf{x}} = \vartheta_{\mathbf{x}}$. The power gain corresponding to the channel effect and the beamforming is deduced from equations 4.2 and 4.4:

$$|\mathbf{h}_{\mathbf{x}} \mathbf{w}_{\mathbf{x}}|^2 = N_t |\rho_{\mathbf{x}}|^2 |\mathbf{a}_t^H(\vartheta_{\mathbf{x}}) \mathbf{a}_t(\varphi_{\mathbf{x}})|^2, \tag{4.5}$$

where $|\rho_{\mathbf{x}}|^2$ is the power gain of the small-scale fading, which in the case of Nakagami-M fading follows a gamma distribution, denoted Gamma(M, $\frac{1}{M}$).

From equation 4.3, the array gain of the transmitter located at $\mathbf{x}$ can be developed as:

$$\begin{aligned}|\mathbf{a}_t^H(\vartheta_{\mathbf{x}})\mathbf{a}_t(\varphi_{\mathbf{x}})|^2 =& \frac{1}{N_t^2}\left|\sum_{i=0}^{N_t-1}\exp\left(j2\pi i(\vartheta_{\mathbf{x}}-\varphi_{\mathbf{x}})\right)\right|^2\\ =& \frac{1}{N_t^2}\left|\frac{1-\exp\left(j2\pi N_t(\vartheta_{\mathbf{x}}-\varphi_{\mathbf{x}})\right)}{1-\exp\left(j2\pi(\vartheta_{\mathbf{x}}-\varphi_{\mathbf{x}})\right)}\right|^2\\ =& \frac{\sin^2\left[\pi N_t(\vartheta_{\mathbf{x}}-\varphi_{\mathbf{x}})\right]}{N_t^2\sin^2\left[\pi(\vartheta_{\mathbf{x}}-\varphi_{\mathbf{x}})\right]}\\ =& G_{\text{act}}(\vartheta_{\mathbf{x}}-\varphi_{\mathbf{x}}),\end{aligned} \tag{4.6}$$

where the last step calls for the definition of the **Fejér kernel** as $G_{\text{act}}(x) \triangleq \frac{\sin^2(\pi N_t x)}{N_t^2\sin^2(\pi x)}$. Although the analytical expression of the kernel is relatively simple, it does not lead to a SG analysis due to the quotient of the sine functions, which cannot be solved analytically to obtain a closed-form expression. An approximated kernel for the antenna pattern is thus used in this thesis. Two possible choices have been considered in the literature:

- **The flat-top antenna pattern:** This is the most common choice in the literature [26]. The pattern is a step function equal to 1 for $|x| \leq \frac{1}{2N_t}$, and otherwise equal to the first minor maximum gain of the actual antenna pattern. Despite being highly tractable, this simplified pattern introduces large errors in the evaluation of the coverage probability. The gap with the actual Fejér kernel is shown on Figure 4.2.
- **The cosine antenna pattern:** This pattern is defined as follows:

$$G_{\cos}(x) = \begin{cases}\cos^2\left(\frac{\pi N_t}{2}x\right) & \text{if } |x| \leq \frac{1}{N_t},\\ 0 & \text{otherwise.}\end{cases} \tag{4.7}$$

  One can observe on Figure 4.2 that this pattern provides a good approximation of the main lobe. The side lobes are however put to zero. Nevertheless, this pattern is the one used throughout this thesis because it meets the trade-off between tractability and accuracy.

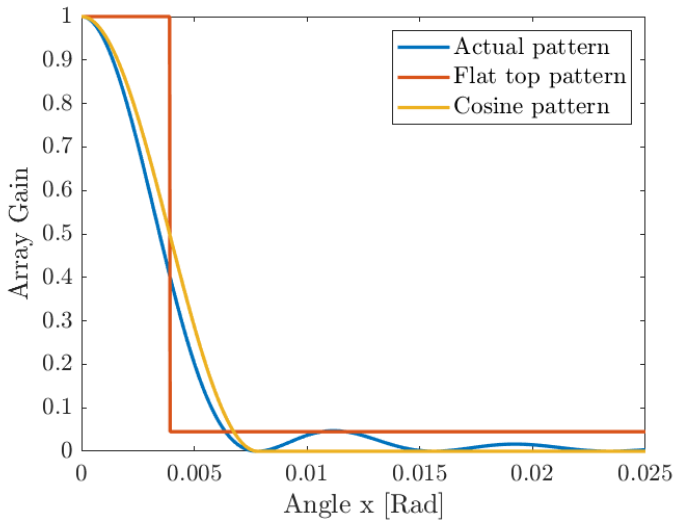

Figure 4.2: Visualisation of the antenna patterns for $N_t = 128$.

Assuming perfect alignment of the beam for the served UE at the origin, the expression of the SINR for the downlink transmission from a BS located at $\mathbf{x}$ is given by:

$$\text{SINR}(\mathbf{x}) = \frac{P_t\beta|\rho_{\mathbf{x}}|^2 r_0^{-\alpha}}{\sigma^2 + \sum_{\mathbf{y}\in\Phi(\mathbf{x})} P_t\beta g_{\mathbf{y}}\|\mathbf{y}\|^{-\alpha}} = \frac{P_t\beta|\rho_{\mathbf{x}}|^2 r_0^{-\alpha}}{\sigma^2 + \mathcal{I}}, \tag{4.8}$$

where $r_0 = \|\mathbf{x}\|$ is the distance between the typical UE and the serving BS, and $g_{\mathbf{y}} = |\rho_{\mathbf{y}}|^2 G_{\cos}(\vartheta_{\mathbf{y}} - \varphi_{\mathbf{y}})$ includes both the small-scale fading gain and the directional antenna array gain. For the array gain of the interfering BSs, $\vartheta_{\mathbf{y}}$ and $\varphi_{\mathbf{y}}$ are independent uniformly distributed random variables over $[-\frac{d}{\lambda}, \frac{d}{\lambda}]$. This statement stems from the isotropic property of the BSs locations.

The power consumption model and the sleeping strategies are the same as the one presented in section 3.1.

4.2 Analytical results

The structure of this section is similar to the corresponding one of the previous chapter. First, the useful lemmas for the derivation of the WCP metric are given. The expressions of the WCP metric for RS and SS are then presented for a general expression of the activity, before specifying it for the described distributions of UEs.

4.2.1 Important Lemmas

First, a useful lemma for the development of the coverage probability is stated. This lemma is used in the proof of Lemma 6.

Lemma 4
If $\frac{d}{\lambda} = \frac{1}{2}$, the array gain $G_{act}(\vartheta_{\mathbf{x}} - \varphi_{\mathbf{x}})$ is equal in distribution to $G_{act}(\frac{d}{\lambda}\theta_{\mathbf{x}})$, where $\theta_{\mathbf{x}}$ is a uniformly distributed random variable over $[-1, 1]$.

A second important lemma states the form of the coverage probability when Nakagami-M fading is assumed. It is used in section 4.2.4 to determine the WCP metric for the system model described in section 4.1.

Lemma 5
The coverage probability of a BS under the assumption of Nakagami-M fading is given by:

$$\mathbb{P}_{cov}(\tau) = \int_{R_{min}}^{R_{max}} \sum_{n=0}^{M-1} \frac{(-\tau M r^{\alpha})^n}{n!(P_t\beta)^n} \mathcal{L}_{N,\mathcal{I}}^{(n)}\left(\frac{\tau M r^{\alpha}}{\beta P_t}; \lambda_{\mathcal{I}}, r\right) f_R(r; \lambda_R) dr. \tag{4.9}$$

- *$\mathcal{L}_{N,\mathcal{I}}^{(n)}$ is the n^{th} derivative of the LT of the noise and interference term $\sigma^2 + \mathcal{I}$*

Note from Lemmas 1 and 5 that the effect of Rayleigh fading is equivalent to the one of Nakagami fading with parameter $M = 1$ and $R_{\max} = +\infty$.

The next lemma provides the expression of the LT of the interference term for the system model defined in section 4.1.

Lemma 6
For a Nakagami-M fading, beamforming, a minimal distance κ to the typical UE and HPPP distributed BSs of intensity $\lambda_{\mathcal{I}}$ are assumed, the LT of the interference term is given by:

$$\mathcal{L}_{\mathcal{I}}(s; \lambda_{\mathcal{I}}, \kappa) = \exp\left[-\frac{2\pi\lambda_{\mathcal{I}}}{N_t} \left\{ \kappa^2 \left[\mathcal{J}_0\left(\frac{-s\beta P_t \kappa^{-\alpha}}{M}\right) - 1 \right] - R_{max}^2 \left[\mathcal{J}_0\left(\frac{-s\beta P_t R_{max}^{-\alpha}}{M}\right) - 1 \right] \right\} \right], \tag{4.10}$$

where:

$$\mathcal{J}_k(x) \triangleq {}_3F_2\left(k+\frac{1}{2}, k-\nu, k+M; k+1, k+1-\nu; x\right). \tag{4.11}$$

${}_pF_q(a_1,...,a_p;b_1,...,b_q;z)$ *is the generalised hypergeometric function and* $\nu \triangleq \frac{2}{\alpha}$.

Given that the noise and the interference terms are independent, the following corollary can be stated:

Corollary 4
For the considered channel model, the LT of the noise and interference term $\sigma^2 + \mathcal{I}$ *is given by:*

$$\mathcal{L}_{N,\mathcal{I}}(s;\lambda_{\mathcal{I}},\kappa) = \exp\left[\eta(s;\lambda_{\mathcal{I}},r)\right], \tag{4.12}$$

where:

$$\eta(s;\lambda_{\mathcal{I}},\kappa) \triangleq -s\sigma^2 - \frac{2\pi\lambda_{\mathcal{I}}}{N_t}\left\{\kappa^2\left[\mathcal{J}_0\left(\frac{-s\beta P_t \kappa^{-\alpha}}{M}\right)-1\right] - R_{max}^2\left[\mathcal{J}_0\left(\frac{-s\beta P_t R_{max}^{-\alpha}}{M}\right)-1\right]\right\}. \tag{4.13}$$

Note that given the independence of the distribution of the BSs and of the UEs, the distribution of the distance between the typical UE and the i^{th} closest BS is the same for the two considered distribution of UEs. Consequently, the expression of f_R stated in Lemma 2 can be used to derive the coverage probability.

4.2.2 Coverage probability for a given serving BS

Before deriving the WCP metric for RS and SS, a general expression for the coverage probability is given for the system model described in section 4.1. This expression is stated in all generality, knowing that the typical UE is served by its i^{th} closest BS.

Proposition 5
In a network with Nagakami-M fading and homogeneously distributed BSs, the coverage probability, when the typical UE is served by the i^{th} *closest BS, is given by:*

$$\mathbb{P}_{cov}^{RS}(\tau|N_{ord}=i) = \int_{R_{min}}^{R_{max}} \left\|\exp\left\{\mathbf{C_M}(r)\right\}\right\|_1 f_{R_i}(r;\lambda_R)dr, \tag{4.14}$$

where:

- $\|\exp\{\cdot\}\|_1$ *is the matrix one norm of the exponential matrix.*
- $\mathbf{C_M}$ *is an* $M \times M$ *lower triangular Toeplitz matrix defined as:*

$$\mathbf{C_M}(r) = \begin{bmatrix} c_0(r) & & & & & \\ c_1(r) & c_0(r) & & & & \\ c_2(r) & c_1(r) & c_0(r) & & & \\ \vdots & \vdots & \vdots & \ddots & & \\ \vdots & \vdots & \vdots & & \ddots & \\ c_{M-1}(r) & \cdots & \cdots & c_2(r) & c_1(r) & c_0(r) \end{bmatrix}, \tag{4.15}$$

in which $c_k(r) = \frac{(-s)^k}{k!}\eta^{(k)}(s;\lambda_{\mathcal{I}},\kappa)$ *with* $s = \frac{\tau M r^\alpha}{\beta P_t}$. *The expression of the* k^{th}

derivative of $\eta(s;\lambda_{\mathcal{I}},\kappa)$ *is given by:*

$$\eta^{(k)}(s;\lambda_{\mathcal{I}},\kappa) = -\mathbb{1}_{(k\leq 1)}\sigma^2 s^{1-k} - \mathbb{1}_{(k=0)}\frac{2\pi\lambda_{\mathcal{I}}}{N_t}\left(R_{max}^2-\kappa^2\right) - \frac{4\sqrt{\pi}\lambda_{\mathcal{I}}}{k!N_t}\frac{\Gamma(M+k)}{\Gamma(M)}\frac{\Gamma(k+\frac{1}{2})}{(2-\alpha k)}\left(\frac{\beta P_t}{M}\right)^k \left[\kappa^{2-\alpha k}\mathcal{J}_k\left(\frac{-s\beta P_t\kappa^{-\alpha}}{M}\right) - R_{max}^{2-\alpha k}\mathcal{J}_k\left(\frac{-s\beta P_t R_{max}^{-\alpha}}{M}\right)\right]. \quad (4.16)$$

4.2.3 WCP metric for RS

As in section 3.2.2, the coverage probability for RS is derived from Proposition 5 by considering an independent thinning operation applied on the HPPP of BSs Φ_{B}. Proposition 6 states the expression of the metric.
As shown in Proposition 2, the WCP metric, when RS is applied, has the same expression as the coverage probability. Hence, it does not depend on the distribution of UEs considered.

Proposition 6
For the system model described in section 4.1, the WCP metric when RS is applied is given by:

$$\mathbb{P}_{\mathrm{WCP}}^{RS}(\tau) = \int_{R_{min}}^{R_{max}} \left\|\exp\left\{\mathbf{C_M}(r)\right\}\right\|_1 f_{R_1}(r;q\lambda_B)dr, \quad (4.17)$$

where the entries of the matrix $\mathbf{C_M}(r)$ *are given by:*

$$c_k(r) = -\mathbb{1}_{(k\leq 1)}(-1)^k\sigma^2\frac{\tau M r^\alpha}{\beta P_t} - \mathbb{1}_{(k=0)}\frac{2\pi q\lambda_B}{N_t}\left(R_{max}^2-r^2\right) - \frac{4(-1)^k\sqrt{\pi}q\lambda_B\tau^k}{(k!)^2N_t}\frac{\Gamma(M+k)}{\Gamma(M)}\frac{\Gamma(k+\frac{1}{2})}{(2-\alpha k)} \left[r^2\mathcal{J}_k(-\tau) - R_{max}^2\left(\frac{r}{R_{max}}\right)^{\alpha k}\mathcal{J}_k\left(-\tau\left(\frac{r}{R_{max}}\right)^\alpha\right)\right]. \quad (4.18)$$

4.2.4 WCP metric for SS

Unlike for RS, the WCP metric for SS is not equivalent to the coverage probability. Its expression is stated in Proposition 7.

Proposition 7
The WCP metric for the system model described in section 4.1, when SS is applied, is given by:

$$\mathbb{P}_{\mathrm{WCP}}^{\mathrm{SS}}(\tau) = \frac{\mathbb{E}\{as(a)\}}{\mathbb{E}\{a\}}\int_{R_{min}}^{R_{max}}\left\|\exp\left\{\mathbf{C_M}(r)\right\}\right\|_1 f_{R_1}(r;\lambda_{\mathrm{B}})dr + \frac{(\mathbb{E}\{a\}-\mathbb{E}\{as(a)\})}{\mathbb{E}\{a\}}\sum_{i=2}^{\infty}\mathbb{E}\{s\}(1-\mathbb{E}\{s\})^{i-2}\int_{R_{min}}^{R_{max}}\left\|\exp\left\{\mathbf{C_M}(r)\right\}\right\|_1 f_{R_i}(r;\lambda_{\mathrm{B}})dr, \quad (4.19)$$

where the entries of the matrix $\mathbf{C_M}(r)$ *have the following expression:*

$$c_k(r) = -\mathbb{1}_{(k\leq 1)}(-1)^k\sigma^2\frac{\tau M r^\alpha}{\beta P_t} - \mathbb{1}_{(k=0)}\frac{2\pi\mathbb{E}\{s\}\lambda_B}{N_t}\left(R_{max}^2 - r^2\right) - \frac{4(-1)^k\sqrt{\pi}\mathbb{E}\{s\}\lambda_B\tau^k}{(k!)^2 N_t}\frac{\Gamma(M+k)}{\Gamma(M)}\frac{\Gamma(k+\frac{1}{2})}{(2-\alpha k)} \left[r^2\mathcal{J}_k\left(-\tau\right) - R_{max}^2\left(\frac{r}{R_{max}}\right)^{\alpha k}\mathcal{J}_k\left(-\tau\left(\frac{r}{R_{max}}\right)^\alpha\right)\right]. \quad (4.20)$$

4.2.5 Modelling of the load

To evaluate the WCP metric for SS, the activity of each BS must be modelled. In section 3.2.3, Proposition 4 states the pmf of the activity for UEs distributed as a HPPP. This expression is still valid for the system model considered in this chapter when the UEs are distributed as a HPPP. However, if the UEs are distributed as a PCP, the pmf of the activity must be adapted. The development of this pmf can be found in [27] and is recalled here.

The pmf is computed for a typical BS, from a HPPP Φ_B of intensity λ_B, that would be located at the origin. As described in section 4.1, the UEs are distributed as a PCP $\Phi_\mathrm{U}^\mathrm{C}$.
The typical association cell $\mathcal{C}_0$ is defined as:

$$\mathcal{C}_0 = \{\mathbf{y}\in\mathbb{R}^2 : \|\mathbf{y}\| \leq \|\mathbf{y}-\mathbf{t}\|, \forall \mathbf{t}\in\Phi_\mathrm{B}\}. \quad (4.21)$$

From this definition, the load of the typical cell is given by the number of UEs within the typical association cell. This can be computed from the random counting measure of $\Phi_\mathrm{U}^\mathrm{C}$ denoted $\Psi_\mathrm{U}(\mathcal{C}_0)$. In order to derive the pmf of the load, $\Psi_\mathrm{U}(\mathcal{C}_0)$ is assumed to be equal to $\Psi_\mathrm{U}(b(\mathbf{0}, R_c))$. The typical cell of the typical BS is thus approximated as a disk of radius R_c centered at the position of the BS. This approximation is inspired by [32, Th. 4] and allows to develop Proposition 8.

Proposition 8
In a network in which the positions of the UEs are given by a PCP $\Phi_\mathrm{U}^\mathrm{C}$*, the pmf of the activity is given by:*

$$f_\mathcal{A}(n) = IDFT\left\{G_{\Phi_{u_0}}\left(e^{j2\pi n/N}\right)\right\}, \quad (4.22)$$

where:

- *IDFT is the inverse discrete Fourier transform and* N *is the number of points for which we compute the activity.*
- $G_{\Phi_{u_0}}$ *is the probability generating function of* $\Psi_\mathrm{U}(\mathcal{C}_0)$*, given by:*

$$G_{\Psi_0}(\theta) = \int_0^\infty \exp\left\{-2\pi\lambda_\mathrm{U}^p\int_0^\infty\left(1-\exp\left[-\overline{m}(1-\theta)\xi(r,w)\right]\right)w dw\right\} f_{R_c}(r)dr, \quad (4.23)$$

in which:

– $\xi(r, w)$ *is given for the two types of* PCP *by:*

$$\xi^{\mathrm{TCP}}(r, w) = 1 - \mathcal{Q}_1(w\sigma_U^{-1}, r\sigma_U^{-1}), \tag{4.24}$$

$$\xi^{\mathrm{MCP}}(r, w) = \frac{1}{r_m^2}\left([\min(r, \max(r_m - w, 0))]^2 + \frac{2}{\pi}\int_{\min(r,|r_m-w|)}^{\min(r,r_m+w)} u \arccos\left(\frac{u^2 + w^2 - r_m^2}{2uw}\right) du\right), \tag{4.25}$$

$\mathcal{Q}_1(\cdot)$ *being the Marcum Q-function.*

– $R_c \sim \text{Nakagami}\left(c, \frac{1}{\pi\lambda_B}\right)$ *so its* pdf *is given by:*

$$f_{R_c}(r) = 2\frac{(\pi\lambda_B)^c}{\Gamma(c)} c^c r^{2c-1} \exp(-\pi\lambda_B c r^2). \tag{4.26}$$

From Proposition 8, it is straightforward to compute the three expectations of the activity needed to compute the WCP metric.

4.3 Numerical Results

In this section, the validity of the analytical expressions obtained in section 4.2 is first confirmed by Monte-Carlo simulations. Then, the analytical expressions are used to determine the influence of some parameters on the EE. For each simulation, the default values from Tables 4.1, 4.2, 4.3 and 4.4 are used unless otherwise stated. The values of the network parameters are from [26], while the values of the BSs and UEs parameters are from [27]. The power consumption parameters are the same as the one considered in section 3.3. Note that for the MC simulations, the true beamforming pattern given by equation 4.6 is used.

Parameters	Values
M	3
α	2.1
$\beta[dB]$	0
q/q_{SS}	0.5
$\tau[dB]$	5
$P_t[dB]$	13
σ^2	10^{-4}
$R_{min}[m]$	1
$R_{max}[m]$	200
N_t	128
$\frac{d}{\lambda}$	0.5

Table 4.1: Network parameters

Parameters	Values
n	10000
$L[m]$	5000

Table 4.2: MC simulation parameters

Parameters	Values
$\lambda_B[m^{-2}]$	$5\ 10^{-5}$
$\lambda_U[m^{-2}]$	10^{-3}
$\lambda_p[m^{-2}]$	$5\ 10^{-5}$
$\overline{m}$	20
σ_U^2	30
$r_m[m]$	50

Table 4.3: BSs and UEs parameters

Parameters	Values
$P_0[W]$	130
$P_{sleep}[W]$	75
Δ_p	4.7

Table 4.4: Power consumption parameters

4.3.1 Validity of the expressions using MC simulations

As in section 3.3.1, the solid lines for each figure represent the results of the MC simulations while the stars represent the values obtained with the analytical expressions.

Figure 4.3 compares the analytical expression of the WCP metric, as a function of the noise variance, with the MC simulations. This comparison is performed for the three types of distribution of UEs defined in section 4.1, and for various strategies. It can be observed that the analytical curves do not fit exactly the simulated curves, but still provide a good approximation. As in the previous chapter, this can be explained by the approximation made by considering that Palm Theory applies for the distribution of the load of the BSs. This approximation is further discussed in chapter 5, where a more complex and more precise model for the activity is considered.
One can observe that the NS strategy is the best choice according to the WCP metric. When all BSs are awake, the average distance to the serving BS is smaller and therefore the received power increases. In the same time, the interference increases as well. Nevertheless, using beamforming is overall advantageous, as the advantages related to an increased received power outweighs the disadvantages related to the increased interference. Another observation is that SS outperforms RS when the proportion of BSs awake is the same. This confirms the benefit related to the use of SS, already observe in chapter 3 for another system model.

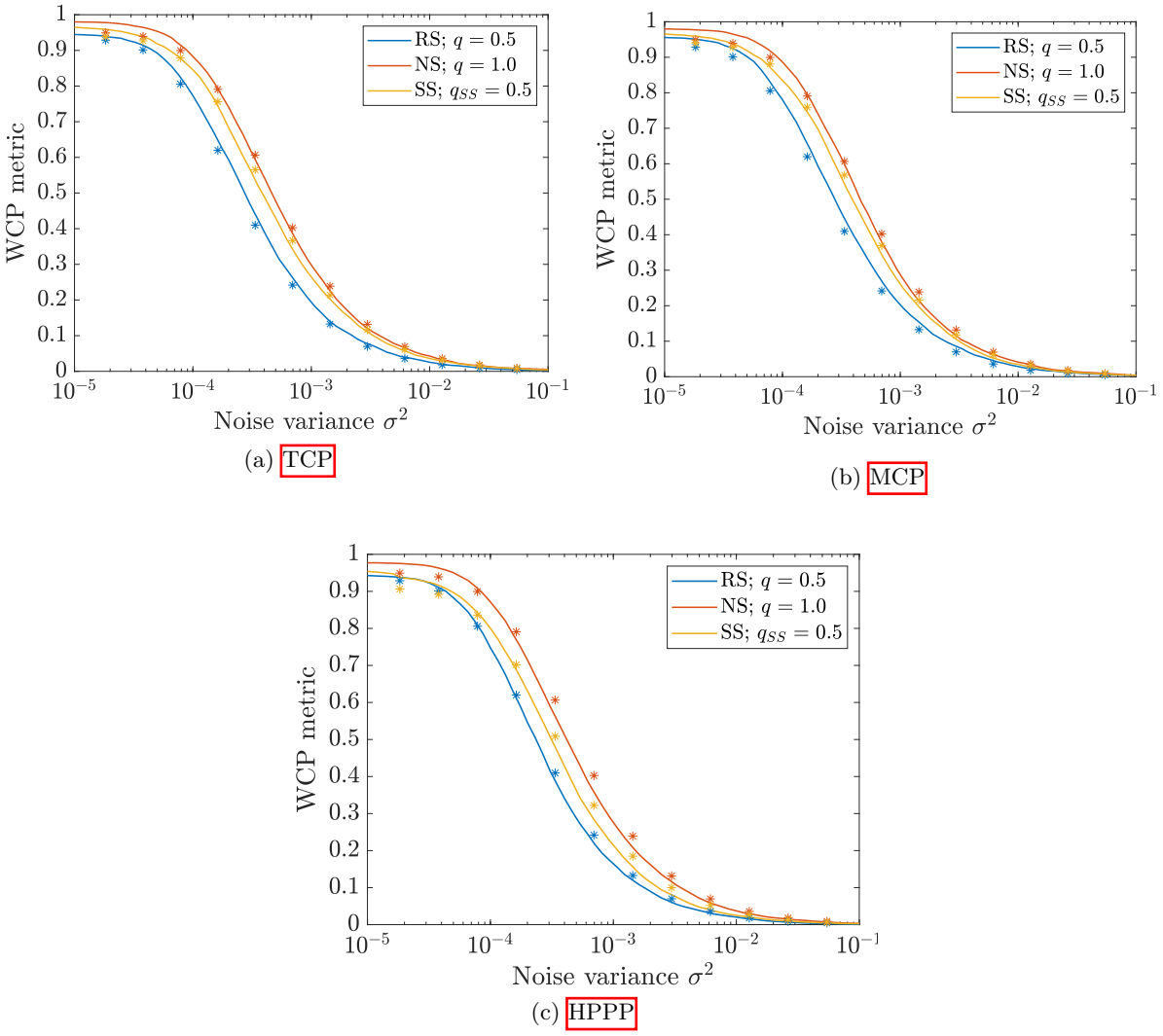

(a) TCP

(b) MCP

(c) HPPP

Figure 4.3: Comparison of analytical and numerical results for Propositions 6 and 7 for the different distribution of Φ_U.

The accuracy of the pmf of the load given in Proposition 8 is confirmed on figure 4.4. Two different densities are used for the HPPP of BSs and for the parent HPPP of the UEs. The simulation is performed for both types of PCP discussed in this thesis, namely the TCP and the MCP. The effect of the clusters can be observed by noticing, for the tested parameters, that the probability to have no UE is higher than the probability to have only one. Since the UEs form different groups in the Euclidean plane, there are some regions without any UE. This is even more significant for the MCP since no UE can be found further than a distance r_m from its cluster center.
The blue and the red curves in figure 4.4 can be compared to the curves of the same color in figure 3.3. While figure 4.4 gives the load for a PCP, figure 3.3 shows the load for a HPPP. The curves are comparable in both case since the density of BSs is the same. The density of UEs is however two times bigger for the PCP than the HPPP. Despite this higher density of UEs, having a load equal to 0 is the most likely event for the PCP while it has a probability close to zero for the HPPP. This is due to the clusters formed by the UEs for the PCP distribution.

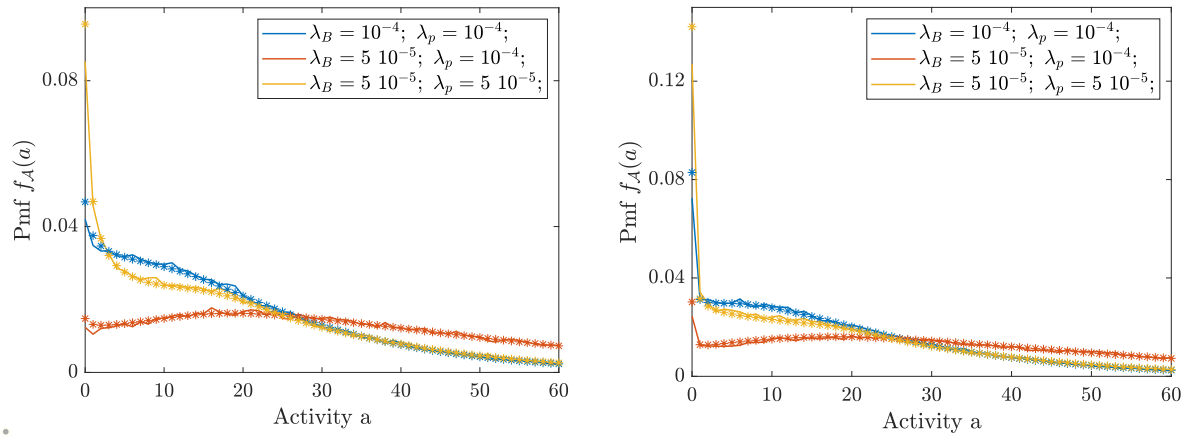

(a) TCP (b) MCP

Figure 4.4: Comparison of analytical and numerical results for the load in Propositions 8 with Φ_U distributed as a PCP.

4.3.2 SG based interpretations

In this subsection, the curves obtained from the analytical expressions are presented. Solid lines are used to represent the results instead of stars as in the previous subsection. Each analysis of parameters or strategy is performed for the three types of UEs distribution, with the same total density of UEs. This total density is computed for a PCP as $\overline{m}\lambda_p$.

Figure 4.5 illustrates the evolution of the EE with respect to the QoS threshold, for different types of strategies and sleeping probabilities. In each case, SS outperforms both RS and NS in terms of EE. However, this conclusion does not apply for the HPPP case. Indeed, for low QoS threshold (i.e. close to 1), RS provides a better EE than the corresponding SS, with the same proportion of sleeping BSs. RS provides a better global coverage over the whole network than SS for which network outage may appear in regions having a low number of UEs. For low values of the QoS threshold, the network outage are less likely for RS, that will serve each UE equally. But when the QoS increases, the network outage will also happen with RS. By awaking BSs in regions with more UEs, SS increases the EE.
One can also observe that the optimal ratio of awake BSs among the tested ones is different for the PCP and the HPPP. A smaller ratio is more efficient for the TCP because the UEs are grouped together. Therefore, awaking only the BSs that are located next to a cluster will provide a high coverage without consuming too much of power. The increase in coverage capacity, that would stem from a higher ratio of active BSs, is not sufficient to compensate the increased power consumption. For a HPPP, the optimal ratio is higher because the network outages must be avoided as much as possible. Indeed, potentially a lot of UEs can be placed in these outage region and a good global coverage is therefore necessary. For the same reasons, the maximum value for the EE is higher for the PCP than for the HPPP. The conclusion is that, for the same density of UEs and BSs, the optimal proportion of awake BSs for SS is smaller when the UEs are grouped together than when they are uniformly distributed over the network.

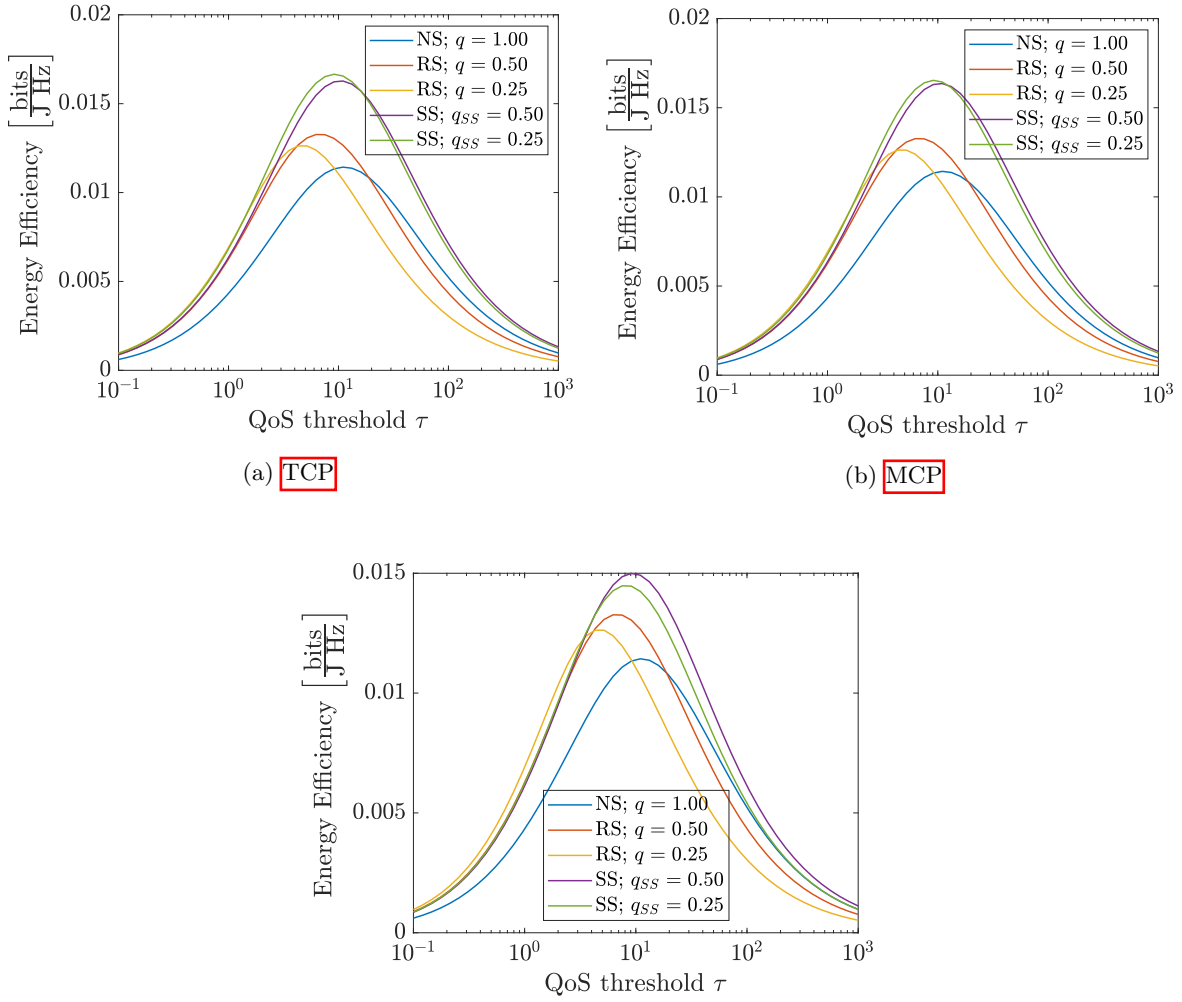

(a) TCP

(b) MCP

(c) HPPP

Figure 4.5: Energy efficiency for different sleeping strategies and level of noise as a function of the QoS threshold τ. Three different distributions of Φ_{U} are considered.

Figure 4.6 compares the evolution of the EE with respect to the noise variance, for various proportions of awake BSs in SS mode. One can observe that, among the tested q_{SS}, both the biggest and the smallest ones provide the worst EE for each level of noise. This shows that an optimal ratio exists between a situation in which all BSs are awake and another one in which almost all BSs are sleeping. In the first case, the WCP metric will be at its highest level, as shown in figure 4.3, but the corresponding power consumption is maximised. In the second one, the power consumption is minimised but still higher than zero due to the non-zero sleeping power consumption P_{sleep}. The corresponding WCP metric tends towards zero when the ratio of awake BSs tends toward zero. There is therefore an optimal ratio that can be found between the two cases.
One can also observe that when the noise variance increases, the different strategies tends to provide the same EE. Therefore, as in figure 3.6, the impact of the power consumption on the EE becomes less significant when the noise variance increases.

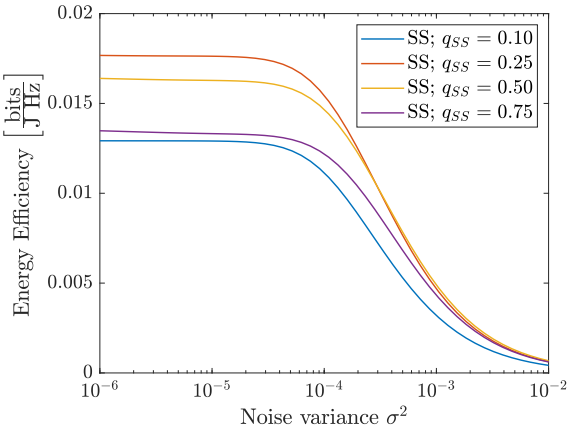

(a) TCP

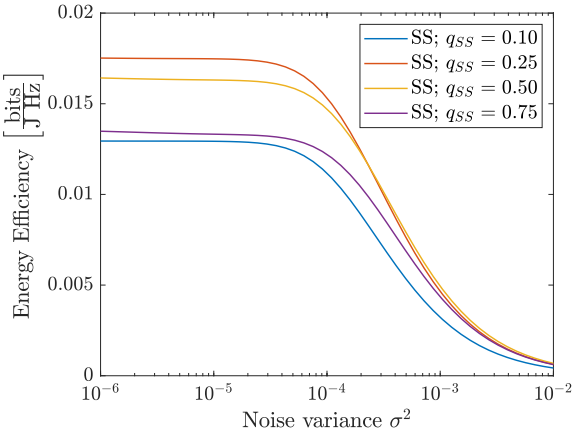

(b) MCP

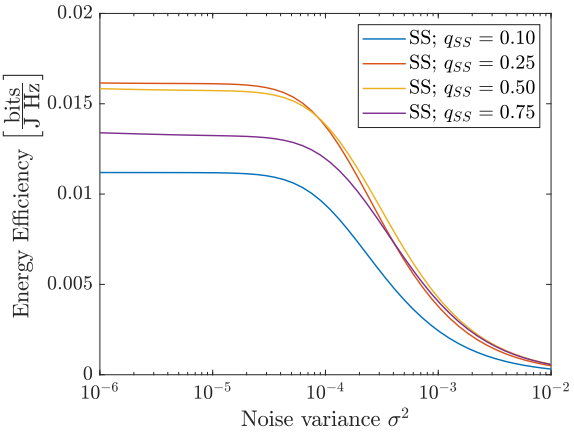

(c) HPPP

Figure 4.6: Energy efficiency for SS as a function of the noise variance with different proportion of awake BSs q_{SS}. Three different distributions of Φ_U are considered.

Figure 4.7 shows the impact of the SS threshold μ. One can observe that the power consumption decreases before the WCP metric, which results in an increased EE. When the threshold μ is high (i.e. bigger than 50), the proportion of awake BSs and the WCP both tend toward zero. The power consumption stays stable at a non zero level because of the sleeping power consumption. Therefore, similarly to what can be seen in figure 3.8, there is an optimal value of μ between the situation in which all BSs are awake and the one in which they are all sleeping.
One can observe that the optimal choice for μ is different according to the density of BSs and to the distribution of UEs. For a fixed density of UEs and BSs, the optimal μ for the HPPP is bigger than the optimal one for the PCP. With the considered parameters, the optimal choice is the same for the MCP and for the TCP. For each distribution, there is only one local maximum for the EE, which is therefore a global one too. Algorithm 1 to find the optimal μ can therefore still be used. This algorithm was described in section 3.3.2.

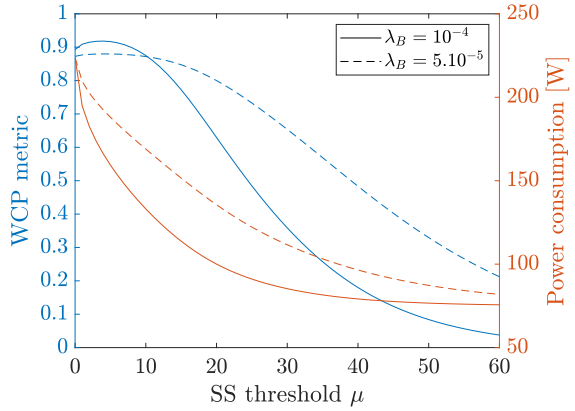

(a) TCP: WCP metric and P_{tot}

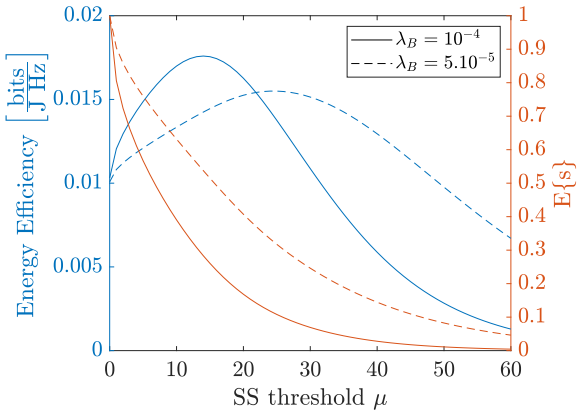

(b) TCP: EE and $\mathbb{E}\{s\}$

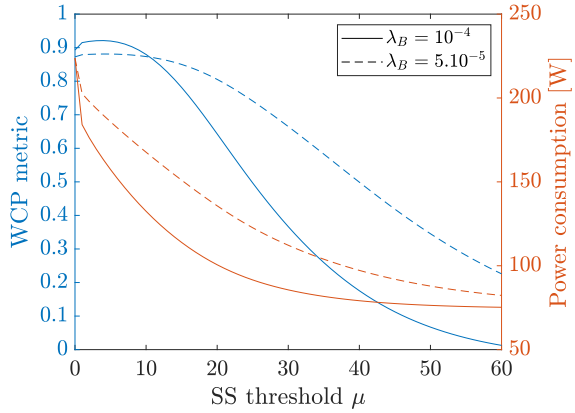

(c) MCP: WCP metric and P_{tot}

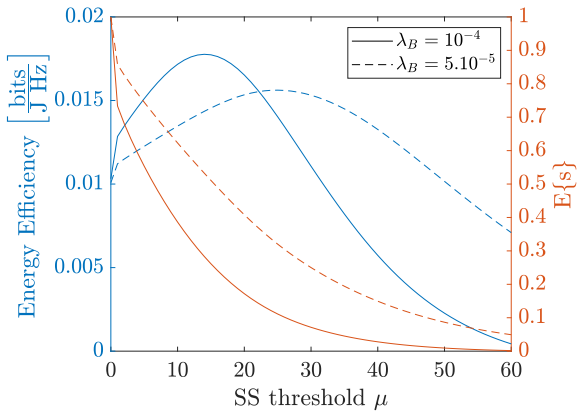

(d) MCP: EE and $\mathbb{E}\{s\}$

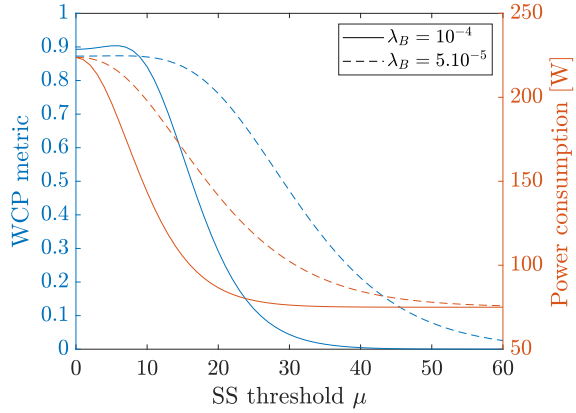

(e) HPPP: WCP metric and P_{tot}

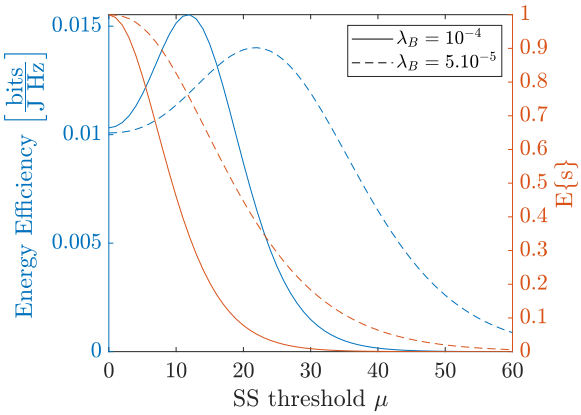

(f) HPPP: EE and $\mathbb{E}\{s\}$

Figure 4.7: Impact of μ on the WCP metric, the power consumption, the EE and the ratio of awake BSs for different density of BSs. Three different distributions of Φ_{U} are considered.

Figure 4.8 shows the optimal EE and the corresponding proportion $\mathbb{E}\{s\}$ of awake BSs for various densities of UEs and BSs. For the two types of PCP, the density of UEs is given by $\overline{m}\lambda_p$, with $\overline{m} = 20$. A first observation is that the optimal EE increases with the density of BSs, for a fixed density of UEs. At the same time, the corresponding $\mathbb{E}\{s\}$ decreases. Therefore, the coverage increases faster than the total power consumption because the awake BSs are located in regions

with a lot of UEs.
It can also be observed that, for an equivalent density of UEs, the EE is higher for the PCPs than for the HPPP. This is explained by the corresponding ratio of awake BSs that can be smaller for the PCP by awaking only the BSs next to a cluster of UEs.
Furthermore, the evolution of the EE with the density of UEs is interesting to study for a given density of BSs. In section 3.3.2, it was observe that the impact of λ_U was small as the corresponding optimal EE and $\mathbb{E}\{s\}$ stayed quite stable. For the system model described in section 4.1, the influence of the density of UEs is significant. For the two types of PCPs, the optimal EE decreases when the density of UEs increases. This can be explained by the fact that the number of cluster increases. As a consequence, it can be observed that the proportion of awake BSs must increase to serve these clusters. This results in an increased power consumption that is not counterbalanced by an increased coverage probability.

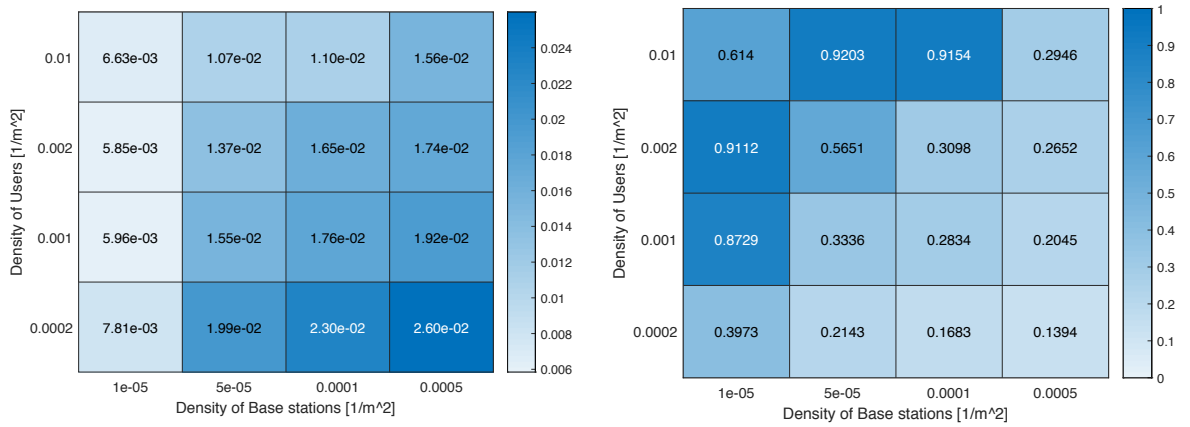

(a) TCP: EE

(b) TCP: $\mathbb{E}\{s\}$

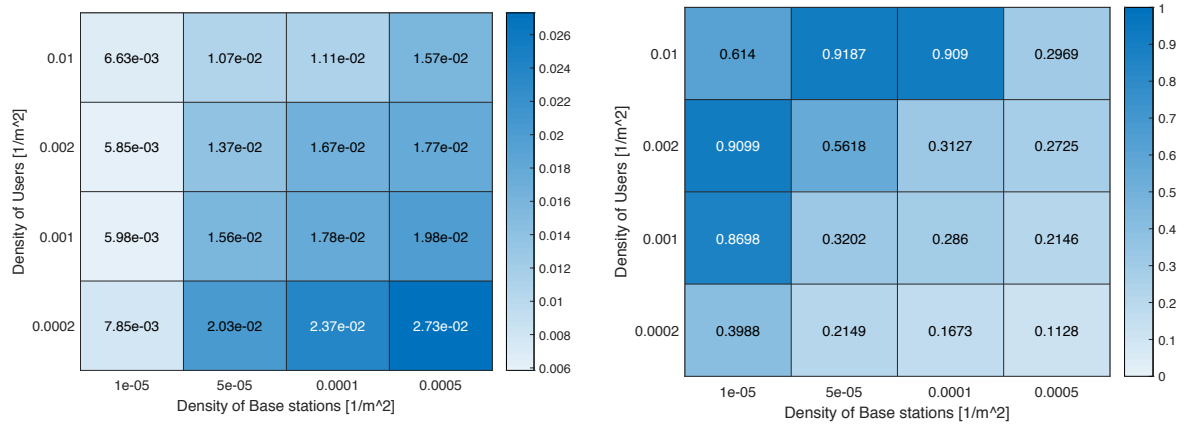

(c) MCP: EE

(d) MCP: $\mathbb{E}\{s\}$

Figure 4.8: Part 1

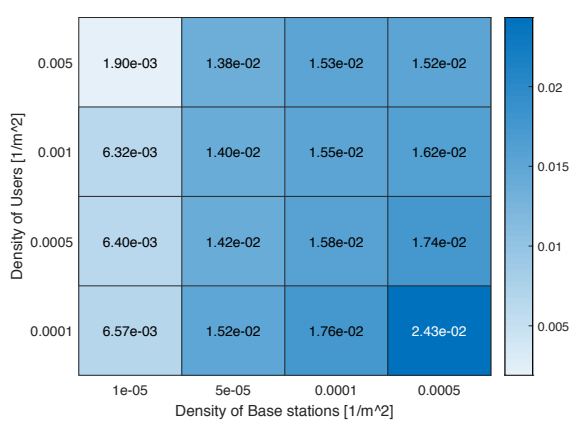

(e) HPPP: EE

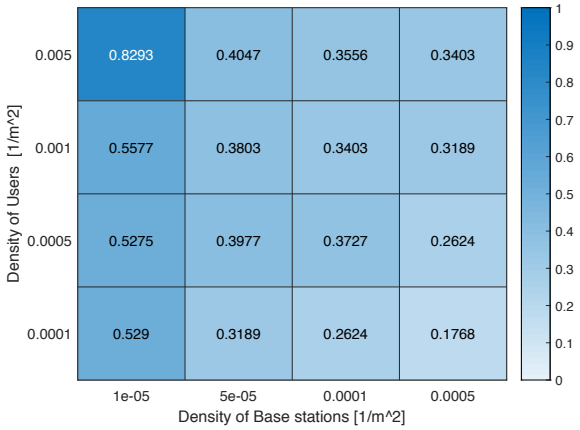

(f) HPPP: $\mathbb{E}\{s\}$

Figure 4.8: Part2: Comparison of the optimised EE for different densities of UEs and BSs. SS with the optimal μ is used in each case and three different distributions of Φ_{U} are considered. The density of UEs for the PCP is given by $\overline{m}\lambda_p$ with $\overline{m} = 20$.

Figure 4.9 depicts the evolution of the WCP metric with the LoS radius R_{max}. Comparing the three subfigures allows to conclude, as the three graphs are very similar, that the impact of the radius does not depend on the type of PP considered for the UEs distribution. Furthermore, one can observe that for small radius (i.e. up to $100[m]$ for $\sigma^2 = 10^{-3}$ and to $150[m]$ for $\sigma^2 = 10^{-4}$), the WCP increases with the radius. This is because the probability to have a serving BS increases with the radius. The smaller the radius, the higher the probability to have no serving BS for the typical UE which leads to network outage. When R_{max} is bigger than $100[m]$ for $\sigma^2 = 10^{-3}$ and than $150[m]$ for $\sigma^2 = 10^{-4}$, the probability to have a serving BS is almost equal to one. However, the number of interfering BSs within the LoS ball increases, which leads to a decreasing WCP. There is thus a trade-off between the two situations for which the WCP metric is optimal. Note however that the WCP eventually stabilises to a non-zero value when the radius tends toward infinity. Indeed, the further the interfering BSs are from the typical UE, the smaller their average contribution to the interference. Therefore, even with an infinite LoS radius, the WCP does not tend towards zero.
The impact of the Nakagami parameter M can also be observed on figure 4.9. One can see that the maximum WCP is obtained for $M = 10$ in each scenario. However, for high values of the LoS radius (i.e. bigger than $350[m]$), the best performances are obtained for lower values of M. Recall that, when M increases, the effect of the fading gain tends toward a delta which would not affect the received signal. Therefore, for $R_{max} > 300[m]$ and $M = 10$, there are more interfering BSs within the LoS ball and their signal is less impacted by the fading. This explains why $M = 10$ provides the worse performances for $R_{max} > 300[m]$.

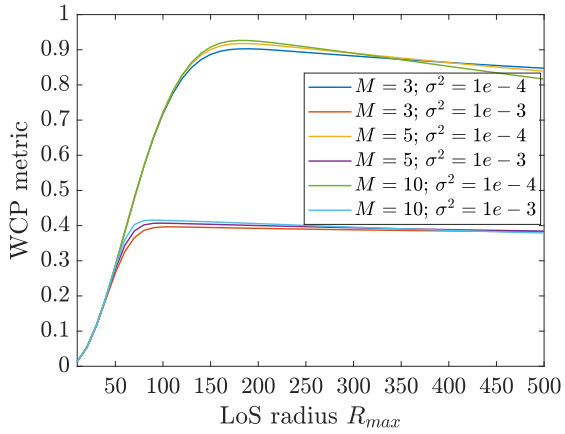

(g) TCP

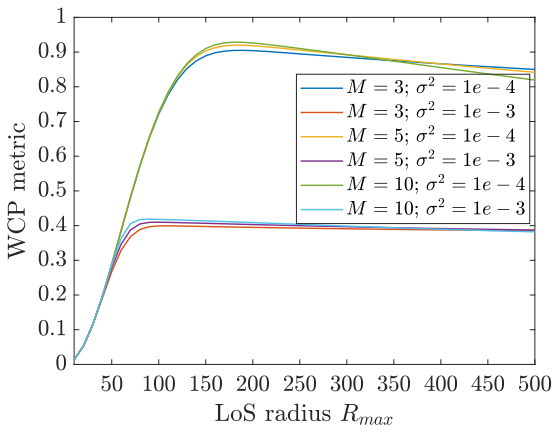

(h) MCP

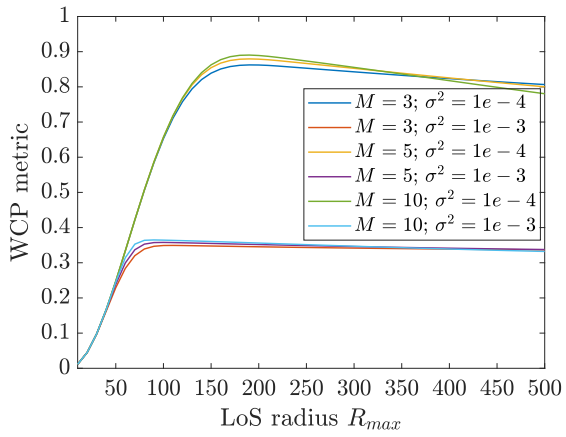

(i) HPPP

Figure 4.9: WCP metric for SS as a function of the LoS radius R_{max} for different values of noise variance σ^2 and Nakagami parameter M. Three different distributions of Φ_{U} are considered.

Figure 4.10 illustrates the impact of the number of antennas on the WCP metric. Let us recall that the number of antennas impacts the beamforming. The more antennas in the uniform linear array, the narrower the transmitted signal. A first observation is that the impact of the number of antennas on the WCP is not different according to the UEs distribution. Indeed, the shape of the graphs on the three subfigures are similar. Overall, it can be observed that the WCP increases with the number of antennas. The slope is higher for low numbers of antennas (i.e. $N_t < 20$). For such number of antennas, the beam of the interfering BSs is wider. Therefore, the probability to interfere with the signal of the serving BS is higher as well. For $N_t \geq 20$, the antennas are already very directive and the benefit from using more antennas decreases. The WCP tends towards the no-interference upper bound represented by the dashed line in each case. Indeed, when N_t tends toward infinity, the antenna pattern in equation 4.7 tends toward a Dirac delta function. Then, the probability for the typical UE to be in the direction of an interfering beam, having a sufficient power to influence the SINR, tends toward zero.

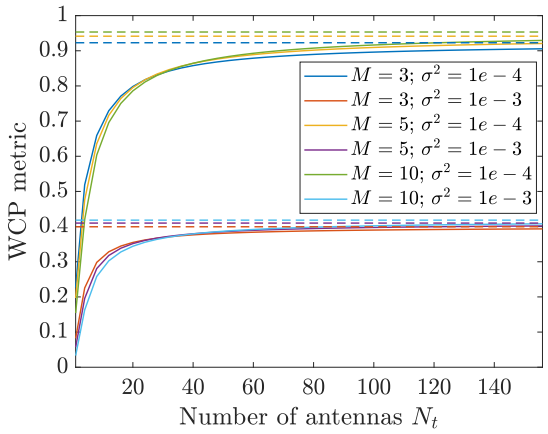

(a) TCP

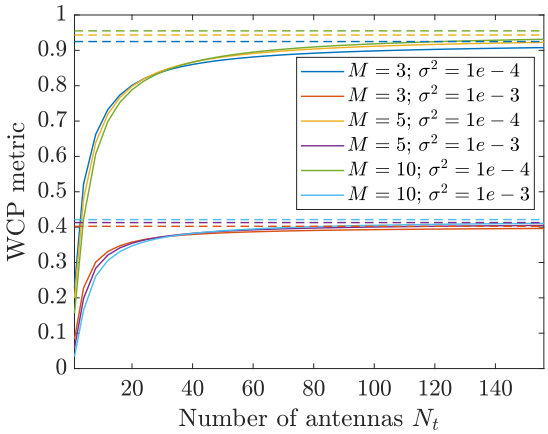

(b) MCP

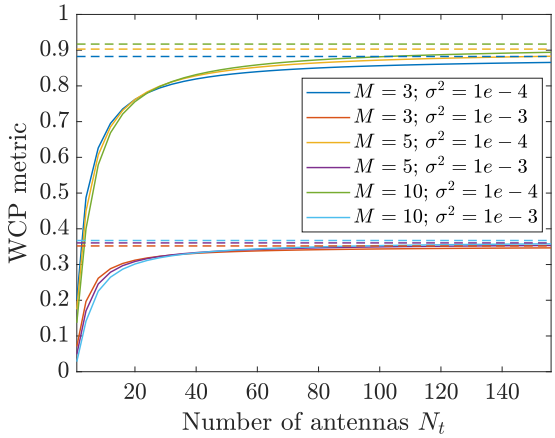

(c) HPPP

Figure 4.10: WCP metric for SS as a function of the number of antennas N_t for different values of noise variance σ^2 and Nakagami parameter M. Three different distributions of Φ_U are considered. The dashed line represents an upper bound on the WCP metric for which there is no interference.

Figure 4.11 shows the evolution of the optimal EE with respect to the transmitting power P_t. Four different numbers of transmitting antennas are compared. It can be observed that the optimal number of antennas is always the biggest one among the tested ones (i.e. $N_t = 128$). This is because the interference decreases when the beam is narrower. Note that this conclusion is only valid because the model sets a zero energetic cost for the number of antennas. One can also observe that the distribution of the UEs and the number of antennas have a small impact on the optimal choice of transmitting power $P_{t,opt}$. Indeed, all EE curves from all graphs have their maximum close to $P_t = 16[W]$. The only exception is $N_t = 1$ for which more power is needed to optimised the EE. The optimal transmitting power satisfies a trade-off between an increasing power consumption and an increasing WCP metric when P_t increases too. For $P_t < P_{t,opt}$, the received power is not sufficient compare to the noise variance in the expression of the SINR. For $P_t > P_{t,opt}$, the increase obtained regarding the WCP metric is not sufficient to balance the increased power consumption. Therefore, in both case the EE is smaller than the optimal one.

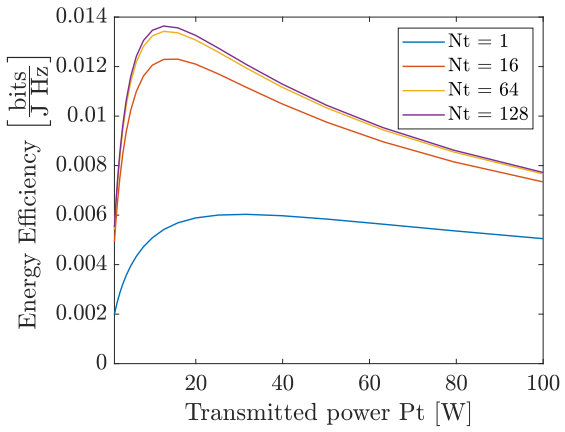

(a) TCP

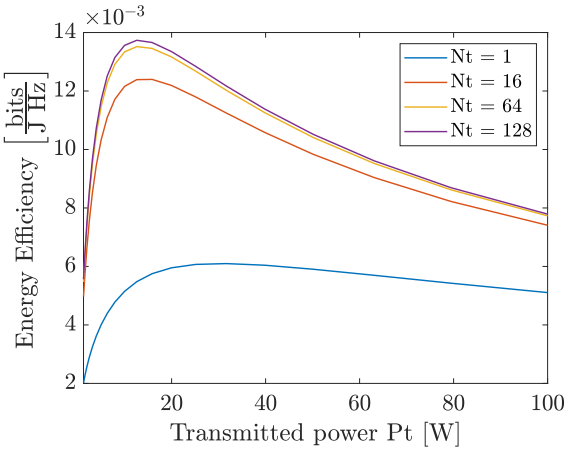

(b) MCP

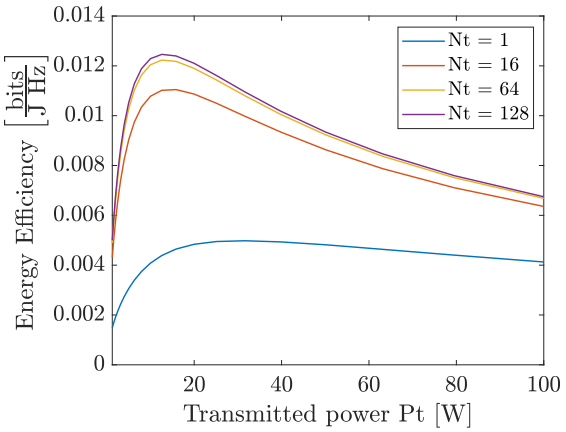

(c) HPPP

Figure 4.11: Impact of P_t on the optimal EE metric for different number of antennas N_t. Three different distributions of Φ_{U} are considered.

Chapter 5

Sleep Control Strategies in 4-Layers Inhomogeneous Millimeter Wave Networks

In this last chapter the impact of sleep control strategies on the EE is studied for a 4-layers inhomogeneous mm-Wave networks. As in the previous chapters, the system model is first described. The derived analytical expressions are then presented. Finally, MC simulations are used to confirm the accuracy of the expressions obtained before performing an analysis based on them.
The contributions of this chapter are manifold. First, the coverage analysis for K-Tier networks performed in [33] is extended to mm-Wave networks with beamforming. Furthermore, the position of the UEs are considered, in the paper, to be given by a PCP for which the cluster centers are BSs. This takes into account the current capacity-driven deployments of BSs which are placed in regions of high UEs density. This thesis extends the paper by introducing in the model sleeping mode strategies in a network with 4 different distributions of UEs and BSs described as different layers. As a consequence, the modelling of the load must be adapted. The modelling used in the previous chapters based on [24] and [27] is thus extended for this purpose. Finally, the expression of the WCP metric is adapted to define a new metric that takes into account the problem expressed in chapter 4, concerning the non-application of Palm Theory, and the multiple tiers network.

5.1 System model

In this chapter a $\hat{K}$-tier inhomogeneous network is considered. Each tier is defined according to one of the 4 following layers:

- **Layer 1: BSs without dependent UEs:** The BSs corresponding to a tier of this layer are distributed as an independent HPPP Φ_i^{BS} of density $\lambda_i^{\text{BS}} > 0$, with a transmit power $P_i > 0$ and a number of transmitting antennas $N_{t,i}$.
- **Layer 2: BSs with dependent UEs:** The BSs corresponding to a tier of this layer are distributed as an independent HPPP Φ_i^{BS} of density $\lambda_i^{\text{BS}} > 0$, with a transmit power $P_i > 0$ and a number of transmitting antennas $N_{t,i}$. UEs are also considered in this layer. They are distributed as a PCP Φ_i^{UE} having Φ_i^{BS} as a parent PP. The BSs form thus the cluster centers of the PCP of UEs. If the cluster is a TCP, the corresponding variance is denoted σ_i^2. If the cluster is a MCP, the corresponding radius is denoted $r_{m,i}$.
- **Layer 3: PCP of UEs:** This layer introduces independent PCPs Φ_i^{UE} of UEs. There is thus no BSs as cluster centers. The parent HPPP has a constant intensity λ_i^p. If the

cluster is a TCP, the corresponding variance is denoted σ_i^2. If the cluster is a MCP, the corresponding radius is denoted $r_{m,i}$.

- **Layer 4: HPPP of UEs:** For a tier of this layer, the UEs are distributed as an independent HPPP Φ_i^{UE} of density $\lambda_i^{\mathrm{UE}} > 0$.

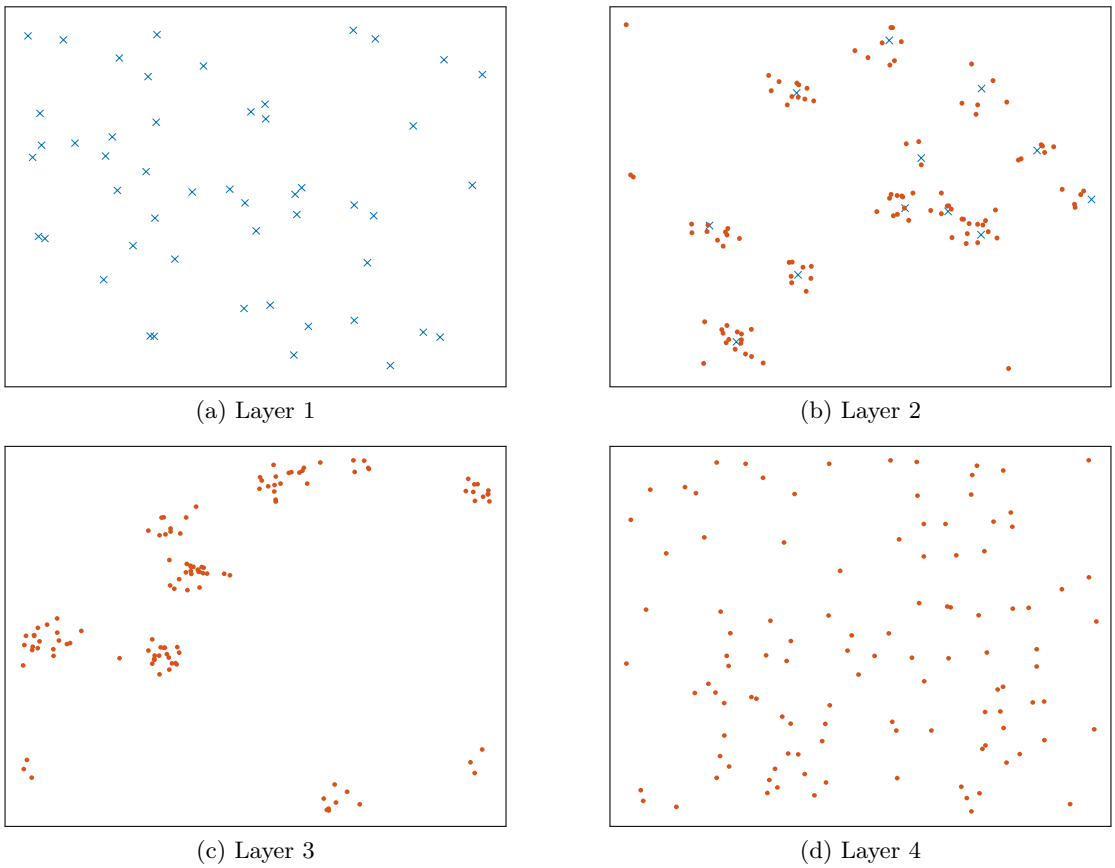

(a) Layer 1 (b) Layer 2

(c) Layer 3 (d) Layer 4

Figure 5.1: Visualisation of a realisation of the 4 types of layers. TCPs are used for the different PCPs. The crosses represent the locations of BSs while the dots represent the locations of the UEs.

The tiers of BSs are thus distributed according to one of the two first layers while the tiers of UEs are distributed according to one of the three last layers. Notice that there is no restriction on the number of tiers that are described according to each of the layers.

The association scheme is based on the average received signal at the UE side. It is not location based as in previous chapters because the power transmitted by two BSs of different tiers can be different. The average power received by a UE at the origin from a BS at $\mathbf{x} \in \Phi_j^{\mathrm{BS}}$ is given by $P_j \|\mathbf{x}\|^{-\alpha}$. The typical UE is thus connected to the closest awake BS in terms of power weighted distance which is defined as $\|\mathbf{x}\| P_j^{-\frac{1}{\alpha}}$.

Among the $\hat{K}$-tiers of BSs and UEs, only K of them are from one of the 2 first layers. For notation convenience, they are denoted by the first K indexes such that the set of indexes of these K tiers is defined as $\mathcal{K} = \{1, 2, \ldots, K\}$. $\hat{I}_k$ is defined as the set of indexes of all the BSs from a tier k.

For the channel model, there is no change with the one described in chapter 4. The channel gain is Nakagami distributed with parameter M and beamforming is considered with the

cosine pattern. The LoS model is applied with maximum radius $R_{\max}$ and the exclusion zone of radius $R_{\min}$ is considered around each BS to avoid problems with the path loss model.

With regard to the sleeping strategies, only SS is considered in this chapter as its advantages over RS have been demonstrated in previous chapters. An activation function $s_k(\cdot)$ is defined for each tier $k \in \mathcal{K}$ with a threshold μ_k. The BS serving the typical UE could be any BS from any tier as all BSs are in open access. The activity is defined as the load of the cell of each BS. The sleeping probability for each BS is thus $\mathbb{E}\{s_k\}$.

The coverage analysis is performed for a typical UE from one of the tiers of UEs. The analysis is thus performed for the three types of layers of UEs. In the case of a typical UE from layer 2, there is a BS at the center of the representative cluster. This BS is located at position $\mathbf{y} \in \Phi_i^{\text{BS}}$. Using Slivnyak's Theorem, the thinned process $\Phi_i^{\text{BS}} \setminus \{\mathbf{y}\}$ has the same distribution as Φ_i^{BS}. For notation convenience, another tier Φ_0^{BS}, which consist only of a single point $\mathbf{y}$, is defined. The tier referred to by index i will thus be the thinned one. The new set of indexes is defined as $\mathcal{K}_0 = \{0\} \bigcup \mathcal{K} = \{0, 1, 2, \ldots, K\}$. Note that the parameters of the 0^{th} tier are derived from the i^{th} one such that $\sigma_0^2 = \sigma_i^2$, $r_{m,0} = r_{m,i}$, $P_0 = P_i$ and $N_{t,0} = N_{t,i}$.

5.2 Analytical results

In this section a new metric adapted from the WCP one is defined and described. The expressions of each term of this metric are then successively derived. The modelling of the load is also adapted to the new system model.

5.2.1 Averaged *K*-tiers weighted coverage probability

Let us first recall the expression of the WCP metric in the specific case of a discrete random variable $\mathcal{A}$ describing the load of the cell of the typical UE:

$$\mathbb{P}_{\text{WCP}}(\tau) = \frac{1}{\mathbb{E}\{a\}} \sum_{a=0}^{\infty} a \mathbb{P}_{cov}(\tau|a) f_{\mathcal{A}}(a). \tag{5.1}$$

One can directly observe that this metric must be adapted for a multi-tier system model as the one described in section 5.1. Indeed, in a single-tier network the activity considered is simply the activity of the closest BS. This is true no matter what sleeping mode is chosen for the BSs. In a multi-tier network however, the closest BS could be from any tier and this must be taken into account in the metric. Furthermore, it was observed in the two previous chapters that Palm theory cannot be applied to characterise the pmf of the load of the closest BS to the typical UE, directly from the load of a typical BS. Section 5.2.7 deals with the adaptations to be made and the impact of the distance between the typical UE and the first BS on the latter's load. By taking these new aspects into account, a new metric called the ***averaged K-tiers weighted coverage probability*** (AKWCP) is defined in Definition 2. In this chapter, the EE is computed from this metric instead of the WCP.

Definition 2 (AKWCP metric)
The averaged K-tiers weighted coverage probability metric is defined as:

$$\mathbb{P}_{\text{AKWCP}} = \sum_{k=0}^{K} \int_{R_{min}}^{R_{max}} \mathbb{P}(k^* = k | r_{k,1}) f_{R_{k,1}}(r_{k,1}|R_{min}) \frac{1}{\mathbb{E}\{a_{k,1}\}} \cdot \Big[\mathbb{E}\{a_{k,1} s_k(a_{k,1})\} \mathbb{P}_{suc}(\tau, r_{k,1} | k^* = k; s_k(a_{k,1}) = 1) + (\mathbb{E}\{a_{k,1}\} - \mathbb{E}\{a_{k,1} s_k(a_{k,1})\}) \mathbb{P}_{cov}(\tau | r_{k,1}; k^* = k; s_k(a_{k,1}) = 0) \Big] dr_{k,1}, \quad (5.2)$$

where:

- *$R_{k,i}$ is the distance between the i^{th} nearest BS of tier k and the typical UE.*
- *$a_{k,i}$ is the activity of the i^{th} nearest BS of tier k.*

The different terms of the AKWCP metric are described successively. First, a sum is performed over each tier of BSs. The purpose of this sum is to distribute the events in which the closest BS to the typical UE belongs to tier k. An integral is then evaluated over the distance to this nearest BS, for which the pdf is given by the term $f_{R_{k,1}}(r_{k,1}|R_{min})$. The term $\mathbb{P}(k^* = k|r_{k^*,1})$ is the probability that the closest BS is from tier k knowing the distance to this closest BS. k^* is the index denoting the tier of this closest BS. The quotient of $\mathbb{E}\{a_{k,1}\}$ could already be found in the WCP metric. It appears because of the weighting of the probability of success by the activity of the cell. Then, between the brackets, two cases are distinguished. The first one is the weighted probability of success knowing that the closest BS is awake. It is a success probability and not a coverage one because there is already an integral performed on the distance to the serving BS. The second term is the weighted coverage probability knowing that the closest BS

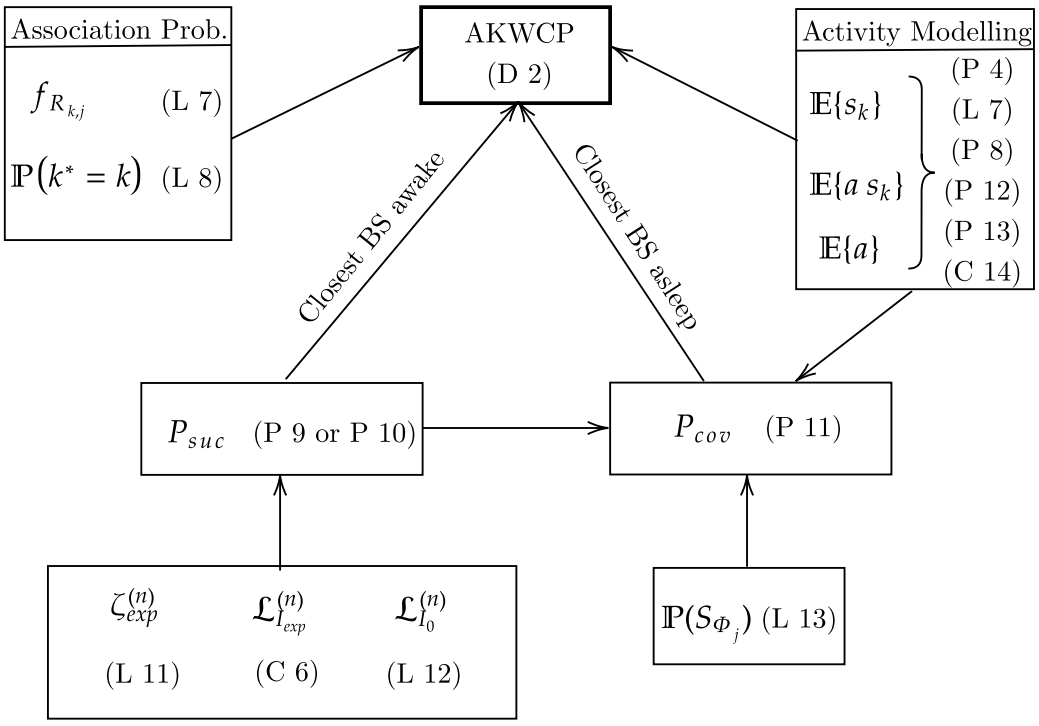

Figure 5.2: Summary of the different quantities to evaluate in order to obtain the expression of the AKWCP metric. The acronyms D, L, P and C stands respectively for Definition, Lemma, Proposition and Corollary.

is sleeping. The tier to which this BS belongs and the distance to this BS are both known when this probability is evaluated.

Figure 5.2 summarises all the terms that have to be evaluated in order to obtained the AKWCP metric. The lemmas, propositions or corollaries corresponding to each term are stated in the next subsections.

5.2.2 Distribution of the distance and association probability

The first term to develop is the distribution of the distance to the typical UE of the i^{th} closest BS tier j. The expression of the corresponding pdfs and ccdfs are stated in Lemma 7.

Lemma 7
The pdf and the ccdf of the distance between the typical UE and the i^{th} closest BS from tier j, given an excluding radius κ, are expressed as:

For $j \in \mathcal{K}$:

$$\underline{pdf:}\quad f_{R_{j,i}}(r_{j,i}|\kappa) = \frac{2(\lambda_j^{BS}\pi)^i}{(i-1)!} r_{j,i}(r_{j,i}^2-\kappa^2)^{i-1}\exp(-\lambda_j^{BS}\pi(r_{j,i}^2-\kappa^2)), \quad r_{j,i}\geq\kappa. \tag{5.3}$$

$$\underline{ccdf:}\ \overline{F}_{R_{j,i}}(r_{j,i}|\kappa) = \sum_{n=0}^{i-1}\frac{(\lambda_j^{BS}\pi)^n}{n!}(r_{j,i}^2-\kappa^2)^n\exp(-\lambda_j^{BS}\pi(r_{j,i}^2-\kappa^2)), \quad r_{j,i}\geq\kappa. \tag{5.4}$$

For $j=0$ and typical UE from a TCP:

$$\underline{pdf:}\quad f_{R_{0,1}}(r_{0,1}|\kappa) = \frac{r_{0,1}}{\sigma_0^2}\exp\left(-\frac{(r_{0,1}^2-\kappa^2)}{2\sigma_0^2}\right), \quad r_{0,1}\geq\kappa. \tag{5.5}$$

$$\underline{ccdf:}\ \overline{F}_{R_{0,1}}(r_{0,1}|\kappa) = \exp\left(-\frac{(r_{0,1}^2-\kappa^2)}{2\sigma_0^2}\right), \quad r_{0,1}\geq\kappa. \tag{5.6}$$

For $j=0$ and typical UE from a MCP:

$$\underline{pdf:}\quad f_{R_{0,1}}(r_{0,1}|\kappa) = \frac{2r_{0,1}}{r_{m,0}^2-\kappa^2}, \quad \kappa\leq r_{0,1}\leq r_{m,0}. \tag{5.7}$$

$$\underline{ccdf:}\ \overline{F}_{R_{0,1}}(r_{0,1}|\kappa) = \frac{r_{m,0}^2-r_{0,1}^2}{r_{m,0}^2-\kappa^2}, \quad \kappa\leq r_{0,1}\leq r_{m,0}. \tag{5.8}$$

Now that the pdf and the ccdf are defined, the expression of the term $\mathbb{P}(k^*=k|r_{k,1})$ is given in Lemma 8.

Lemma 8
For the system model described in section 5.1, the probability that the closest BS is from tier k, knowing the distance to the closest BS of this tier, is given by:

$$\mathbb{P}(k^*=k|r_{k,1}) = \prod_{j\in\mathcal{K}_1\setminus\{k\}}\overline{F}_{R_{j,i}}(\overline{P}_{k,j}r_{k,1}|R_{min}), \tag{5.9}$$

where $\overline{P}_{kj} = \left(\frac{P_j}{P_k}\right)^{1/\alpha}$.

5.2.3 Characterisation of the interference

The next step in the development of the AKWCP metric is the characterisation of the interference, in order to derive the probability of success when the typical UE is served by the i^{th} BS from tier j. The location of the serving BS is denoted $\mathbf{x}_{j,i}$. Since the typical UE is connected to the closest BS in terms of power weighted distance, there exists no active BS from tier k, $\forall k \in \mathcal{K}_0$, within a disc of radius $\kappa_{jk} = \overline{P}_{jk}\|\mathbf{x}_{j,i}\|$ centered at the typical UE location. This disc is denoted $b(\mathbf{0}, \kappa_{j,k})$. The interference from the k^{th} tier is thus defined as:

$$\mathcal{I}_{(j,i;k)}(\|\mathbf{x}_{j,i}\|) = \sum_{\mathbf{y}_k \in \tilde{\Phi}_k^{\mathrm{BS}} \setminus b(\mathbf{0},\kappa_{jk})} P_k \beta g_k \|\mathbf{y}_k\|^{-\alpha}, \tag{5.10}$$

where $\tilde{\Phi}_k^{\mathrm{BS}}$ is the PPP of tier k obtained after independent thinning with probability $\mathbb{E}\{s_k\}$. The total interference is obtained by summing the contribution of each tier to obtain:

$$\mathcal{I}^{tot}_{(j,i)}(\|\mathbf{x}_{j,i}\|) = \sum_{k=0}^{K} \mathcal{I}_{(j,i;k)}(\|\mathbf{x}_{j,i}\|). \tag{5.11}$$

From this expression, the SINR at the typical UE, when it is served by the BS located at $\mathbf{x}_{j,i}$, can be written as:

$$\mathrm{SINR}(\mathbf{x}_{j,i}) = \frac{P_j \beta |\rho|^2 \|\mathbf{x}_{j,i}\|^{-\alpha}}{\sigma^2 + \mathcal{I}^{tot}_{(j,i)}(\|\mathbf{x}_{j,i}\|)}. \tag{5.12}$$

At this point, a first observation is that expression 5.12 does not depend on the index of the serving BS. Indeed, only the corresponding tier and the distance to the BS have an impact. Therefore, a per-tier success probability can be derived and the interference term can be denoted $\mathcal{I}^{tot}_j$.

The probability of success when the typical UE is served by a BS of tier j located at $\mathbf{x}_j$ is given by:

$$\mathbb{P}_{suc}(\tau, \mathbf{x}_j) = \sum_{n=0}^{M-1} \frac{(-\tau M r_j^{\alpha})^n}{n!(P_j\beta)^n} \mathcal{L}^{(n)}_{N,\mathcal{I}^{tot}_j}\left(\frac{\tau M r_j^{\alpha}}{\beta P_j}; r_j\right). \tag{5.13}$$

This expression is obtained from the general expression of the coverage probability given in Lemma 5 and by defining $r_j = \|\mathbf{x}_j\|$. To further develop the success probability, the LT transform of the noise and interference term is given in Corollary 5, while Lemma 10 states the LT transform of the interference term alone. To proof Lemma 10, the expression for the LT of the coefficient g is required. Therefore, Lemma 9 first states this transform.

Lemma 9
The LT transform of the term g, including both the small scale fading gain and the directional antenna array gain, is given for $s \in \mathbb{R}$ by:

$$\mathcal{L}_g(s) = 1 - \frac{2}{N_t} + \int_0^{2/N_t} \left(1 + \frac{s\cos^2(\frac{\pi N_t}{4}\theta)}{M}\right)^{-M} d\theta. \tag{5.14}$$

Lemma 10
The LT transform of the interference term, when the serving BS is from tier j located at a distance r_j of the typical UE, is given by:

$$\mathcal{L}_{\mathcal{I}^{tot}_j}(s) = \prod_{k=0}^{K} \mathcal{L}_{\mathcal{I}_k}(s) \tag{5.15}$$

$$= \mathcal{L}_{\mathcal{I}_0}(s) \prod_{k=1}^{K} \mathcal{L}_{\mathcal{I}_k}(s), \tag{5.16}$$

where $\mathcal{L}_{\mathcal{I}_k}(s)$ is the LT of the interference from the k^{th} tier.

The LT transform of the interference from the k^{th} tier for $k \in \mathcal{K}$ is given by:

$$\mathcal{L}_{\mathcal{I}_k}(s) = \exp\left[-\zeta_k(s)\right], \tag{5.17}$$

where:

$$\zeta_k(s) = \frac{2\pi\mathbb{E}\{s_k\}\lambda_k^{BS}}{N_{t,k}}\left\{\kappa^2\left[\mathcal{J}_0\left(\frac{-s\beta P_k\kappa_{jk}^{-\alpha}}{M}\right)-1\right] - R_{max}^2\left[\mathcal{J}_0\left(\frac{-s\beta P_k R_{max}^{-\alpha}}{M}\right)-1\right]\right\}. \tag{5.18}$$

For the interference from tier $k=0$, different case have to be taken into account:

- *If the typical UE is not from a tier of layer 2 then $\mathcal{L}_{\mathcal{I}_0}(s)=1$.*
- *If $j=0$, then $\mathcal{L}_{\mathcal{I}_0}(s)=1$.*
- *If $j\neq 0$, then*

$$\mathcal{L}_{\mathcal{I}_0}(s) = (1-\mathbb{E}\{s_0\}) + \mathbb{E}\{s_0\}\left(1-\frac{2}{N_{t,k}}\right)\left(1-\overline{F}_{R_{0,1}}(R_{max}|\kappa_{j0})\right) + \mathbb{E}\{s_0\}\int_{\kappa_{j0}}^{R_{max}}\int_0^{2/N_{t,0}}\left(1+\frac{sP_0\beta r_{0,1}^{-\alpha}\cos^2(\frac{\pi N_{t,0}}{4}\theta)}{M}\right)^{-M} f_{R_{0,1}}(r_{0,1}|\kappa_{j0})\, d\theta\, dr_{0,1}. \tag{5.19}$$

Corollary 5
The LT of the noise and interference term $\sigma^2+\mathcal{I}_j^{tot}$ is given by:

$$\begin{aligned}\mathcal{L}_{N,\mathcal{I}_j^{tot}}(s;r_j) &= \exp\left(-s\sigma^2\right)\mathcal{L}_{\mathcal{I}_j^{tot}}(s)\\ &= \mathcal{L}_{\mathcal{I}_0}(s)\exp\left(\zeta_{exp}(s)\right)\\ &= \mathcal{L}_{\mathcal{I}_0}(s)\mathcal{L}_{\mathcal{I}_{exp}}(s)\end{aligned} \tag{5.20}$$

where:

$$\zeta_{exp}(s) = -s\sigma^2 - \sum_{k=1}^{K}\zeta_k(s). \tag{5.21}$$

A first observation from Corollary 5 and Lemma 10 is that, when the typical UE is not from layer 2, the LT transform of the noise and interference term is not an exponential. Therefore, the success probability cannot be computed with an exponential matrix, as it was done in chapter 4.

The next step in the development of the success probability, is to compute the successive derivatives of the $\zeta_{exp}(s)$ and $\mathcal{L}_{\mathcal{I}_0}(s)$. This is done respectively in Lemmas 11 and 12, while Corollary 6 states the derivatives of $\mathcal{L}_{\mathcal{I}_{exp}}$.

Lemma 11
The l^{th} derivative of the exponent term ζ_{exp} in the LT of the noise and interference

term is given by:

$$\zeta_{exp}^{(l)}(s) = -\mathbb{1}_{(l\leq 1)}\sigma^2 s^{1-l} - \sum_{k=1}^{K} \zeta_k^{(l)}(s), \tag{5.22}$$

where:

$$\zeta_k^{(l)}(s) = \mathbb{1}_{(l=0)} \frac{2\pi\mathbb{E}\{s_k\}\lambda_k^{BS}}{N_{t,k}} \left(R_{max}^2 - \kappa_{jk}^2\right) + \frac{4\sqrt{\pi}\mathbb{E}\{s_k\}\lambda_k^{BS}}{l! N_{t,k}} \frac{\Gamma(M+l)}{\Gamma(M)} \frac{\Gamma(l+\frac{1}{2})}{(2-\alpha l)} \left(\frac{\beta P_k}{M}\right)^l \left[\kappa_{jk}^{2-\alpha l} \mathcal{J}_l\left(\frac{-s\beta P_k \kappa_{jk}^{-\alpha}}{M}\right) - R_{max}^{2-\alpha l} \mathcal{J}_l\left(\frac{-s\beta P_k R_{max}^{-\alpha}}{M}\right)\right]. \tag{5.23}$$

Corollary 6
The l^{th} derivative of $\mathcal{L}_{\mathcal{I}_{exp}}$ can be computed by recursion from:

$$\mathcal{L}_{exp}^{(l)}(s) = \sum_{n=0}^{l-1} \binom{l-1}{n} \zeta_{exp}^{l-n}(s) \mathcal{L}_{exp}^{i}(s), \quad \text{for } l \geq 1, \tag{5.24}$$

knowing that $\mathcal{L}_{\mathcal{I}_{exp}}^{(0)}(s) = \exp(\zeta_{exp}(s))$.

Lemma 12
The l^{th} derivative of the LT transform of the interference from tier 0 can have two different forms:

- *If the typical UE is not from a tier of layer 2 or if $j = 0$ then*

$$\mathcal{L}_{\mathcal{I}_0}^{(l)}(s) = \begin{cases} 1 & \text{if } l = 0, \\ 0 & \text{otherwise.} \end{cases} \tag{5.25}$$

- *If $j \neq 0$, then*

$$\mathcal{L}_{\mathcal{I}_0}^{(l)}(s) = \int_{\kappa_{j,0}}^{R_{max}} \int_0^{2/N_{t,0}} \mathbb{E}\{s_0\} \left(1 + \frac{sP_0\beta r_{0,1}\cos^2\left(\frac{\pi N_{t,0}}{4}\theta\right)}{M}\right)^{-(M+l)} \left(\frac{-P_0\beta}{M}\right)^l (M)_l \cos^{2l}\left(\frac{\pi N_{t,0}}{4}\theta\right) r_{0,1}^{-l\alpha} f_{R_{0,1}}(r_{0,1}|\kappa_{j,0}) d\theta dr_{0,1} + \mathbb{1}_{(l=0)}(1 - \mathbb{E}\{s_0\}) + \mathbb{1}_{(l=0)}\mathbb{E}\{s_0\}\left(1 - \frac{2}{N_{t,0}}\right)\left(1 - \overline{F}_{R_{0,1}}(R_{max}|\kappa_{j,0})\right). \tag{5.26}$$

5.2.4 Success probability

Using the lemmas from previous subsection, the probability of success stated in equation 5.13 can be developed. The expression when the typical UE is not from a tier of layer 2 is stated in Proposition 9. For a typical UE from a tier of layer 2, if $j = 0$, then the same proposition gives the correct expression, while Proposition 10 states the probability for $j \neq 0$.

Proposition 9
The success probability when the typical UE is served by a BS of tier j located at $\mathbf{x}_j$, for the cases where the typical UE is not from a tier of layer 2 or when the typical UE

is from a tier of layer 2 but $j = 0$, is given by:

$$\mathbb{P}_{suc}(\tau, \mathbf{x}_j) = \left\| \exp\left\{ \mathbf{C}_{\mathbf{M}}(r_j) \right\} \right\|_1, \tag{5.27}$$

where $r_j = \|\mathbf{x}_j\|$ and the entries of the matrix $\mathbf{C}_{\mathbf{M}}(r_j)$ are given by:

$$\begin{aligned} c_l(r) = &-\mathbb{1}_{(l\leq 1)}(-1)^l \sigma^2 \frac{\tau M r_j^\alpha}{\beta P_j} - \sum_{k=1}^{K} \mathbb{1}_{(l=0)} \frac{2\pi \mathbb{E}\{s_k\} \lambda_k^{BS}}{N_{t,k}} \left(R_{max}^2 - \kappa_{jk}^2 \right) \\ &- \sum_{k=1}^{K} \frac{4(-1)^l \sqrt{\pi} \mathbb{E}\{s_k\} \lambda_k^{BS} \tau^l}{(l!)^2 N_{t,k}} \frac{\Gamma(M+l)}{\Gamma(M)} \frac{\Gamma(l+\frac{1}{2})}{(2-\alpha l)} \\ &\left[r_j^2 \left(\frac{P_k}{P_j} \right)^{2/\alpha} \mathcal{J}_l(-\tau) - R_{max}^2 \left(\frac{r_j}{R_{max}} \right)^{\alpha l} \left(\frac{P_k}{P_j} \right)^l \mathcal{J}_l\left(-\tau \frac{P_k}{P_j} \left(\frac{r_j}{R_{max}} \right)^\alpha \right) \right]. \end{aligned} \tag{5.28}$$

Proposition 10
The success probability, when the typical UE is from a tier of layer 2 and served by a BS of tier $j \neq 0$ located at $\mathbf{x}_j$, is given by:

$$\mathbb{P}_{suc}(\tau, \mathbf{x}_j) = \sum_{l=0}^{M-1} \frac{(-\tau M r_j^\alpha)^l}{l! (P_j \beta)^l} \sum_{n=0}^{l} \binom{n}{k} \mathcal{L}_{\mathcal{I}_0}^{(l-n)} \left(\frac{\tau M r_j^\alpha}{\beta P_j} \right) \mathcal{L}_{\mathcal{I}_{exp}}^{(n)} \left(\frac{\tau M r_j^\alpha}{\beta P_j} \right), \tag{5.29}$$

where the n^{th} derivative of $\mathcal{L}_{\mathcal{I}_0}(s)$ and $\mathcal{L}_{\mathcal{I}_{exp}}(s)$ are respectively given by equation 5.26 of Lemma 12 and by equation 5.24 of Corollary 6.

In the expression of the AKWCP metric defined in equation 5.2, the success probability $\mathbb{P}_{suc}(\tau, r_{k,1} | k^* = k; s_k(a_{k,1}) = 1)$ can be computed using either Proposition 9, either Proposition 10. This probability of success is defined when the typical UE is served by the closest BS in terms of power weighted distance, located at distance $r_{k,1}$.

5.2.5 Coverage probability

One last term in the AKWCP metric is not yet defined. This term is denoted $\mathbb{P}_{cov}(\tau | r_{k,1}; k^* = k; s_k(a_{k,1}) = 0)$ and refers to the coverage probability of the network when the closest BS in terms of power weighted distance is sleeping. The distance to this sleeping BS is known and denoted $r_{k,1}$. The tier corresponding to this BS is denoted k^*. The distance $r_{k,1}$ results in an exclusion region of serving BSs around the typical UE depending on the power transmitted by each tier.

In order to calculate this coverage probability, the coverage provided by each tier is developed as a weighted sum such that:

$$\begin{aligned} \mathbb{P}_{cov}(\tau | r_{k,1}; k^* = k; s_k(a_{k,1}) = 0) = &\mathbb{P}_{cov,k^*}(\tau | r_{k,1}; k^* = k; s_k(a_{k,1}) = 0) \\ &+ \sum_{j \in \mathcal{K}_0 \setminus \{k^*\}} \mathbb{P}_{cov,j}(\tau | r_{k,1}; k^* = k; s_k(a_{k,1}) = 0) \end{aligned} \tag{5.30}$$

The coverage probability of tier j must be weighted by the probability of being connected to this tier. The corresponding event is denoted S_{Φ_j} so $\mathbb{P}(S_{\Phi_j} | r_c)$ represents the probability to be connected to tier j, knowing the distance r_c to the closest awake BS from this tier. This probability is stated in Lemma 13. Then, Proposition 11 states the expression of the coverage probability in equation 5.30.

Lemma 13
The probability to be connected to a given tier, knowing the distance r_c to the closest awake BS from this tier, is given by:

For $j = k^*$:

$$\mathbb{P}(S_{\Phi_{k^*}}|r_c; r_{k,1}; k^* = k; s_k(a_{k,1}) = 0) = \mathbb{E}\{s_{k^*}\} \prod_{m\in\mathcal{K}_0\setminus\{k^*\}} \prod_{n\in\hat{I}_m} \left((1 - \mathbb{E}\{s_m\}) + \overline{F}_1(m,n) - \overline{F}_1(m,n)(1 - \mathbb{E}\{s_m\})\right), \quad (5.31)$$

where $\overline{F}_1(m,n) = \overline{F}_{R_{m,n}}(\overline{P}_{k^*,m} r_c | \overline{P}_{k,m} r_{k,1})$.

For $j \in \mathcal{K}_0 \setminus \{k^*\}$:

$$\mathbb{P}(S_{\Phi_j}|r_c; r_{k,1}; k^* = k; s_k(a_{k,1}) = 0) = \mathbb{E}\{s_j\} \prod_{n\in\hat{I}_{k^*}\setminus\{1\}} \left((1 - \mathbb{E}\{s_{k^*}\}) + \overline{F}_2(j,n) - \overline{F}_2(j,n)(1 - \mathbb{E}\{s_{k^*}\})\right) \prod_{m\in\mathcal{K}_0\setminus\{j,k^*\}} \prod_{n\in\hat{I}_m} \left((1 - \mathbb{E}\{s_m\}) + \overline{F}_3(j,m,n) - \overline{F}_3(j,m,n)(1 - \mathbb{E}\{s_m\})\right), \quad (5.32)$$

where $\overline{F}_2(j,n) = \overline{F}_{R_{k^*,n}}(\overline{P}_{j,k^*} r_c | r_{k,1})$ and $\overline{F}_3(j,m,n) = \overline{F}_{R_{m,n}}(\overline{P}_{j,m} r_c | \overline{P}_{k,m} r_{k,1})$.

Proposition 11
The coverage probability from a tier j, weighted by the probability to be connected to this particular tier, when the closest BS in terms of power weighted distance is asleep and located at a distance $r_{k,1}$, can take two different forms:

For $j = k^*$:

$$\mathbb{P}_{cov,k^*}(\tau|r_{k,1}; k^* = k; s_k(a_{k,1}) = 0) = \int_{r_{k,1}}^{R_{max}} \mathbb{P}(S_{\Phi_{k^*}}|r_c; r_{k,1}; k^* = k; s_k(a_{k,1}) = 0) \mathbb{P}_{suc}(\tau, r_c|S_{\Phi_{k^*}}) \sum_{i=2}^{|\hat{I}_{k^*}|} (1 - \mathbb{E}\{s_{k^*}\})^{i-2} f_{R_{k^*,i}}(r_c|r_{k,1})\, dr_c, \quad (5.33)$$

where $|\hat{I}_{k^*}|$ is the cardinality of the set of index of the BSs from tier k^*.

For $j \in \mathcal{K}_0 \setminus \{k^*\}$:

$$\mathbb{P}_{cov,j}(\tau|r_{k,1}; k^* = k; s_k(a_{k,1}) = 0) = \int_{\overline{P}_{k,j} r_{k,1}}^{R_{max}} \mathbb{P}(S_{\Phi_j}|r_c; r_{k,1}; k^* = k; s_k(a_{k,1}) = 0) \mathbb{P}_{suc}(\tau, r_c|S_{\Phi_j}) \sum_{i=1}^{|\hat{I}_j|} (1 - \mathbb{E}\{s_j\})^{i-1} f_{R_{j,i}}(r_c|\overline{P}_{k,j} r_{k,1})\, dr_c. \quad (5.34)$$

5.2.6 Modelling of the load

To evaluate the AKWCP metric, the activity of each BS must be modelled. This section aims to develop a general expression for the pmf of the load of the BSs from each tier. In this thesis, the characterisation of the load is performed considering the same power transmission for all tiers, and for a typical BS located at the origin.

For a BS from layer 1, the UEs served by the BS can be from an independent HPPP (the corresponding load is denoted load A), from an independent PCP without any BS as cluster centers (denoted load B), and from an independent PCP with BSs as cluster centers (denoted load C). It is the same for a BS from layer 2 except that it can also serve UEs from the dependent PCP (denoted load D). Once the pmf of the four types of loads are define, the total load must still be derived. The location of the UEs from each source is independent, so the loads from each source are assumed to be independent as well. With this assumption, the total load is thus obtained by summing the load from each source. The total pmf is then given by the pmf of a sum of independent variables. This assumption of independence is discussed in section 5.3 using MC simulations.

In order to derive the pmf of load A and B, observe that the BSs from all tiers are distributed as independent HPPPs with different intensities. This allows to benefit from the principle of superposition of independent HPPPs, resulting in a HPPP with intensity equal to the sum of the respective intensities. This summed intensity is denoted $\lambda_{tot}^{\mathrm{BS}} = \sum_{k=0}^{K} \lambda_k^{\mathrm{BS}}$. Hence, for the characterisation of load A, the expression from Proposition 4 can simply be used by replacing the intensity of the HPPP of BSs by the total intensity $\lambda_{tot}^{\mathrm{BS}}$. Similarly, the characterisation of load B is obtained from Proposition 8 by replacing the intensity of the HPPP of BSs by the total intensity $\lambda_{tot}^{\mathrm{BS}}$. A direct observation is that the expression of the load does not depend directly on the intensity of the tier to which the BS belongs, but only depends on the total intensity of BSs.

For the characterisation of the pmf of load C, the expression cannot be found in the literature. However, one can observe that the situation is the same as the one described in load B except that there is a BS at the cluster center. This aspect is taken into account in Proposition 12 to adapt the expression of the load stated in Proposition 8.

Proposition 12 (Load C)
The pmf of the activity from an independent PCP of tier j with BSs as cluster centers can be obtained from Proposition 8 by replacing the expression of the probability generating function of $\Psi_{\mathrm{U}}(\mathcal{C}_0)$, in equation 4.23, by:

$$G_{\Psi_0}(\theta) = \int_0^{\infty} \exp\left\{ -2\pi\lambda_j^{\mathrm{BS}} \int_{2r}^{\infty} \left(1 - \exp\left[-\overline{m}_j(1-\theta)\xi_j(r,w)\right]\right) w dw \right\} f_{R_c}(r) dr, \quad (5.35)$$

in which $\xi_j(r,w)$ is given by equations 4.24 and 4.25 with the parameters of tier j for the PCP.

The last pmf to develop describes the distribution of the load from the UEs having the BS of interest as a cluster center. The position of the UEs are thus linked to the position of the BS. The expression of the load in Proposition 8 is adapted in Proposition 13 to characterise load D.

Proposition 13 (Load D)
The pmf of the activity, from the UEs having the BS of interest from tier j as a cluster center, can be obtained from Proposition 8 by replacing the expression of the probability generating function of $\Psi_{\mathrm{U}}(\mathcal{C}_0)$, in equation 4.23, by:

$$G_{\Psi_0}(\theta) = \int_0^{\infty} \exp\left[-\overline{m}(1-\theta)\xi(r,0)\right] f_{R_c}(r) dr, \quad (5.36)$$

in which $\xi(r,0)$ is given for the two types of PCP by:

$$\xi^{\text{TCP}}(r,0) = 1 - \exp\left(-\frac{r^2}{2\sigma_j^2}\right), \tag{5.37}$$

$$\xi^{\text{MCP}}(r,0) = \frac{\min(r^2, r_{m,j}^2)}{r_{m,j}^2}. \tag{5.38}$$

Now that the 4 types of loads have been defined, the pmf of the total load of a BS can be determined. To do so, lets recall first how to determine the pmf of the sum of two independent discrete random variables. Let X and Y be two independent discrete random variables. Their respective pmf is denoted by p_X and p_Y. Then, the pmf of the sum variable $Z = X + Y$ is given by:

$$p_Z(z) = \sum_{y \in R_Y} p_X(z-y) p_Y(y), \tag{5.39}$$

where R_Y is the support of p_Y.

For a BS of layer 1, the total pmf is obtained by summing the pmf from load A for a HPPP with intensity λ_{tot}^{UE} equal to the sum of the intensities of all tiers of layer 4, with the pmf from load B for all tiers of layer 3 and the pmf from load C for all tiers of layer 2. The same is done for a BS of layer 2 except that the load D is added only for the tier to which the BS belongs.

5.2.7 Adaptation regarding Palm theory

As it has been seen in the previous subsections, Palm theory states that the distribution for a typical BS located at the origin holds for any BS selected uniformly at random among all the BSs of a PP. However, in the development of the AKWCP metric, the activity is defined for the load of the closest BS to the typical UE. This is not a random selection and Palm theory does not actually apply. In previous chapters, this had an impact on the accuracy of the developed analytical expressions, but this effect was neglected. In this chapter, the load developed for the typical BS is assumed to be correct for all BSs except for the closest one to the typical UE. For this BS, two adaptations are performed and described in this subsection.

The first effect that has to be taken into account is that the closest BS to the typical UE has at least one UE within its Voronoï region. Otherwise, it would not be the closest one. The pmf of the load must therefore be adapted. This is described in Lemma 14.

Lemma 14
The total pmf of the load of the closest BS to the typical UE must be adapted. The adaptation has to be performed on the pmf of the load (denoted $f_A(n)$) from the PP to which the typical UE belongs, before summing up the contribution from all tiers. The adapted pmf is given by:

$$f_A(n|n \geq 1) = \begin{cases} \frac{f_A(n)}{1-f_A(0)} & \text{if } n \geq 1, \\ 0 & \text{otherwise.} \end{cases} \tag{5.40}$$

The pmf that must be adapted depends on the layer to which the typical UE belongs, but also depend on the tier to which the closest BS belongs. The different cases are described successively:

For a typical UE of tier j from layer 2:
If the closest BS is from tier 0, the load D corresponding to tier j must be adapted. Otherwise, it is the load C corresponding to tier j.

For a typical UE of tier j from layer 3:
Load B corresponding to tier j must be adapted.

For a typical UE of tier j from layer 4:
Load A corresponding to tier j must be adapted.

The adaptation from Lemma 14 is not the only change to perform to the pmf of the activity of the closest BS. Up to now, the load of the closest BS of tier $k^* = k$ was assume to be independent from its distance to the typical UE denoted $r_{k^*,1}$. However, with the assumption of a circular Voronoï region described in section 4.2.5, this is no longer true. Indeed, the radius R_c of the Voronoï region of the closest BS must be at least bigger than the distance $r_{k^*,1}$ to the typical UE. Otherwise, the typical UE would not be in the Voronoï region of the closest BS. By contradiction, this BS would not be the closest one. In order to take this effect into account, the circular shape hypothesis must be applied to load A. The distribution of the number of UEs from a HPPP of intensity λ^{UE} in a cell of area A is given by:

$$\text{Dist}(n|A) \overset{(a)}{=} \frac{(\lambda^{UE}A)^n}{n!}\exp(-\lambda^{UE}A). \tag{5.41}$$

(a) is obtained from equation 2.8. By integrating equation 5.41 on the distribution of R_c, load A, under the assumption of the circular region $A = \pi R_c^2$, is given by:

$$f_{Load\ A}(n) = \int_{R_c} \text{Dist}(n|A = \pi r^2) f_{R_c}(r) dr, \tag{5.42}$$

where f_{R_c} is given in Proposition 8. Corollary 7 states that the assumption of the circular Voronoï region does not change the distribution of load A when there is no constrain on R_c.

Corollary 7
Under the assumption of the circular Voronoï region, when there is no constrain on the radius R_c, the activity follows a NB distribution $NB(c, p_s)$ with the same parameters as Proposition 4.

Now that all types of loads are defined with the circular Voronoï region assumption, the change to apply can be described. For each pmf contributing to the distribution of the total load of the closest BS, the integration on R_c must be performed from $r_{k^*,1}$ to infinity instead of 0 to infinity. The pdf of the radius R_c must also be adapted and is given by:

$$f_{R_c|r_{k^*,1}}(r; c, \Omega) = \frac{f_{R_c}(r; c, \Omega)}{\overline{F}_{R_c}(r_{k^*,1})}, \quad r \geq r_{k^*,1}, \tag{5.43}$$

where $\Omega = \frac{1}{\pi\lambda_B}$ and $\overline{F}_{R_c}$ is the ccdf of R_c given by the regularised upper incomplete gamma function $Q\left(c, \frac{c}{\Omega} r_{k^*,1}^2\right)$.

5.3 Numerical Results

In this section, the validity of the model for the load developed in section 5.2.6 is first assessed through MC simulations for a typical BS. Then, the accuracy of the analytical expression of the AKWCP metric is verified using MC simulations for a typical UE. The simulations also allow to verify the benefit of the adaptation of the pmf described in section 5.2.7. Finally, the analytical expression of the AKWCP metric is used to observe the evolution of the EE with the noise variance.

The development of the AKWCP has been carried out in all generality for a network of $\hat{K}$ tiers. A specific network must thus be defined for the simulations. In this thesis, four tiers are considered, each of them belonging to one of the four defined layers:

- **Tier k = 1 of Layer 1:** HPPP of BSs of density $\lambda_1^{\text{BS}} = 5\ 10^{-5}[m^{-2}]$.
- **Tier k = 2 of Layer 2:** HPPP of BSs of density $\lambda_1^{\text{BS}} = 10^{-5}[m^{-2}]$. The position of the BSs are the cluster centers of a TCP of UEs, with parameter $\overline{m}_2 = 20$ and $\sigma_2^2 = \frac{200}{\pi}$.
- **Tier k = 3 of Layer 3:** TCP of UEs of parent density $\lambda_3^p = 10^{-4}[m^{-2}]$. The other parameters are $\overline{m}_3 = 10$ and $\sigma_3^2 = \frac{200}{\pi}$.
- **Tier k = 4 of Layer 4:** HPPP of UEs of density $\lambda_4^{\text{UE}} = 5\ 10^{-4}[m^{-2}]$.

With regard to the values of the network parameters, MC simulation parameters and power consumption parameters, no change is made compare to chapter 4.3. They can thus be found respectively in Table 4.1, 4.2 and 4.4. The only exception is that $n = 50000$ iterations have been made for each MC simulation.

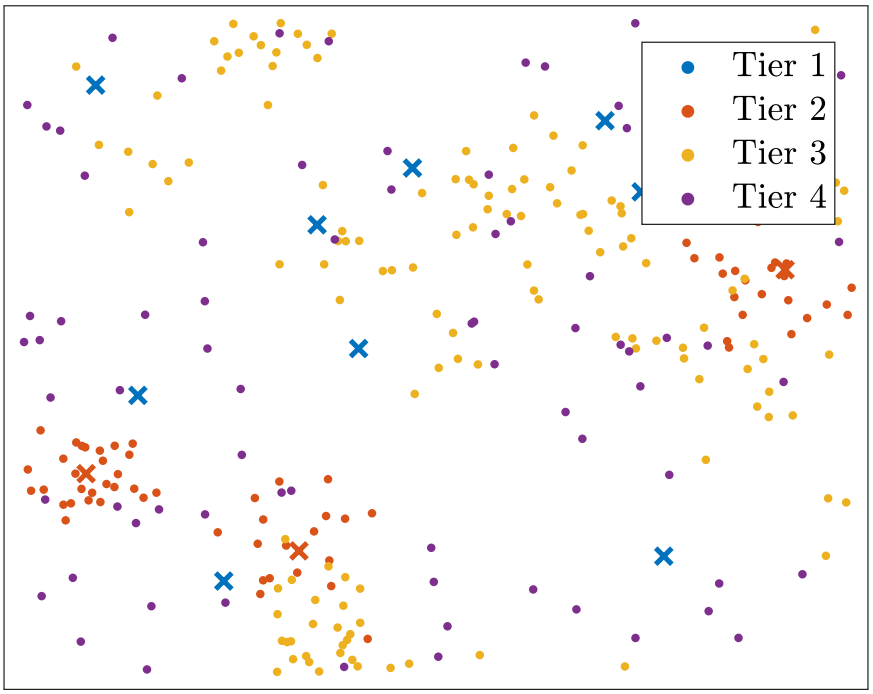

Figure 5.3: Visualisation of a realisation of the 4-tiers network considered for the simulations of chapter 5. The crosses represent the locations of the BSs while the dots represent the locations of the UEs

5.3.1 MC simulations for the load modelling

Preliminary note: For each figure, the solid lines represent the result of the MC simulation while the stars represent the values obtained with the analytical expressions.

Figure 5.4 depicts the accuracy of the analytical model characterising the pmf of the load from each possible source. The MC simulations are performed for a typical BS located at the origin. It can be observe that the analytical models provide a good approximation of the MC simulations for load A and B, despite the circular Voronoï assumption made to develop the model. However, a gap between the two curves can be observed for load C and D.
One can observe that load C is the one having the smallest contribution to the total load. In this case, the UEs are clustered around a BS. Therefore, most of these UEs are served by their corresponding BS. This would however not be true anymore if the variance of the cluster σ_2^2 increases, as in that specific case the UEs of a cluster would be more spread over the network.

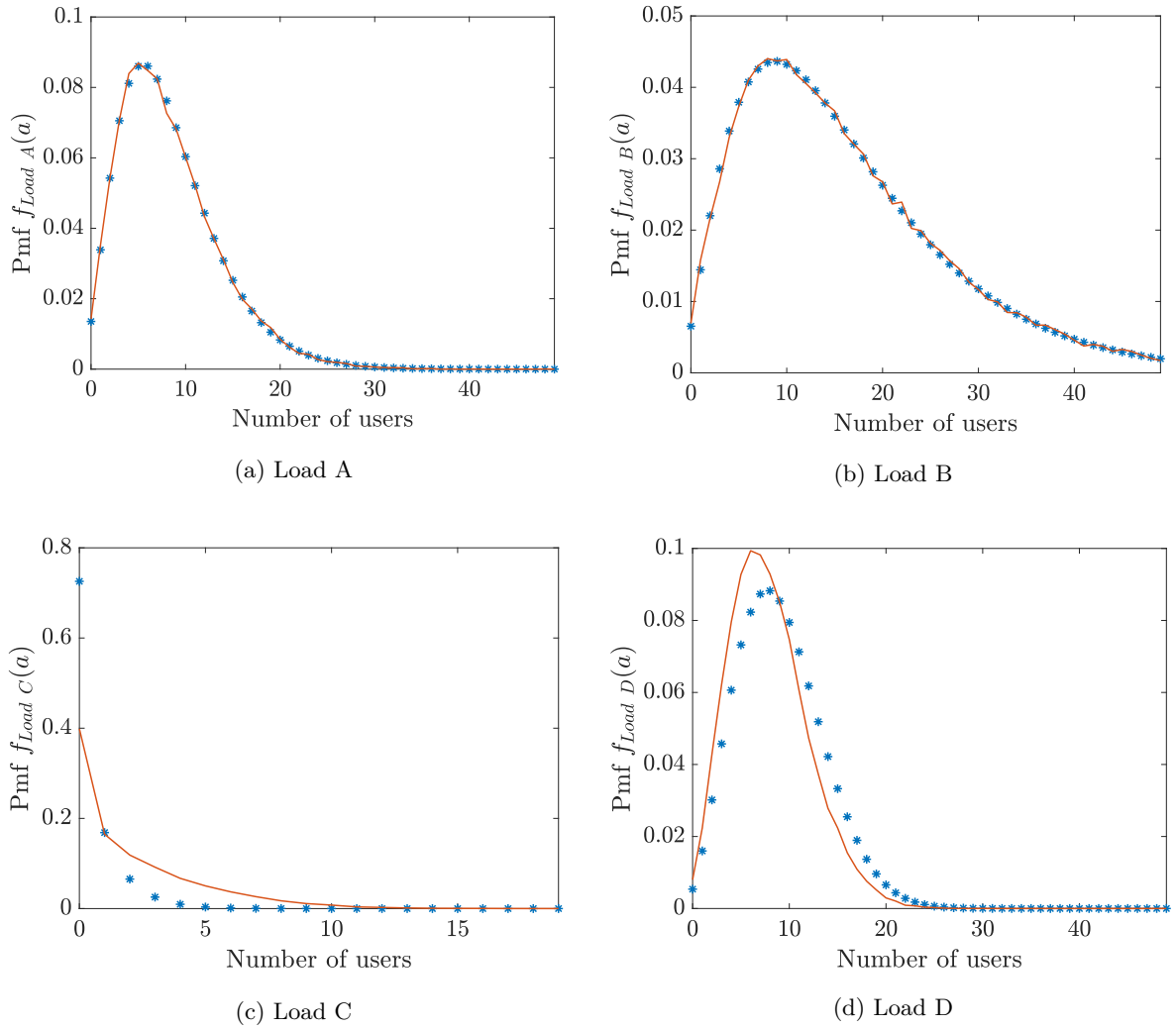

(a) Load A

(b) Load B

(c) Load C

(d) Load D

Figure 5.4: Comparison of analytical and numerical results for the pmf of the 4 types of loads, for a typical BS located at the origin.

Figure 5.5 compares the analytical result with a MC simulation for the pmf of the load of the BSs of tier 1 and 2. No adaptation on the pmf, such as the one described in section 14, is performed as the model is given here for a typical BS located at the origin. Despite the relatively good accuracy obtained for load A, B, C and D, as observed in figure 5.4, pmf 1 and 2, computed from a sum of independent variable, are not as accurate. This shows that the assumption of independence between the respective loads does not hold.
Some interpretations can be made to explain the interaction between the different loads, despite the independence of the positions of the UEs from each source. Indeed, if the contribution from load A, to the total number of UEs within the Voronoï region of the typical BS, is smaller than its mean contribution, then the one from the other loads has a higher probability to be smaller than their mean one as well. One of the reason for this could be that load A is small because a BS is located next to the typical BS. Therefore, this neighboring BS will serve UEs, from each tier, that are located close to the typical BS. This will decrease their contribution to the total load of this BS.
The provided explanation is not exhaustive and many other interactions can have an impact on the distribution of the load. The effect of these interactions can be observe on figure 5.4 as the curve provided by the MC simulation has a higher standard deviation than the one provided by the analytical results. Unfortunately, SG does not provide tools to take these

effects into account and to compute an exact expression of the total load from load A, B, C and D. The independence approximation made in this thesis provides a tractable and intuitive way of computing the distribution of the load for complex network configuration. The next subsection discuss the impact of this approximation on the accuracy of the AKWCP metric.

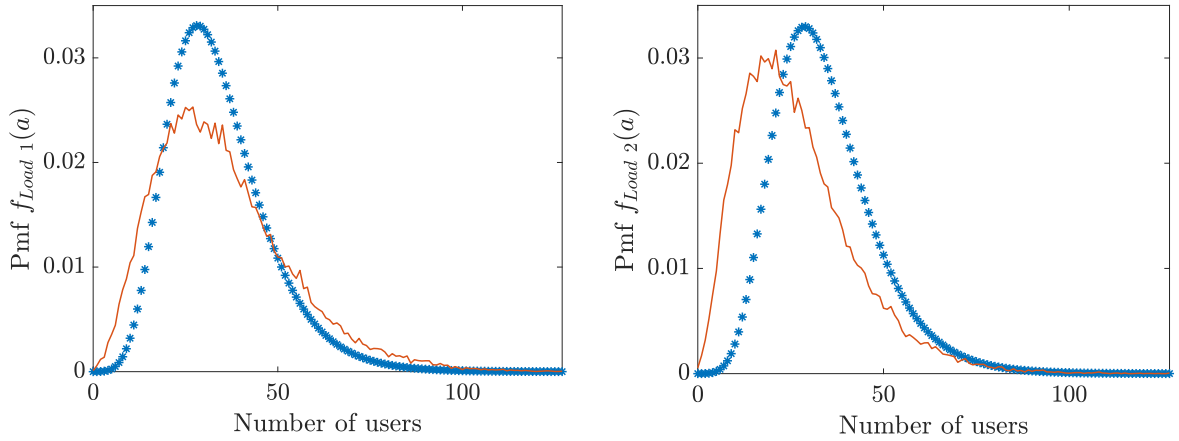

(a) Pmf 1

(b) Pmf 2

Figure 5.5: Comparison of analytical and numerical results for the pmf of the load for the BSs of tier 1 and 2.

5.3.2 MC simulations for the AKWCP metric

Preliminary note: the evaluation of the AKWCP metric is computationally expensive so external resources have been used to obtain the analytical curves of the next graphs. Computational resources have been provided by the supercomputing facilities of the Université catholique de Louvain (CISM/UCL) and the Consortium des Équipements de Calcul Intensif en Fédération Wallonie Bruxelles (CÉCI) funded by the Fond de la Recherche Scientifique de Belgique (F.R.S.-FNRS) under convention 2.5020.11 and by the Walloon Region.

Figure 5.6 compares the evolution, with respect to the noise variance, of the analytical expression of the AKWCP metric, with a MC simulation. It can be observed that the result provided by the analytical expression provides an accurate approximation of the simulated curve. The small gap between the two curves can be explained by the different assumptions made when developing the analytical expression.
It can be observed that the AKWCP metric is higher for the UEs of tier 2. Recall that these UEs are distributed as a TCP with BSs as cluster centers. For a network provider, there is thus a real benefit in terms of AKWCP metric of having a BS placed at the center of a cluster of UEs.
The curves for the UEs of tier 3 and 4 are very similar. This shows that, if the network provider does not place intentionally the BSs according to the position of the cluster of UEs, all UEs will have access to the same service. Indeed, UEs from tier 4 that are very spread over the network and UEs from tier 3 that form clusters over the network have similar values for the AKWCP metric.

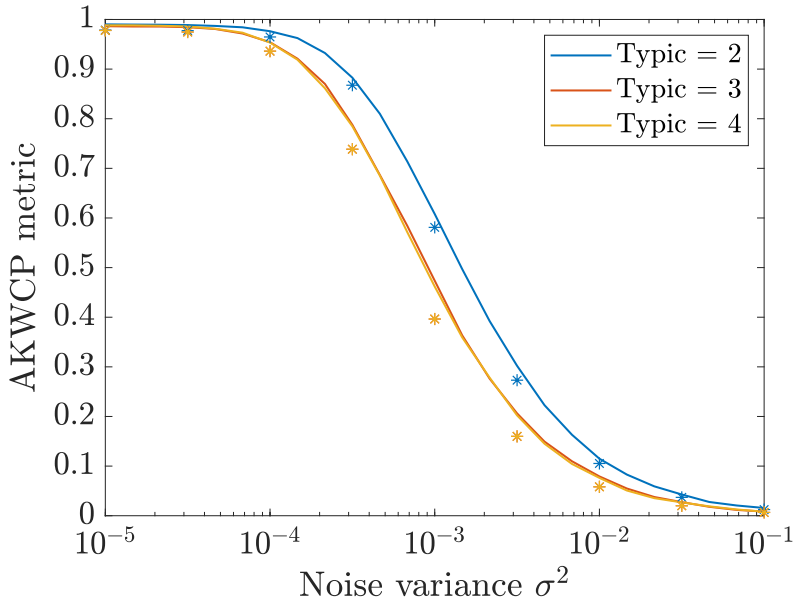

Figure 5.6: Comparison of analytical and numerical results for the AKWCP metric defined in Definition 2. The expression is evaluated for a typical UE from tier 2, 3 or 4.

Figure 5.7 compares the evolution of the AKWCP metric for different simulations with the analytical solution. The MC simulation curve is obtained by running a complete MC simulation, as it was performed for the different comparisons of this thesis. The position of all BSs and UEs are generated according to their corresponding PP distribution. Two other "fake" simulations are performed and are denoted A-MC and NA-MC. In these "fake" configurations, only the position of the BSs are generated at each iteration. For the considered system model, the UEs have only an effect on the activity of each BSs. Therefore, their influence can be replaced in the "fake" MC simulations by the developed analytical model of the load. In other words, instead of counting the number of UEs within the Voronoï region of each BS to determine their activity, the load is randomly generated from the developed analytical pmf. For the A-MC simulation, the adapted analytical model, described in section 5.2.7, is used, while for the NA-MC simulation, the non-adapted one is used. The purpose of this simulation is to verify the impact of the model developed to characterise the load on the accuracy of the AKWCP metric.
It can be observed that the A-MC simulation fits the MC simulation for a typical UE from tier 3 and 4, while a small gap can be observed for a typical UE from tier 2. This shows that the approximations made for the analytical model of the load have a negligible impact on the accuracy of the AKWCP metric. Furthermore, the fact that the NA-MC curve does not fit the MC simulation shows the benefit of the adapted model of the load developed in this thesis.

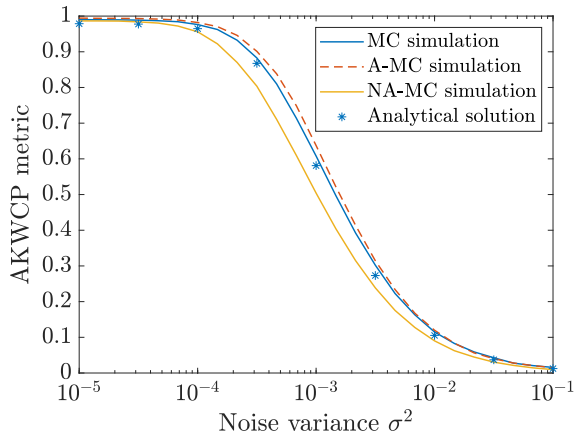

(a) Typic = 2

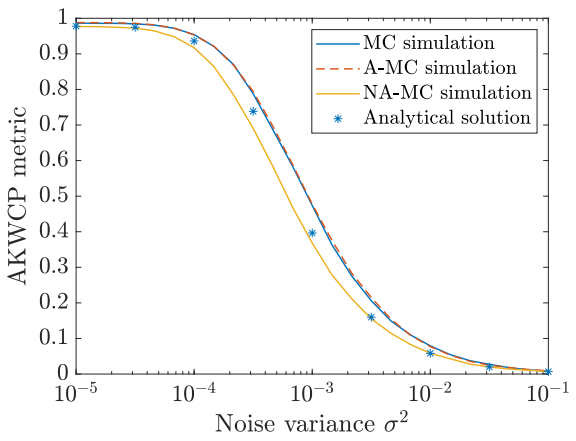

(b) Typic = 3

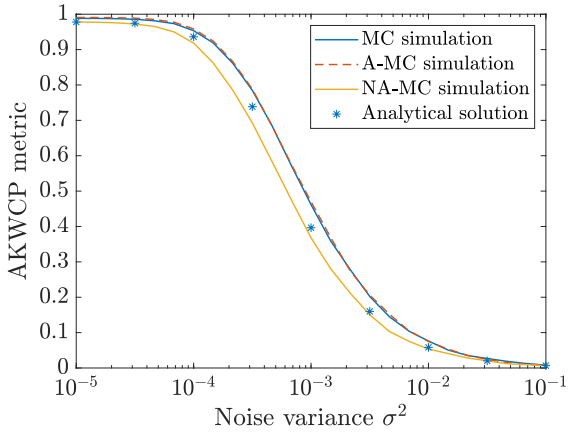

(c) Typic = 4

Figure 5.7: Comparison of the analytical solution of the AKWCP metric with a MC simulation, a fake adapted MC simulation (denoted AMC) and a fake non-adapted MC simulation (denoted NAMC). The comparison is performed for 3 types of typical UE.

5.3.3 SG based interpretations

Figure 5.8 depicts the evolution of the EE with respect to the noise variance. For this figure, the solid lines are obtained from the results of the analytical expression. Different proportion of awake BSs q_{SS} are compared for the three types of typical UE. One can observe that, among the tested values of q_{SS}, the smallest proportion (i.e. $q_{SS} = 0.25$) provides the best EE for most values of noise. When the noise variance increases, the gap between the different strategies decreases and their respective EE tend towards 0.

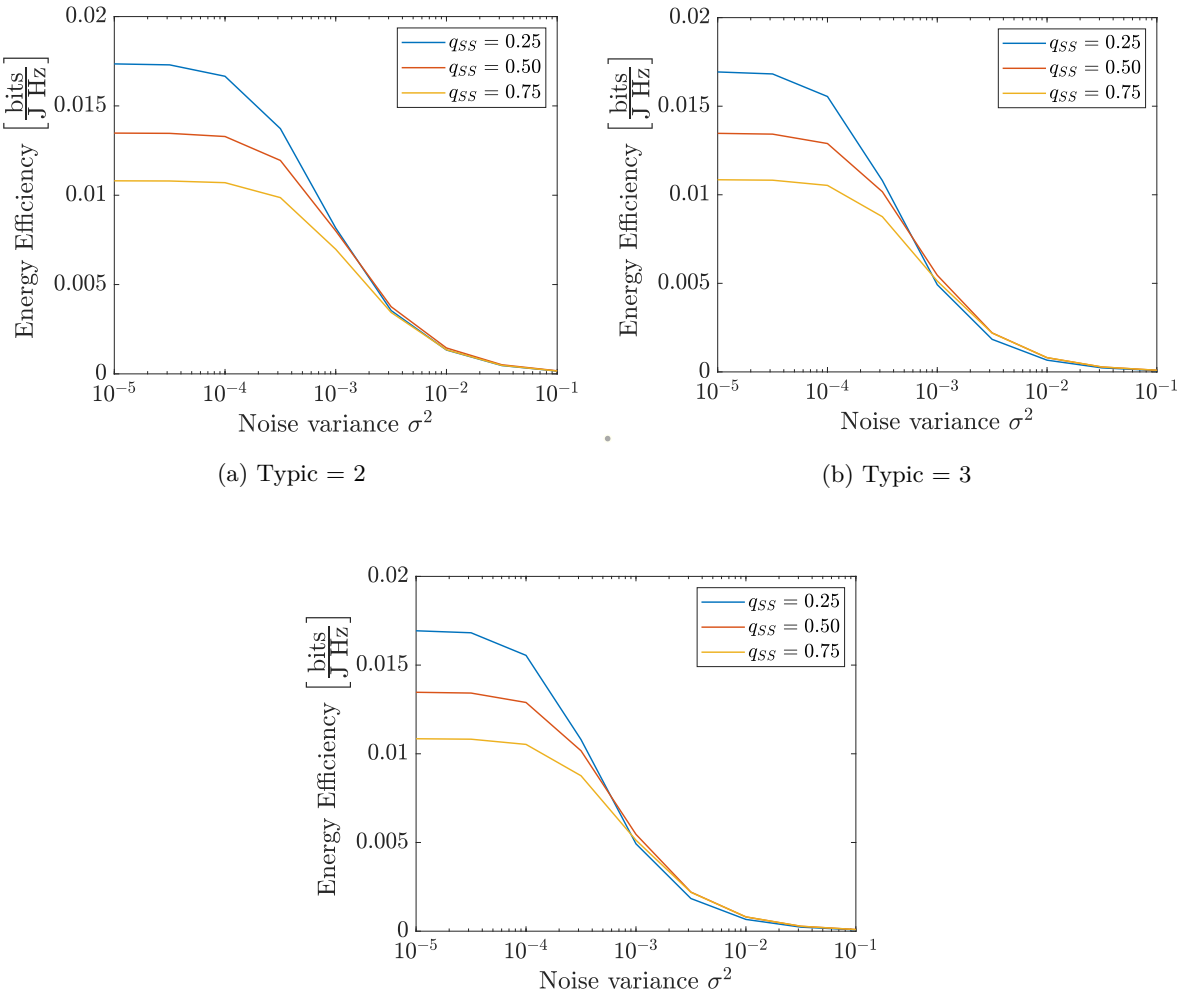

(a) Typic = 2

(b) Typic = 3

(c) Typic = 4

Figure 5.8: EE for different proportion of awake BSs with SS. The comparison is performed for 3 types of typical UE.

Chapter 6

Conclusion

In this thesis, a general framework to study the benefit of sleep mode strategies in wireless communication networks has been presented. SG has been used to develop analytical expressions characterising the evolution of the EE for the different system models considered.

First, a simple system model in which the UEs and the BSs are independently and homogeneously distributed over the network has been analysed. The simple model of Rayleigh fading has been used to evaluate the WCP metric. This new metric extends the coverage probability to show the benefit of sleep mode strategies in terms of EE. The impact of the densities of UEs and of BSs on the performances has been studied and the benefit of SS over RS has been proven for this simple system model.

Next, some of the features of 5G cellular networks, such as beamforming and mm-Wave, have been considered in a new scenario. The metrics developed in the previous chapter have been adapted to these new characteristics. Clustered UEs distributions have been introduced in the model to reflect more realistic situations. The impact of the system parameters on the EE and the WCP has been analysed in order to identify good practices for network providers.

Finally, a general and tractable multi-tier configuration of network has been presented to study the inherent inhomogeneous architecture of 5G networks. For this purpose, four different layers of BSs and UEs have been considered. A new metric, namely the AKWCP, has been defined to study this system model and to correct the inaccuracy observed in the simpler models used in the previous chapters. A characterisation of the distribution of the load for each BS has been derived and adaptations have been performed to integrate the concepts of Palm theory. MC simulations have been used to validate the accuracy of the obtained models and to evaluate the benefits of adapting the load model.

In future works, the system model studied in the last chapter could be further exploited:

- The assumed independence of the loads from different PP of UEs has been shown to be inaccurate in the characterisation of the load in chapter 5. Despite providing an intuitive and tractable way of approximating the total load, the presented model could be improved. For this purpose, instead of deriving the loads from each PP independently and then adding their contribution, the probability generating function of the total load could be directly computed by benefiting from the independence of the PPs. This would lead to a more complex integral that would solve the current issue on the load and therefore improve the accuracy of the characterisation of said load.

- The expression that was developed for the AKWCP metric is very flexible and is based on an average received power association scheme. Therefore, different transmitting power

can be used in each tier. However, the current model for the activity, used to evaluate the metric, is developed for a network with universal power transmission. By developing the analytical expressions characterising the load, for BSs with different transmitting powers, a more realistic network model featuring macro, micro, pico and femto cells could be studied.

- A more complete model for the power consumption would be interesting to study to take into account more aspects in the evaluation of the EE. In this thesis, the energetic cost of the deployment of BSs and of the use of multiple antennas has not been studied.
- The influence of the network parameters would be interesting to study using the general framework presented in chapter 5. Different network configurations can be compared together to derive best practices for network providers wishing to implement GREEN communications.
- A more complex sleeping strategy could be developed to include intermediate modes of transmision. In this thesis, the BSs are either awake (they transmit with maximum power) or asleep (they do not transmit at all). The impact on the EE of adding stand-by modes with intermediate transmitting powers would be interesting to study in order to develop more efficient sleeping strategies.

Finally, with the sleeping strategy developed in this thesis, each BS decides of its sleeping mode independently of the one chosen by neighbouring BSs. This simple scheme is sub-optimal. An interactive decision scheme, such as the one presented in [34], would allow to optimise the sleeping strategy of the full network. However, an analysis of such network is not possible with SG. It would then be interesting to compare the performances, in terms of EE, of an interactive sleeping strategies with the analytical model developed in this thesis. The performances of the interactive scheme would be obtained using MC simulations.

Bibliography

[1] Amitabha Ghosh, Andreas Maeder, Matthew Baker, and Devaki Chandramouli. 5g evolution: A view on 5g cellular technology beyond 3gpp release 15. *IEEE Access*, 7:127639–127651, 2019.

[2] Wei Hong, Zhi Hao Jiang, Chao Yu, Debin Hou, Haiming Wang, Chong Guo, Yun Hu, Le Kuai, Yingrui Yu, Zhengbo Jiang, Zhe Chen, Jixin Chen, Zhiqiang Yu, Jianfeng Zhai, Nianzu Zhang, Ling Tian, Fan Wu, Guangqi Yang, Zhang-Cheng Hao, and Jian Yi Zhou. The role of millimeter-wave technologies in 5g/6g wireless communications. *IEEE Journal of Microwaves*, 1(1):101–122, 2021.

[3] S. O'Dea. Number of mobile (cellular) subscriptions worldwide from 1993 to 2019. Published on December 3, 2020 on statistica.com. <https://www.statista.com/statistics/262950/global-mobile-subscriptions-since-1993/> accessed on 13 August 2021.

[4] Pimmy Gandotra, Rakesh Kumar Jha, and Sanjeev Jain. Green communication in next generation cellular networks: A survey. *IEEE Access*, 5:11727–11758, 2017.

[5] Pimmy Gandotra and Rakesh Kumar Jha. Next generation cellular networks and green communication. In *2018 10th International Conference on Communication Systems Networks (COMSNETS)*, pages 522–524, 2018.

[6] Hauke Holtkamp, Gunther Auer, Samer Bazzi, and Harald Haas. Minimizing base station power consumption. *IEEE Journal on Selected Areas in Communications*, 32(2):297–306, 2014.

[7] Wonil Roh, Ji-Yun Seol, Jeongho Park, Byunghwan Lee, Jaekon Lee, Yungsoo Kim, Jaeweon Cho, Kyungwhoon Cheun, and Farshid Aryanfar. Millimeter-wave beamforming as an enabling technology for 5g cellular communications: theoretical feasibility and prototype results. *IEEE Communications Magazine*, 52(2):106–113, 2014.

[8] Chang Liu, Balasubramaniam Natarajan, and Hongxing Xia. Small cell base station sleep strategies for energy efficiency. *IEEE Transactions on Vehicular Technology*, 65(3):1652–1661, 2016.

[9] Wenson Chang, Wen-Yen Cheng, Zhao-Ting Meng, and Szu-Lin Su. Energy-efficient sleep strategy with variant sleep depths for open-access femtocell networks. *IEEE Communications Letters*, 23(4):708–711, 2019.

[10] Jan García-Morales, Guillem Femenias, and Felip Riera-Palou. Energy-efficient access-point sleep-mode techniques for cell-free mmwave massive mimo networks with non-uniform spatial traffic density. *IEEE Access*, 8:137587–137605, 2020.

[11] Gunther Auer, Vito Giannini, Claude Desset, Istvan Godor, Per Skillermark, Magnus Olsson, Muhammad Ali Imran, Dario Sabella, Manuel J. Gonzalez, Oliver Blume, and Albrecht

Fehske. How much energy is needed to run a wireless network? *IEEE Wireless Communications*, 18(5):40–49, 2011.

[12] Marco Di Renzo. Intro to stochastic geometry & point processes, September 2016. Course on Random graphs and Wireless Commun. networks, Oxford University.

[13] Jeffrey G. Andrews, Francois Baccelli, and Radha Krishna Ganti. A tractable approach to coverage and rate in cellular networks. *IEEE Transactions on Communications*, 59(11):3122–3134, 2011.

[14] Anjin Guo and Martin Haenggi. Spatial stochastic models and metrics for the structure of base stations in cellular networks. *IEEE Transactions on Wireless Communications*, 12(11):5800–5812, 2013.

[15] Christopher Z Mooney. *Monte carlo simulation*. Number 116. Sage, 1997.

[16] Harpreet S. Dhillon Jeffrey G. Andrews, Abhishek K. Gupta. A primer on cellular network analysis using stochastic geometry. Published on October 5, 2016 on Arxiv.org. <https://arxiv.org/pdf/1604.03183.pdf> accessed on 7 April 2021.

[17] Hesham ElSawy, Ahmed Sultan-Salem, Mohamed-Slim Alouini, and Moe Z. Win. Modeling and analysis of cellular networks using stochastic geometry: A tutorial. *IEEE Communications Surveys Tutorials*, 19(1):167–203, 2017.

[18] Martin Haenggi. *Stochastic Geometry for Wireless Networks*. Cambridge University Press, 2012.

[19] H. Paul Keeler. Simulating a homogeneous poisson point process on a rectangle, August 6, 2018. Website: <https://hpaulkeeler.com/poisson-point-process-simulation/> accessed on 20 Mars 2021.

[20] Chiranjib Saha, Mehrnaz Afshang, and Harpreet S. Dhillon. 3gpp-inspired hetnet model using poisson cluster process: Sum-product functionals and downlink coverage. *IEEE Transactions on Communications*, 66(5):2219–2234, 2018.

[21] H. Paul Keeler. Simulating a thomas cluster point process, December 28, 2018. Website: <https://hpaulkeeler.com/simulating-a-thomas-cluster-point-process/> accessed on 14 April 2021.

[22] H. Paul Keeler. Simulating a matérn cluster point process, November 30, 2018. Website: <https://hpaulkeeler.com/simulating-a-matern-cluster-point-process/> accessed on 14 April 2021.

[23] Yong Sheng Soh, Tony Q. S. Quek, Marios Kountouris, and Hyundong Shin. Energy efficient heterogeneous cellular networks. *IEEE Journal on Selected Areas in Communications*, 31(5):840–850, 2013.

[24] Bhathiya Pilanawithana, Saman Atapattu, and Jamie Evans. Distribution of number of users per cell in a poisson wireless network with shadowing. In *2016 Australian Communications Theory Workshop (AusCTW)*, pages 153–156, 2016.

[25] A. Okabe, B. Boots, K. Sugihara, and S. N. Chiu. *Spatial Tessellations Concepts and Applications of Voronoi Diagrams*, chapter Poisson Voronoi Diagrams, pages 345 – 346. 2nd ed of JOHN WILEY & SONS.

[26] Xianghao Yu, Jun Zhang, Martin Haenggi, and Khaled B. Letaief. Coverage analysis for millimeter wave networks: The impact of directional antenna arrays. *IEEE Journal on Selected Areas in Communications*, 35(7):1498–1512, 2017.

[27] Chiranjib Saha and Harpreet S. Dhillon. Load on the typical poisson voronoi cell with clustered user distribution. *IEEE Wireless Communications Letters*, 9(9):1361–1365, 2020.

[28] Andrew Thornburg, Tianyang Bai, and Robert W. Heath. Performance analysis of outdoor mmwave ad hoc networks. *IEEE Transactions on Signal Processing*, 64(15):4065–4079, 2016.

[29] Tianyang Bai and Robert W. Heath. Coverage and rate analysis for millimeter-wave cellular networks. *IEEE Transactions on Wireless Communications*, 14(2):1100–1114, 2015.

[30] A.A.M. Saleh and R. Valenzuela. A statistical model for indoor multipath propagation. *IEEE Journal on Selected Areas in Communications*, 5(2):128–137, 1987.

[31] Jeffrey G. Andrews, Tianyang Bai, Mandar N. Kulkarni, Ahmed Alkhateeb, Abhishek K. Gupta, and Robert W. Heath. Modeling and analyzing millimeter wave cellular systems. *IEEE Transactions on Communications*, 65(1):403–430, 2017.

[32] P.D. Mankar, P. Parida, H.S. Dhillon, and M. Haenggi. Distance from the nucleus to a uniformly random point in the 0-cell and the typical cell of the poisson-voronoi tessellation, 2019. [Online] available: arXiv:1907.03635.

[33] Chiranjib Saha and Harpreet S. Dhillon. Downlink coverage probability of k-tier hetnets with general non-uniform user distributions. In *2016 IEEE International Conference on Communications (ICC)*, pages 1–6, 2016.

[34] Arif Dataesatu, Pornpawit Boonsrimuang, Kazuo Mori, and Pisit Boonsrimuang. Energy efficiency enhancement in 5g heterogeneous cellular networks using system throughput based sleep control scheme. In *2020 22nd International Conference on Advanced Communication Technology (ICACT)*, pages 549–553, 2020.

[35] P. Henrici and Karreman Mathematics Research Collection. *Applied and Computational Complex Analysis: Power series*. Applied and Computational Complex Analysis. Wiley, 1974.

Appendix A

Proofs

A.1 Proofs of the Lemmas

Proof of Lemma 1

The coverage probability can be developed from its definition in equation 2.19. The distance to the serving BS is denoted $R = \|\mathbf{x}\|$, with a corresponding pdf f_R:

$$\begin{aligned}\mathbb{P}_{cov}(\tau) &= \int_{R_{\min}}^{\infty} \mathbb{P}\left[\mathrm{SINR}(\mathbf{x}) > \tau | r\right] f_R(r;\lambda_B) dr \\ &\overset{(a)}{=} \int_{R_{\min}}^{\infty} \mathbb{P}\left[\frac{P_t\ h\ r^{-\alpha}}{\sigma^2 + \mathcal{I}} > \tau \middle| r\right] f_R(r;\lambda_B) dr \\ &= \int_{R_{\min}}^{\infty} \underbrace{\mathbb{P}\left[h > \frac{r^{\alpha}\tau(\sigma^2+\mathcal{I})}{P_t}\middle| r\right]}_{\{1\}} f_R(r;\lambda_B) dr. \end{aligned} \tag{A.1}$$

(a) is obtained from the definition of the SINR in equation 3.2. Since $h \sim Exp(1)$, the ccdf of an exponential distribution given by $\mathbb{P}[h > T] = \exp(-T)$ can be used to expand the term $\{1\}$:

$$\begin{aligned}\{1\} &= \mathbb{E}_{\mathcal{I}}\left[\mathbb{P}\left[h > \frac{r^{\alpha}\tau(\sigma^2+\mathcal{I})}{P_t}\middle| r, \mathcal{I}\right]\right] \\ &= \mathbb{E}_{\mathcal{I}}\left[\exp\left(\frac{-r^{\alpha}\tau(\sigma^2+\mathcal{I})}{P_t}\right)\middle| r\right] \\ &= \exp\left(\frac{-r^{\alpha}\tau\sigma^2}{P_t}\right)\mathbb{E}_{\mathcal{I}}\left[\exp\left(\frac{-r^{\alpha}\tau\mathcal{I}}{P_t}\right)\middle| r\right] \\ &\overset{(b)}{=} \mathcal{L}_N\left(\frac{-r^{\alpha}\tau}{P_t}\right)\mathcal{L}_{\mathcal{I}}\left(\frac{-r^{\alpha}\tau}{P_t}\right), \end{aligned}$$

where (b) is obtained by identification of the definition of the LT. Introducing $\{1\}$ back in equation A.1 finishes the proof.

■

Proof of Lemma 2

The ccdf of the distance to the i^{th} closest BS can be written as follows:

$$\begin{aligned}
\bar{F}_{R_i}(R;\lambda_R) &= \mathbb{P}(R_i > R) \\
&= \mathbb{P}\left(\text{Having less than } i \text{ BSs in area } \pi(R^2 - R_{\min}^2)\right) \\
&= \sum_{n=0}^{i-1} \mathbb{P}\left[\Psi\left(\pi(R^2 - R_{\min}^2)\right) = n\right] \\
&\overset{(a)}{=} \sum_{n=0}^{i-1} \frac{(\pi\lambda_{\mathrm{R}})^n \left(R^2 - R_{\min}^2\right)^n}{n!} \exp\left(-\lambda_{\mathrm{R}}\pi(R^2 - R_{\min}^2)\right).
\end{aligned}$$

(a) follows from equation 2.8 for a HPPP of intensity λ_{R}. The pdf can be obtained by derivation of the ccdf:

$$\begin{aligned}
f_{R_i}(r_i;\lambda_R) &= -\frac{d\bar{F}_{R_i}(r_i;\lambda_R)}{dr_i} \\
&= -\sum_{n=0}^{i-1} \frac{(\pi\lambda_{\mathrm{R}})^n 2r_i \left(r_i^2 - R_{\min}^2\right)^{n-1}}{(n-1)!} \exp\left(-\lambda_{\mathrm{R}}\pi(r_i^2 - R_{\min}^2)\right) \\
&\quad + \sum_{n=0}^{i-1} \frac{(\pi\lambda_{\mathrm{R}})^{n+1} 2r_i \left(r_i^2 - R_{\min}^2\right)^{n}}{n!} \exp\left(-\lambda_{\mathrm{R}}\pi(r_i^2 - R_{\min}^2)\right) \\
&\overset{(b)}{=} \frac{2(\pi\lambda_{\mathrm{R}})^i}{(i-1)!} r_i (r_i^2 - R_{\min}^2)^{i-1} \exp\left(-\pi\lambda_{\mathrm{R}}(r_i^2 - R_{\min}^2)\right).
\end{aligned}$$

(b) is obtained after a variable change to simplify terms between the two sums.

■

Proof of Lemma 3

The LT of the interference term $\mathcal{I} = \sum_{\mathbf{y}\in\Phi_{\mathrm{B}}(\mathbf{x})} P_t\ h\ \|\mathbf{y}\|^{-\alpha}$ can be developed as:

$$\begin{aligned}
\mathcal{L}_{\mathcal{I}}(s;\lambda_{\mathcal{I}}) &= \mathbb{E}\left[\exp\left(-s\mathcal{I}\right)\right] \\
&= \mathbb{E}_{\Phi_{\mathrm{B}}(\mathbf{x}),h}\left[\prod_{\mathbf{y}\in\Phi_{\mathrm{B}}(\mathbf{x})} \exp\left(-sP_t\ h\ \|\mathbf{y}\|^{-\alpha}\right)\right] \\
&= \mathbb{E}_{\Phi_{\mathrm{B}}(\mathbf{x})}\left[\prod_{\mathbf{y}\in\Phi_{\mathrm{B}}(\mathbf{x})} \mathbb{E}_h\left[\exp\left(-sP_t\ h\ \|\mathbf{y}\|^{-\alpha}\right)\right]\right] \\
&\overset{(a)}{=} \mathbb{E}_{\Phi_{\mathrm{B}}(\mathbf{x})}\left[\prod_{\mathbf{y}\in\Phi_{\mathrm{B}}(\mathbf{x})} \frac{1}{1 + sP_t\|\mathbf{y}\|^{-\alpha}}\right] \\
&\overset{(b)}{=} \exp\left(-2\pi\lambda_{\mathcal{I}} \int_r^{\infty} \left(1 - \frac{1}{1 + sP_t\ v^{-\alpha}}\right) v dv\right),
\end{aligned}$$

where (a) follows from the LT of a exponential random variable with parameter $\lambda = 1$. (b) is obtained by denoting $r = \|\mathbf{x}\|$ and using, with polar coordinates, the PGFL for a HPPP, given in equation 2.10, outside the ball $b(\mathbf{0}, r)$.

To finish the proof the LT transform is evaluated for $s = \frac{r^\alpha \tau}{P_t}$:

$$\begin{aligned}\mathcal{L}_{\mathcal{I}}\left(\frac{r^\alpha\tau}{P_t};\lambda_{\mathcal{I}}\right) &= \exp\left(-2\pi\lambda_{\mathcal{I}}\int_r^\infty\left(1-\frac{1}{1+\tau\left(\frac{r}{v}\right)^\alpha}\right)vdv\right)\\ &= \exp\left(-2\pi\lambda_{\mathcal{I}}\int_r^\infty\left(\frac{\tau}{\tau+\left(\frac{r}{v}\right)^\alpha}\right)vdv\right)\\ &\overset{(c)}{=} \exp\left(-\pi\lambda_{\mathcal{I}}r^2\underbrace{\int_{\tau^{-2/\alpha}}^\infty\frac{\tau^{2/\alpha}}{1+u^{\alpha/2}}du}_{\rho(\tau,\alpha)}\right),\end{aligned}$$

where (c) is obtained by applying the variable change $u = \left(\frac{v}{\tau^{1/\alpha}r}\right)^2$.

■

Proof of Lemma 4

The goal is to proof that $G_{\text{act}}(\vartheta_{\mathbf{x}} - \varphi_{\mathbf{x}})$ is equal in distribution to $G_{\text{act}}(\frac{d}{\lambda}\theta_{\mathbf{x}})$ knowing that $\frac{d}{\lambda} = \frac{1}{2}$ and that $\vartheta_{\mathbf{x}}, \varphi_{\mathbf{x}} \overset{i.i.d.}{\sim} \text{Uniform}[-\frac{d}{\lambda}, \frac{d}{\lambda}]$.

Three variables $X \triangleq \frac{\lambda}{d}\vartheta_{\mathbf{x}}$, $Y \triangleq \frac{\lambda}{d}\varphi_{\mathbf{x}}$ and $W \triangleq \theta_{\mathbf{x}}$ can be defined. Hence, $X, Y \overset{i.i.d.}{\sim} \text{Uniform}[-1,1]$ and the difference random variable $W = X - Y$ is distributed as:

$$\begin{aligned}f_W(w) &\overset{(a)}{=} \int_{-\infty}^{\infty} f_{X,Y}(x, x-w)dx\\ &= \int_{-\infty}^{\infty}\frac{1}{4}\mathbb{1}_{[-1,1]}(x)\mathbb{1}_{[-1,1]}(x-w)dx\\ &= \frac{1}{4}\int_{-1}^{1}\mathbb{1}_{[-1,1]}(x-w)dx,\end{aligned} \tag{A.2}$$

where $\mathbb{1}_{[-1,1]}(\cdot)$ is the indicator function on the set $[-1,1]$. (a) follows from the definition of the pdf of the difference of two random variables. The integral in equation A.2 can be solved by considering three different intervals for w:

$$f_W(w) = \begin{cases}\frac{1}{4}(2-w) & \text{if } w \in [0,2],\\ \frac{1}{4}(2+w) & \text{if } w \in [-2,0[,\\ 0 & \text{otherwise.}\end{cases} \tag{A.3}$$

The function G_{act} having a period of 1, setting $\frac{d}{\lambda} = \frac{1}{2}$ allows the following statement:

$$\begin{cases}G_{\text{act}}(\frac{\theta_{\mathbf{x}}}{2}) = G_{\text{act}}(\frac{1}{2}(\theta_{\mathbf{x}}-2)) & \text{if } \theta_{\mathbf{x}} \in [0,1],\\ G_{\text{act}}(\frac{\theta_{\mathbf{x}}}{2}) = G_{\text{act}}(\frac{1}{2}(\theta_{\mathbf{x}}+2)) & \text{if } \theta_{\mathbf{x}} \in [-1,0[.\end{cases} \tag{A.4}$$

The distribution of $\theta_{\mathbf{x}}$ can thus be changed accordingly without changing the distribution of $G_{\text{act}}(\frac{\theta_{\mathbf{x}}}{2})$:

$$f_{\theta_{\mathbf{x}}}(w) = \begin{cases}\frac{1}{4}(2-w) + \frac{1}{4}(2+(w-2)) = \frac{1}{2} & \text{if } w \in [0,1],\\ \frac{1}{4}(2+w) + \frac{1}{4}(2-(w+2)) & \text{if } w \in [-1,0[,\\ 0 & \text{otherwise.}\end{cases} \tag{A.5}$$

Finally, $\theta_{\mathbf{x}} \sim \text{Uniform}[-1,1]$ follows from equation A.5.

■

Proof of Lemma 5

From its definition in equation 2.19, the coverage probability can be developed as follows:

$$\begin{aligned}
\mathbb{P}_{\text{cov}}(\tau) &\overset{(a)}{=} \mathbb{E}_r\left[\mathbb{P}\left(\frac{P_t\beta|\rho_{\mathbf{x}}|^2 r^{-\alpha}}{\sigma^2+\mathcal{I}} > \tau\right)\right] \\
&= \int_{R_{\min}}^{R_{\max}} \mathbb{P}\left[|\rho_{\mathbf{x}}|^2 > \frac{\tau r^{\alpha}}{P_t\beta}(\sigma^2+\mathcal{I})\right] f_R(r;\lambda_R)dr \\
&\overset{(b)}{=} \int_{R_{\min}}^{R_{\max}} \sum_{n=0}^{M-1} \frac{(\tau M r^{\alpha})^n}{n!} \mathbb{E}_{\mathcal{I}}\left[(\sigma^2+\mathcal{I})^n \exp(-\tau M r^{\alpha}(\sigma^2+\mathcal{I}))\right] f_R(r;\lambda_R)dr \\
&\overset{(c)}{=} \int_{R_{\min}}^{R_{\max}} \sum_{n=0}^{M-1} \frac{s^n}{n!} \mathbb{E}_{\mathcal{I}}\left[(\sigma^2+\mathcal{I})^n \exp(-s(\sigma^2+\mathcal{I}))\right] f_R(r;\lambda_R)dr. \qquad \text{(A.6)}
\end{aligned}$$

(a) is obtained using the definition of the SINR given in equation 4.8. (b) follows from the ccdf of the gamma distributed channel coefficient, given by:

$$\overline{F}(x;k,\theta) = \sum_{i=0}^{k-1} \frac{1}{i!}\left(\frac{x}{\theta}\right)^i \exp\left(\frac{-x}{\theta}\right). \qquad \text{(A.7)}$$

(c) is obtained by defining $s = \tau M r^{\alpha}$.
The noise and the interference term being independent, the LT transform of the sum of these two random variables can be written as:

$$\mathcal{L}_{N,\mathcal{I}} = \mathbb{E}_{\mathcal{I}}\left[\exp(-s(\sigma^2+\mathcal{I}))\right]. \qquad \text{(A.8)}$$

The n^{th} derivative of this term is given by:

$$\mathcal{L}^{(n)}_{N,\mathcal{I}} = (-1)^n \mathbb{E}_{\mathcal{I}}\left[(\sigma^2+\mathcal{I})^n \exp(-s(\sigma^2+\mathcal{I}))\right]. \qquad \text{(A.9)}$$

Identifying this derivative in equation A.6 finishes the proof.

■

Proof of Lemma 6

From its definition, the LT transform of the interference term can be developed as:

$$\begin{aligned}
\mathcal{L}_{\mathcal{I}}(s) =& \mathbb{E}_{\mathcal{I}}\left[\exp(-s\mathcal{I})\right] \\
=& \mathbb{E}_{\mathcal{I}}\left[\exp\left(-s\sum_{\mathbf{y}\in\Phi_B(\mathbf{x})} \beta P_t g_{\mathbf{y}} \|\mathbf{y}\|^{-\alpha}\right)\right] \\
\overset{(a)}{=}& \mathbb{E}_{\Phi_B(\mathbf{x})}\left[\prod_{\mathbf{y}\in\Phi_B(\mathbf{x})} \mathbb{E}_g\left\{\exp\left(-s\beta P_t g\|\mathbf{y}\|^{-\alpha}\right)\right\}\right]. \\
\overset{(b)}{=}& \exp\left\{-\pi\lambda_{\mathcal{I}} \underbrace{2\int_{\kappa}^{R_{\max}} \left(1-\mathbb{E}_g\left[-s\beta P_t g r^{-\alpha}\right]\right) r dr}_{\{1\}}\right\}. \qquad \text{(A.10)}
\end{aligned}$$

(a) is obtained from all $g_{\mathbf{y}}$ that are i.i.d. random variables. (b) comes from the PGFL of a HPPP and by defining κ as the lower bound of the distance between the typical UE and the nearest interfering BS.
One can observe that the expectation over g is an integral so the expression of the term {1}

in equation A.10 involves a double integral. According to Fubini's theorem, the order of the two integrals can be swapped. Using this theorem, the term $\{1\}$ of equation A.10 can thus be further developed as follows:

$$\begin{aligned}
\{1\} =& 2\ \mathbb{E}_g\left[\int_{\kappa}^{R_{\max}} \left(1-\exp(-s\beta P_t g r^{-\alpha})\right) r dr\right] \\
\overset{(c)}{=}& R_{\max}^2 - \kappa^2 + 2\mathbb{E}_g\left[\int_{\kappa}^{R_{\max}} r\exp(-s' g r^{-\alpha}) dr\right] \\
\overset{(d)}{=}& R_{\max}^2 - \kappa^2 - \mathbb{E}_g\left[\nu (s'g)^{\nu} \int_{s' g R_{\max}^{-\alpha}}^{s' g \kappa^{-\alpha}} \frac{\exp(-t)}{t^{\nu+1}} dt\right] \\
=& R_{\max}^2 - \kappa^2 - \nu\mathbb{E}_g\left[(s'g)^{\nu}\int_{s' g R_{\max}^{-\alpha}}^{\infty} \frac{\exp(-t)}{t^{\nu+1}} dt - (s'g)^{\nu}\int_{s' g \kappa^{-\alpha}}^{\infty} \frac{\exp(-t)}{t^{\nu+1}} dt\right].
\end{aligned} \tag{A.11}$$

(c) is from the definition of $s' \triangleq s\beta P_t$. (d) is obtained by the variable change $t = s' g r^{-\alpha}$ and by defining $\nu \triangleq \frac{2}{\alpha}$.
Next, recall the definition of the generalised exponential integral in equation A.12 and its series expansion in equation A.13:

$$E_p(z) = z^{p-1}\int_z^{\infty} \frac{\exp(-t)}{t^p} dt \tag{A.12}$$

$$= z^{p-1}\Gamma(1-p) - \sum_{k=0}^{\infty} \frac{(-z)^k}{k!(1-p+k)}. \tag{A.13}$$

By identifying the definition of $E_p(z)$, equation A.11 can be developed as:

$$\begin{aligned}
\{1\} =& R_{\max}^2 - \kappa^2 - \nu\kappa^2\mathbb{E}_g\left[E_{\nu+1}(s' g \kappa^{-\alpha})\right] + \nu R_{\max}^2\mathbb{E}_g\left[E_{\nu+1}(s' g R_{\max}^{-\alpha})\right] \\
\overset{(e)}{=}& \nu R_{\max}^2 \sum_{k=1}^{\infty} \frac{(-s' R_{\max}^{-\alpha})^k}{k!(k-\nu)}\mathbb{E}_g[g^k] - \nu\kappa^2 \sum_{k=1}^{\infty} \frac{(-s'\kappa^{-\alpha})^k}{k!(k-\nu)}\mathbb{E}_g[g^k].
\end{aligned} \tag{A.14}$$

To further develop the term $\{1\}$, the moments of g must be computed. From Lemma 4 $g = |\rho|^2 G_{\cos}(\frac{d}{\lambda}\theta)$. The two factor being independent, the k^{th} moment of g can be computed as:

$$\mathbb{E}_g[g^k] = \mathbb{E}_{|\rho|^2}\left[(|\rho|^2)^k\right]\mathbb{E}_{\theta}\left[G_{\cos}\left(\frac{d}{\lambda}\theta\right)^k\right], \tag{A.15}$$

with $\frac{d}{\lambda} = \frac{1}{2}$. Since $|\rho|^2 \sim \text{Gamma}(M, \frac{1}{M})$, the first term of equation A.15 can be computed, from the moment generating function of the gamma distribution given by $M_{|\rho|^2}(t) = (1-\frac{t}{M})^{-M}, \forall t < M$, as follows:

$$\begin{aligned}
\mathbb{E}_{|\rho|^2}\left[(|\rho|^2)^k\right] &= M_{|\rho|^2}^{(k)}(0) \\
&= \left(\frac{1}{M}\right)^k \frac{(M+k-1)!}{(M-1)!} \\
&= \frac{\Gamma(M+k)}{M^k\Gamma(M)}.
\end{aligned} \tag{A.16}$$

The second term of equation A.15 can be developed, knowing that $\theta \sim \text{Uniform}[-1,1]$, as follows:

$$\begin{aligned}\mathbb{E}_\theta\left[G_{\cos}\left(\frac{d}{\lambda}\theta\right)^k\right] =& \mathbb{E}_\theta\left[G_{\cos}\left(\frac{\theta}{2}\right)^k\right] \\ =& \frac{1}{2}\int_{-1}^{1} G_{\cos}^{2k}\left(\frac{x}{2}\right)dx \\ =& \frac{1}{2}\int_{\frac{-2}{N_t}}^{\frac{2}{N_t}} \cos^{2k}\left(\frac{\pi N_t}{4}x\right)dx \\ \overset{(f)}{=}& \frac{4}{\pi N_t}\int_0^{\frac{\pi}{2}} cos^{2k}(u)du. \end{aligned} \tag{A.17}$$

(f) is obtained from the variable change $u = \frac{\pi N_t}{4}x$ and from the parity of the function $cos^{2k}(x)$ for $k \in \mathbb{N}$.
Recall the various equivalent expression of the Euler Beta function $B(x,y)$ defined for $\Re(x) > 0, \Re(y) > 0$:

$$B(x,y) = \int_0^1 t^{x-1}(1-t)^{y-1}dt \tag{A.18}$$

$$= 2\int_0^{\frac{\pi}{2}} (\sin(\theta))^{2x-1}(\cos(\theta))^{2y-1}d\theta \tag{A.19}$$

$$= \frac{\Gamma(x)\Gamma(y)}{\Gamma(x+y)} \tag{A.20}$$

Equation A.17 can be further developed by identifying equation A.19:

$$\begin{aligned}\mathbb{E}_\theta\left[G_{\cos}\left(\frac{d}{\lambda}\theta\right)^k\right] =& \frac{2}{\pi N_t}B\left(\frac{1}{2}, k+\frac{1}{2}\right) \\ \overset{(g)}{=}& \frac{2}{\sqrt{\pi}N_t}\frac{\Gamma\left(k+\frac{1}{2}\right)}{k!}. \end{aligned} \tag{A.21}$$

(g) is obtained by replacing the Beta function with its form given in equation A.20 and by using the Gamma function identities $\Gamma(\frac{1}{2}) = \sqrt{\pi}$ and $\Gamma(k+1) = k!$.
The expression of the k^{th} moment of g in equation A.15 can thus be rewritten, using equations A.16 and A.21, as:

$$\mathbb{E}_g[g^k] = \frac{2}{\sqrt{\pi}N_t}\frac{\Gamma(M+k)\Gamma\left(k+\frac{1}{2}\right)}{k!M^k\Gamma(M)}. \tag{A.22}$$

This expression could directly be inserted in equation A.14. But before doing so, the following identity is defined:

$$H(z) \triangleq \sum_{k=1}^{\infty}\frac{(-z)^k}{k!(k-\nu)}\mathbb{E}_g[g^k]. \tag{A.23}$$

$H(z)$ is developed to identify its expression in equation A.14.

$$\begin{aligned} H(z) =& \frac{2}{\sqrt{\pi}N_t}\sum_{k=1}^{\infty}\frac{(-z)^k}{k!(k-\nu)}\frac{\Gamma(M+k)\Gamma\left(k+\frac{1}{2}\right)}{k!M^k\Gamma(M)} \\ =& \frac{2}{\nu N_t} + \frac{2}{\sqrt{\pi}N_t}\sum_{k=0}^{\infty}\frac{(-z)^k}{k!(k-\nu)}\frac{\Gamma(M+k)\Gamma\left(k+\frac{1}{2}\right)}{k!M^k\Gamma(M)} \\ \overset{(h)}{=}& \frac{2}{\nu N_t}\left(1 - {}_3F_2\left(\frac{1}{2}, -\nu, M; 1, 1-\nu; -\frac{z}{M}\right)\right). \end{aligned} \tag{A.24}$$

(h) is obtained by the definition of the generalised hypergeometric function:

$$ {}_pF_q(a_1,...,a_p;b_1,...,b_q;z) = \sum_{n=0}^{\infty} \left(\frac{(a_1)_n ... (a_p)_n}{(b_1)_n ... (b_q)_n} \right) \left(\frac{z^n}{n!} \right), \tag{A.25} $$

where $(a)_k$ and $(b)_k$ are pochhammer symbols defined as:

$$ (x)_n = \frac{\Gamma(x+n)}{\Gamma(x)} = x(x+1)...(x+n-1). \tag{A.26} $$

Finally, identifying equation A.24 into equation A.14 gives the final form of term {1} which can be inserted in equation A.10 to finish the proof.

■

Proof of Lemma 7

For $j \in \mathcal{K}$, the Φ_j^{BS} are independent HPPPs with respect to the typical UE. The situation is thus the same as Lemma 2 except that the minimal distance is κ and not R_{min}. Therefore, the expression of the pdf and of the ccdf directly follows from the proof of Lemma 2.

For $j = 0$, the situation is different since the position of the typical UE depends on the position of the BS which is at the center of the corresponding cluster. There is a predefined distance distribution depending on the type of PCP considered. For a TCP and a MCP, this distribution is given respectively by equations A.27 and A.28 [27]:

$$ f_{R_0}^{\text{TCP}}(x) = \frac{x}{\sigma_0^2} \exp\left(-\frac{x^2}{2\sigma_0^2} \right), \quad x \geq 0, \tag{A.27} $$

$$ f_{R_0}^{\text{MCP}}(x) = \frac{2x}{r_{m,0}^2}, \quad 0 \leq x \leq r_{m,0}. \tag{A.28} $$

The corresponding ccdfs are obtained by integrating the pdfs from x to infinity. Their expressions are given in equations A.29 and A.30:

$$ \overline{F}_{R_0}^{\text{TCP}}(x) = \exp\left(-\frac{x^2}{2\sigma_0^2} \right), \quad x \geq 0, \tag{A.29} $$

$$ \overline{F}_{R_0}^{\text{MCP}}(x) = 1 - \frac{x^2}{r_{m,0}^2}, \quad 0 \leq x \leq r_{m,0}. \tag{A.30} $$

The last step to obtain the desired pdf and ccdf is to conditioned the obtained expressions on the known minimal distance κ. Using Bayes rule, the final expressions stated in the lemma are obtained from $f_{R_0}(x|\kappa) = \frac{f_{R_0}(x)}{\overline{F}_{R_0}(\kappa)}$, for $x \geq \kappa$, and from $\overline{F}_{R_0}(x|\kappa) = \frac{\overline{F}_{R_0}(x)}{\overline{F}_{R_0}(\kappa)}$, for $x \geq \kappa$.

■

Proof of Lemma 8

The proof of this lemma is inspired by the proof of Lemma 1 in [33]. Let $\mathcal{E}_j$ be the event that the closest BS in terms of power weighted distance is from the j^{th} tier. This event can be defined in terms of its indicator function:

$$ \mathbb{1}\left(\arg\max_{j \in \mathcal{K}_0} P_j R_{j,1}^{-\alpha} = j \right) = \bigcap_{k \in \mathcal{K}_0 \setminus \{j\}} \mathbb{1}(R_{k,1} > \overline{P}_{jk} R_{j,1}), \tag{A.31} $$

where $\overline{P}_{jk} = \left(\frac{P_k}{P_j}\right)^{1/\alpha}$. The next step consists in computing the probability of the event $\mathcal{E}_j$ knowing the distance $R_{j,1} = r_{j,1}$:

$$\begin{aligned}\mathbb{P}(\mathcal{E}_j | R_{j,1} = r_{j,1}) &= \mathbb{E}\left[\bigcap_{k\in\mathcal{K}_0\setminus\{j\}} \mathbb{1}(R_{k,1} > \overline{P}_{jk} R_j) \middle| R_{j,1} = r_{j,1}\right] \\ &= \prod_{k\in\mathcal{K}_0\setminus\{j\}} \mathbb{P}(R_{k,1} > \overline{P}_{jk} r_{j,1}) \\ &= \prod_{k\in\mathcal{K}_0\setminus\{j\}} \overline{F}_{R_{k,1}}(\overline{P}_{jk} r_{j,1}).\end{aligned}$$

Using the expression of the ccdf with the excluding radius R_{min} finishes the proof.

■

Proof of Lemma 9

From its definition, the LT transform of g can be written as:

$$\begin{aligned}\mathcal{L}_g(s) &= \mathbb{E}_g\left[\exp(-sg)\right] \\ &= \mathbb{E}_{|\rho|^2,\tilde{\theta}}\left[\exp\left(-s|\rho|^2 G_{cos}\left(\frac{d}{\lambda}\tilde{\theta}\right)\right)\right] \\ &\overset{(a)}{=} \mathbb{E}_{\tilde{\theta}}\left\{\mathbb{E}_{|\rho|^2}\left[\exp\left(-s|\rho|^2 G_{cos}\left(\frac{d}{\lambda}\tilde{\theta}\right)\right)\middle|\tilde{\theta}\right]\right\}. \end{aligned} \tag{A.32}$$

(a) is obtained from the law of total expectation.
Recall the distribution of the two concern variables:

$$\begin{cases} |\rho|^2 & \sim \text{Gamma}(k = M, \theta = \frac{1}{M}), \\ \tilde{\theta} & \sim \text{Uniform}[-1, 1] \quad \text{assuming } \frac{d}{\lambda} = \frac{1}{2}. \end{cases}$$

Recall also the moment generating function of a random variable $X \sim \text{Gamma}(k, \theta)$ is well known and given for $t \in \mathbb{R}$ by:

$$M_X(t) = \mathbb{E}_X\left[\exp(tX)\right] = (1 - \theta t)^{-k}, \quad \forall t < \frac{1}{\theta}. \tag{A.33}$$

Considering only real values for s, the expression of the LT in equation A.32 can be further developed as:

$$\begin{aligned}\mathcal{L}_g(s) &= \mathbb{E}_{\tilde{\theta}}\left[M_{|\rho|^2}\left(-s\ G_{cos}\left(\frac{1}{2}\tilde{\theta}\right)\right)\right] \\ &\overset{(b)}{=} \mathbb{E}_{\tilde{\theta}}\left[\left(1 + \frac{s\ G_{cos}\left(\frac{1}{2}\tilde{\theta}\right)}{M}\right)^{-M}\right] \\ &= \frac{1}{2}\int_{-1}^{1}\left(1 + \frac{s\ G_{cos}\left(\frac{1}{2}\tilde{\theta}\right)}{M}\right)^{-M} d\tilde{\theta}. \end{aligned} \tag{A.34}$$

(b) follows from the definition of the moment generating function in equation A.33 and by observing that $-s\ G_{cos}\left(\frac{1}{2}\tilde{\theta}\right) \leq 0 < M$. Recall the expression of $G_{cos}\left(\frac{1}{2}x\right)$:

$$G_{cos}\left(\frac{1}{2}\tilde{\theta}\right) = \begin{cases} \cos^2\left(\frac{\pi N_t}{4}x\right) & \text{if } |x| \leq \frac{2}{N_t}, \\ 0 & \text{otherwise.} \end{cases}$$

Inserting this expression into equation A.34 and evaluating the integral finishes the proof.

■

Proof of Lemma 10

In this proof, the expression of the LT of the interference term is developed. Recall the expression of this term given in equation 5.11:

$$\mathcal{I}_j^{tot}(r_j) = \sum_{k=0}^{K} \mathcal{I}_{(j;k)}(r_j), \tag{A.35}$$

where $r_j = \|\mathbf{x}_j\|$. The interference from each tier being independent, the expression of the LT can be written as:

$$\mathcal{L}_{\mathcal{I}_j^{tot}}(s) = \prod_{k=0}^{K} \mathcal{L}_{\mathcal{I}_k}(s), \tag{A.36}$$

where $\mathcal{L}_{\mathcal{I}_k}(s)$ is the LT of the interference from the k^{th} tier. This term is developed successively for $k \in \mathcal{K}$ and $k = 0$.

For $k \in \mathcal{K}$, the position of the typical UE is completely independent from the one of the BSs of tier k. Therefore, the position of the interfering BSs can be seen as an independent HPPP of intensity $\lambda_{\mathcal{I}_k} = \mathbb{E}\{s_k\}\lambda_k^{\text{BS}}$. The LT transform for $k \in \mathcal{K}$ is thus given by lemma 6 with:

- $\lambda_{\mathcal{I}} = \lambda_{\mathcal{I}_k} = \mathbb{E}\{s_k\}\lambda_k^{\text{BS}}$.
- $\kappa = \kappa_{jk} = \overline{P}_{jk} r_j$.
- $P_t = P_k$.

For the interference from $k = 0$, different cases have to be taken into account:

- If the typical UE is not from a tier of layer 2, there is no BS in tier 0 so $\mathcal{L}_{\mathcal{I}_0}(s) = 1$.
- If $j = 0$, there is no interference from this term since the BS of tier 0 is the serving one. So $\mathcal{L}_{\mathcal{I}_0}(s) = 1$ in this case as well.
- If $j \neq 0$, there is interference from one BS which is the cluster center.

The LT of the interference term in the third case can be developed from its definition as follows:

$$\begin{aligned}
\mathcal{L}_{\mathcal{I}_0}(s) =& \mathbb{E}_{g,R_{0,1},a_{0,1}}\left[\exp(-sP_0\beta g R_{0,1}^{-\alpha} s_0(a_{0,1}))|R_{0,1} \geq \kappa_{j0}\right] \\
=& (1 - \mathbb{E}\{s_0\}) + \mathbb{E}\{s_0\}\mathbb{E}_{g,R_{0,1}}\left[\exp(-sP_0\beta g R_{0,1}^{-\alpha})|R_{0,1} \geq \kappa_{j0}\right] \\
=& (1 - \mathbb{E}\{s_0\}) + \mathbb{E}\{s_0\}\mathbb{E}_{R_{0,1}}\left[\mathcal{L}_g(sP_0\beta R_{0,1}^{-\alpha})|R_{0,1} \geq \kappa_{j0}\right] \\
\overset{(a)}{=}& (1 - \mathbb{E}\{s_0\}) + \mathbb{E}\{s_0\}\mathbb{E}_{R_{0,1}}\left[1 - \frac{2}{N_{t,0}} + \int_0^{2/N_{t,0}} \left(1 + \frac{sP_0\beta R_{0,1}^{-\alpha}\cos^2(\frac{\pi N_{t,0}}{4}\theta)}{M}\right)^{-M} d\theta \middle| R_{0,1} \geq \kappa_{j0}\right] \\
\overset{(b)}{=}& (1 - \mathbb{E}\{s_0\}) + \mathbb{E}\{s_0\}\left(1 - \frac{2}{N_{t,0}}\right)\left(1 - \overline{F}_{R_{0,1}}(R_{max}|\kappa_{j0})\right) \\
&+ \mathbb{E}\{s_0\}\int_{\kappa_{j0}}^{R_{max}}\int_0^{2/N_{t,0}} \left(1 + \frac{sP_0\beta r_{0,1}^{-\alpha}\cos^2(\frac{\pi N_{t,0}}{4}\theta)}{M}\right)^{-M} f_{R_{0,1}}(r_{0,1}|\kappa_{j0})\, d\theta\, dr_{0,1}.
\end{aligned}$$

(a) follows from Lemma 9 and (b) is obtained by replacing the expectation on $R_{0,1}$ by an integral from κ_{j0} to R_{max} since non-LoS interference is neglected.

■

Proof of Lemma 11

The expression of $\zeta_{exp}(s)$ is stated in equation 5.21 and recalled here after:

$$\zeta_{exp}(s) = -s\sigma^2 - \sum_{k=1}^{K} \zeta_k(s).$$

The l^{th} derivative of $\zeta_k(s)$ is given by:

$$\zeta_k^{(l)}(s) = \mathbb{1}_{(l=0)} \frac{2\pi\mathbb{E}\{s_k\}\lambda_k^{\text{BS}}}{N_{t,k}} \left(R_{\max}^2 - \kappa_{jk}^2\right) + \frac{4\sqrt{\pi}\mathbb{E}\{s_k\}\lambda_k^{\text{BS}}}{k!N_{t,k}} \frac{\Gamma(M+l)}{\Gamma(M)} \frac{\Gamma(l+\frac{1}{2})}{(2-\alpha l)} \left(\frac{\beta P_t}{M}\right)^l \left[\kappa_{jk}^{2-\alpha l} \mathcal{J}_l\left(\frac{-s\beta P_k \kappa_{jk}^{-\alpha}}{M}\right) - R_{\max}^{2-\alpha l} \mathcal{J}_l\left(\frac{-s\beta P_k R_{\max}^{-\alpha}}{M}\right)\right]. \quad \text{(A.37)}$$

To finish the proof, observe that $\zeta_{exp}(s)$ is given by a sum so its successive derivatives can be computed as the sum of the derivatives.

■

Proof of Lemma 12

The computation of this derivative is straightforward from the definition of this term in Lemma 10.

■

Proof of Lemma 13

In the development of $\mathbb{P}(S_{\Phi_j}|r_c; r_{k,1}; k^* = k; s_k(a_{k,1}) = 0)$, two different cases must be handled independently:

- $j = k^*$,
- $j \in \mathcal{K}_0 \setminus \{k^*\}$.

For $j = k^*$, the typical BS is connected at this tier if at least one BS is awake. A BS from this tier is awake with probability $\mathbb{E}\{s_{k^*}\}$. Secondly, all BSs from all other tiers must be either asleep or further away from the typical UE in terms of power-weighted distance than the serving BS at tier j. It is calculated as the sum of the probability of being asleep with the probability of being further away, minus the joint probability. Mathematically, the probability of connection to tier k^* is thus given by:

$$\mathbb{P}(S_{\Phi_{k^*}}|r_c; r_{k,1}; k^* = k; s_k(a_{k,1}) = 0) = \mathbb{E}\{s_{k^*}\} \prod_{m \in \mathcal{K}_0 \setminus \{k^*\}} \prod_{n \in \hat{I}_m} \left((1 - \mathbb{E}\{s_m\}) + \overline{F}_1(m,n) - \overline{F}_1(m,n)(1 - \mathbb{E}\{s_m\})\right), \quad \text{(A.38)}$$

where $\overline{F}_1(m,n) = \overline{F}_{R_{m,n}}(\overline{P}_{k^*,m} r_c | \overline{P}_{k,m} r_{k,1})$.

For $j \in \mathcal{K}_0 \setminus \{k^*\}$, the typical BS is connected at this tier if at least one BS is awake as it was the case for $j = k^*$. A BS from this tier is awake with probability $\mathbb{E}\{s_j\}$. Then, it is known that the closest BS from tier k^* is sleeping. The others must either be asleep, either be further away in terms of power-weighted distance. Finally, the same applies for all other BSs from all other tiers except that the sleeping state of the closest one is unknown. Mathematically, the

probability of connection to tier $j \in \mathcal{K}_0 \setminus \{k^*\}$ is thus given by:

$$\mathbb{P}(S_{\Phi_j}|r_c; r_{k,1}; k^* = k; s_k(a_{k,1}) = 0) = \mathbb{E}\{s_j\} \prod_{n \in \hat{I}_{k^*} \setminus \{1\}} \Big((1 - \mathbb{E}\{s_{k^*}\}) + \overline{F}_2(j,n) - \overline{F}_2(j,n)(1 - \mathbb{E}\{s_{k^*}\})\Big) \prod_{m \in \mathcal{K}_0 \setminus \{j,k^*\}} \prod_{n \in \hat{I}_m} \Big((1 - \mathbb{E}\{s_m\}) + \overline{F}_3(j,m,n) - \overline{F}_3(j,m,n)(1 - \mathbb{E}\{s_m\})\Big), \quad \text{(A.39)}$$

where $\overline{F}_2(j,n) = \overline{F}_{R_{k^*,n}}(\overline{P}_{j,k^*} r_c | r_{k,1})$ and $\overline{F}_3(j,m,n) = \overline{F}_{R_{m,n}}(\overline{P}_{j,m} r_c | \overline{P}_{k,m} r_{k,1})$.

■

Proof of Lemma 14

Let us denote two events and their corresponding probabilities:

- $\mathcal{E}_n$ is the event that the load is equal to n. The corresponding probability is $\mathbb{P}(\mathcal{E}_n)$.
- $\mathcal{E}_u$ is the event that the load is bigger or equal to 1. The corresponding probability is $\mathbb{P}(\mathcal{E}_u)$.

Using Bayes rule, the probability $\mathbb{P}(\mathcal{E}_n|\mathcal{E}_u)$ is given by:

$$\mathbb{P}(\mathcal{E}_n|\mathcal{E}_u) = \frac{\mathbb{P}(\mathcal{E}_u|\mathcal{E}_n)\ \mathbb{P}(\mathcal{E}_n)}{\mathbb{P}(\mathcal{E}_u)}. \quad \text{(A.40)}$$

In this expression, $\mathbb{P}(\mathcal{E}_n) = f_{\mathcal{E}_n}(n)$ is the already defined probability of having n UEs within the Voronoï region, $\mathbb{P}(\mathcal{E}_u) = 1 - \mathbb{P}(\mathcal{E}_0) = 1 - f_{\mathcal{E}_0}$ and $\mathbb{P}(\mathcal{E}_u|\mathcal{E}_n) = 1$ if $n \geq 1$ and 0 otherwise. $f_{\mathcal{E}_n}$ denotes the pmf of the load. Therefore the adapted probability is given by:

$$f_{\mathcal{E}_n|\mathcal{E}_u}(n) = \begin{cases} \frac{f_{\mathcal{E}_n}(n)}{1 - f_{\mathcal{E}_n}(0)} & \text{if } n \geq 1, \\ 0 & \text{otherwise.} \end{cases} \quad \text{(A.41)}$$

■

A.2 Proofs of the Propositions

Proof of Proposition 1

The coverage probability is obtained by identifying the following terms in Lemma 1:

- $f_R(r;\lambda_R)$ is given by Lemma 2 with $i=1$ and $\lambda_{\mathrm{R}} = q\lambda_{\mathrm{B}}$ since the typical UE is served by the closest BS of a HPPP with intensity $q\lambda_{\mathrm{B}}$
- The LT of the interference term is given by Lemma 3 with $\lambda_{\mathcal{I}} = q\lambda_{\mathrm{B}}$ since the interfering BSs are distributed as a HPPP with intensity $q\lambda_{\mathrm{B}}$.

■

Proof of Proposition 2

The coverage probability in the case of random sleeping being independent from the activity of the BSs, equation 3.14 can be developed as follows:

$$\begin{aligned}\mathbb{P}^{RS}_{\mathrm{WCP}}(\tau) &= \frac{\mathbb{P}^{RS}_{cov}(\tau)}{\mathbb{E}\{a\}}\int_{\mathbb{A}} a_1 f_{\mathcal{A}}(a_1)da_1 \\ &= \frac{\mathbb{P}^{RS}_{cov}(\tau)}{\mathbb{E}\{a\}}\mathbb{E}\{a\} \\ &= \mathbb{P}^{RS}_{cov}(\tau).\end{aligned}$$

■

Proof of Proposition 3

The WCP metric given in equation 3.14 can be developed as:

$$\begin{aligned}\mathbb{P}^{SS}_{\mathrm{WCP}}(\tau) &\overset{(a)}{=} \frac{1}{\mathbb{E}\{a\}}\int_{\mathbb{A}} a_1 \Big(\mathbb{P}_{cov}(\tau|N_{\mathrm{ord}}=1)\mathbb{P}(N_{\mathrm{ord}}=1|a_1) \\ &\quad + \mathbb{P}_{cov}(\tau|N_{\mathrm{ord}}>1)\mathbb{P}(N_{\mathrm{ord}}>1|a_1)\Big) f_{\mathcal{A}}(a_1)da_1 \\ &\overset{(b)}{=} \frac{1}{\mathbb{E}\{a\}}\int_{\mathbb{A}} a_1 \Big(\mathbb{P}_{cov}(\tau|N_{\mathrm{ord}}=1)s(a_1) + \mathbb{P}_{cov}(\tau|N_{\mathrm{ord}}>1)(1-s(a_1))\Big) f_{\mathcal{A}}(a_1)da_1 \\ &= \frac{1}{\mathbb{E}\{a\}}\Big(\mathbb{E}\{as(a)\}\mathbb{P}_{cov}(\tau|N_{\mathrm{ord}}=1) + \left(\mathbb{E}\{a\} - \mathbb{E}\{as(a)\}\right)\mathbb{P}_{cov}(\tau|N_{\mathrm{ord}}>1)\Big). \quad \text{(A.42)}\end{aligned}$$

(a) is obtained by splitting the probability into the probabilities of the events of the nearest BS being awake and asleep. (b) follows from the definition of the SS.
$\mathbb{P}_{cov}(\tau|N_{\mathrm{ord}}>1)$ is the coverage probability when the first BS is sleeping. It can be written as follows by splitting again the probability into the probabilities of the events of the connection to each BS:

$$\mathbb{P}_{cov}(\tau|N_{\mathrm{ord}}>1) = \sum_{i=2}^{\infty}\mathbb{P}_{cov}(\tau|N_{\mathrm{ord}}=i)\mathbb{P}(N_{\mathrm{ord}}=i|N_{\mathrm{ord}}>1). \quad \text{(A.43)}$$

Both terms can be expressed independently:

- $\mathbb{P}(N_{\mathrm{ord}}=i|N_{\mathrm{ord}}>1)$ is the probability that the i^{th} BS is awake and that the $i-1$ closer BSs are sleeping, knowing that the first one is sleeping. Mathematically this can be expressed as:

$$\mathbb{P}(N_{\mathrm{ord}}=i|N_{\mathrm{ord}}>1) = \mathbb{E}\{s\}(1-\mathbb{E}\{s\})^{i-2}. \quad \text{(A.44)}$$

- $\mathbb{P}_{cov}(\tau|N_{\text{ord}}=i)$, for $i \in \mathbb{N}\setminus\{0\}$, is given by Lemma 1, in which $f_R(r;\lambda_R) = f_{R_i}(r;\lambda_B)$ is given by Lemma 2 and $\mathcal{L}_{\mathcal{I}}$ is given by Lemma 3 (with $\lambda_{\mathcal{I}} = \mathbb{E}\{s\}\lambda_B$).

Introducing equations A.43 and A.44 into equation A.42 and using Lemma 1 as described finishes the proof.

■

Proof of Proposition 4

The distribution number of UEs n per cell is denoted as $\text{Dist}(n)$. Since the UEs are distributed as a HPPP of intensity λ_{U}, this distribution is given, for a know cell area A, by:

$$\begin{aligned}\text{Dist}(n|A) &= \mathbb{P}\left(n \text{ UE in area } A\right)\\ &\overset{(a)}{=} \frac{(\lambda_{\text{U}}A)^n}{n!}\exp(-\lambda_{\text{U}}A).\end{aligned} \tag{A.45}$$

(a) is obtained from equation 2.8. The distribution of a BS cell area A can be approximated with a gamma function:

$$f_A(x) = \frac{(c\lambda_{\text{B}})^c}{\Gamma(c)}x^{c-1}\exp\left(-c\lambda_{\text{B}}x\right), \tag{A.46}$$

where $c = 3.575$ [25].
Using equations A.45 and A.46, $\text{Dist}(n)$ can be developed as follows:

$$\begin{aligned}\text{Dist}(n) &= \int_0^\infty \text{Dist}(n|A=x)f_A(x)dx\\ &= \frac{(c\lambda_{\text{B}})^c\lambda_{\text{U}}^n}{\Gamma(c)n!}\int_0^\infty x^n x^{c-1}\exp(-x(\lambda_{\text{U}}+c\lambda_{\text{B}}))dx\\ &\overset{(b)}{=} \frac{(c\lambda_{\text{B}})^c\lambda_{\text{U}}^n}{\Gamma(c)\Gamma(n+1)}\frac{1}{((\lambda_{\text{U}}+c\lambda_{\text{B}}))^{n+c}}\int_0^\infty t^{n+c-1}\exp(-t)dt\\ &\overset{(c)}{=} \frac{(c\lambda_{\text{B}})^c\lambda_{\text{U}}^n}{\Gamma(c)\Gamma(n+1)}\frac{1}{((\lambda_{\text{U}}+c\lambda_{\text{B}}))^{n+c}}\Gamma(n+c)\\ &= \frac{\Gamma(n+c)}{\Gamma(n+1)\Gamma(c)}\left(\frac{1}{1+c\lambda_B/\lambda_U}\right)^n\left(\frac{c\lambda_B/\lambda_U}{1+c\lambda_B/\lambda_U}\right)^c.\end{aligned}$$

(b) is obtained by a variable change $t = x(\lambda_{\text{U}}+c\lambda_{\text{B}})$ and using the identity $\Gamma(n+1) = n!$. (c) is obtained by identification of the definition of the gamma function $\Gamma(z) = \int_0^\infty t^{z-1}\exp(-t)dt$.

■

Proof of Proposition 5

This proof is partly inspired by appendix A of [26]. Defining $x_n \triangleq \frac{(-s)^n}{n!}\mathcal{L}_{N,\mathcal{I}}^{(n)}(s)$, the coverage probability in Lemma 5 can be expressed as:

$$\mathbb{P}_{\text{cov}}(\tau|N_{\text{ord}}=i) = \int_{R_{\min}}^{R_{\max}}\sum_{n=0}^{M-1}x_n f_{R_i}(r;\lambda_R)dr. \tag{A.47}$$

In this expression, x_n has to be evaluated for $s = \frac{\tau M r^\alpha}{\beta P_t}$. Notice that $x_0 = \mathcal{L}_{N,\mathcal{I}}(s) \overset{(a)}{=} \exp\left[\eta(s)\right]$. (a) is a consequence of Corollary 4. The first derivative of the Laplace transform is thus given by $\mathcal{L}_{N,\mathcal{I}}^{(1)}(s) = \eta^{(1)}(s)\mathcal{L}_{N,\mathcal{I}}(s)$ using the derivative chain rule. Using Leibniz's formula for the n^{th}

derivative of a product of two functions, the term x_n can be expressed as:

$$\begin{aligned} x_n =& \frac{(-s)^n}{n!} \frac{d^{n-1}}{ds^{n-1}} \left\{ \mathcal{L}^{(1)}_{N,\mathcal{I}}(s) \right\} \\ =& \frac{(-s)^n}{n!} \sum_{i=0}^{n-1} \binom{n-1}{i} \eta^{(n-i)}(s) \mathcal{L}^{(i)}_{N,\mathcal{I}}(s) \\ =& \sum_{i=0}^{n-1} \frac{(n-i)}{n} \frac{(-s)^{n-i}}{(n-i)!} \eta^{(n-i)}(s) \frac{(-s)^i}{i!} \mathcal{L}^{(i)}_{N,\mathcal{I}}(s) \\ \overset{(b)}{=}& \sum_{i=0}^{n-1} \frac{(n-i)}{n} c_{n-i} x_i. \end{aligned} \tag{A.48}$$

(b) is obtained by defining $c_k \triangleq \frac{(-s)^k}{k!} \eta^{(k)}(s)$.
At this point, x_n is thus expressed by the recursive form of equation A.48. In order to solve this recursive form, two power series are defined as follows:

$$C(z) \triangleq \sum_{n=0}^{\infty} c_n z^n, \tag{A.49}$$

$$X(z) \triangleq \sum_{n=0}^{\infty} x_n z^n = \sum_{n=0}^{\infty} \sum_{i=0}^{n-1} \frac{(n-i)}{n} c_{n-i} x_i z^n. \tag{A.50}$$

Note that the first derivative of $C(z)$ is given by:

$$C^{(1)}(z) = \sum_{n=0}^{\infty} n c_n z^{n-1}. \tag{A.51}$$

The first derivative of $X(z)$ can be developed as follows:

$$\begin{aligned} X^{(1)}(z) &= \sum_{n=0}^{\infty} \sum_{i=0}^{n-1} (n-i) c_{n-i} x_i z^{n-1} \\ &= \sum_{n=0}^{\infty} \sum_{i=0}^{\infty} n c_n x_i z^{n+i-1} \\ &= \underbrace{\left(\sum_{n=0} n c_n z^{n-1} \right)}_{C^{(1)}(z)} \underbrace{\left(\sum_{i=0} x_i z^i \right)}_{X(z)} \\ &= C^{(1)}(z) X(z). \end{aligned} \tag{A.52}$$

The solution of the differential equation in A.52 is given by $X(z) = \exp\{C(z)\}$. Using this result, the coverage probability in equation A.47 can be expressed as follows:

$$\begin{aligned} \mathbb{P}_{\text{cov}}(\tau | N_{\text{ord}} = i) &= \int_{R_{\min}}^{R_{\max}} \sum_{n=0}^{M-1} \frac{1}{n!} X^{(n)}(z) \Big|_{z=0} f_{R_i}(r; \lambda_R) dr \\ &= \int_{R_{\min}}^{R_{\max}} \sum_{n=0}^{M-1} \frac{1}{n!} \frac{d^n}{dz^n} \Big\{ \exp(C(z)) \Big\} \Big|_{z=0} f_{R_i}(r; \lambda_R) dr \\ &\overset{(c)}{=} \int_{R_{\min}}^{R_{\max}} \left\| \exp\left\{ \mathbf{C_M}(r) \right\} \right\|_1 f_{R_i}(r; \lambda_R) dr. \end{aligned}$$

(c) is obtained from [35, p. 14], in which it is shown that the first M coefficients of the power series $\exp(C(z))$ form the first column of the matrix exponential $\exp\{\mathbf{C_M}(r)\}$.

The last step to finish the proof is thus to compute the k^{th} derivative of $\eta(s)$, in order to express the coefficients c_k. First, the expression of the k^{th} derivative of a hypergeometric function is recalled:

$$\frac{d^n}{dz^n}{}_3F_2(a_1,a_2,a_3;b_1,b_2;z) = \frac{(a_1)_n(a_2)_n(a_3)_n}{(b_1)_n(b_2)_n}{}_3F_2(a_1+n,a_2+n,a_3+n;b_1+n,b_2+n;z). \quad \text{(A.53)}$$

Then the k^{th} derivative of $\eta(s)$ is computed as follows:

$$\begin{aligned}\eta^{(k)}(s;\lambda_{\mathcal{I}},\kappa) = &-\mathbb{1}_{(k\leq 1)}\sigma^2 s^{1-k} - \mathbb{1}_{(k=0)}\frac{2\pi\lambda_{\mathcal{I}}}{N_t}\left(R_{\max}^2-\kappa^2\right)\\ &- \frac{4\sqrt{\pi}\lambda_{\mathcal{I}}}{k!N_t}\frac{\Gamma(M+k)}{\Gamma(M)}\frac{\Gamma(k+\frac{1}{2})}{(2-\alpha k)}\left(\frac{\beta P_t}{M}\right)^k\\ &\left[\kappa^{2-\alpha k}\mathcal{J}_k\left(\frac{-s\beta P_t\kappa^{-\alpha}}{M}\right) - R_{\max}^{2-\alpha k}\mathcal{J}_k\left(\frac{-s\beta P_t R_{\max}^{-\alpha}}{M}\right)\right]. \quad \text{(A.54)}\end{aligned}$$

Equation A.54 is obtained from its expression given in Corollary 4 and by identifying the following terms:

$$\begin{cases}\left(\frac{1}{2}\right)_k = \frac{\Gamma(k+\frac{1}{2})}{\Gamma(\frac{1}{2})} = \frac{\Gamma(k+\frac{1}{2})}{\sqrt{\pi}},\\ (M)_k = \frac{\Gamma(M+k)}{\Gamma(M)},\\ (1)_k = k!,\\ \frac{(-\nu)_k}{(1-\nu)_k} = \frac{2}{2-\alpha k}.\end{cases}$$

■

Proof of Proposition 6

The expression of the coverage probability can be obtained from Proposition 5 by identifying:

$$\begin{cases}\lambda_R = q\lambda_{\mathrm{B}} \text{ and } \lambda_{\mathcal{I}} = q\lambda_{\mathrm{B}} \text{ due to the independent thinning operation,}\\ N_{\mathrm{ord}} = 1 \text{ since only the first BS is serving,}\\ \kappa = r \text{ because the minimal distance to the interferer is the distance to the serving BS.}\end{cases}$$

The WCP metric is then directly obtained from the coverage probability according to Proposition 2.

■

Proof of Proposition 7

This proposition is proven following the same steps as in the proof of Proposition 3 to end up with this expression:

$$\begin{aligned}\mathbb{P}_{\mathrm{WCP}}^{SS}(\tau) = &\frac{\mathbb{E}\{as(a)\}}{\mathbb{E}\{a\}}\mathbb{P}_{\mathrm{cov}}(\tau|N_{\mathrm{ord}}=1)\\ &+ \frac{(\mathbb{E}\{a\}-\mathbb{E}\{as(a)\})}{\mathbb{E}\{a\}}\sum_{i=2}^{\infty}\mathbb{E}\{s\}(1-\mathbb{E}\{s\})^{i-2}\mathbb{P}_{\mathrm{cov}}(\tau|N_{\mathrm{ord}}=i). \quad \text{(A.55)}\end{aligned}$$

The expression of the coverage probabilities are obtained from Proposition 5 by identifying:

$$\begin{cases}\lambda_R = \lambda_{\mathrm{B}} \text{ and } \lambda_{\mathcal{I}} = \mathbb{E}\{s\}\lambda_{\mathrm{B}} \text{ due to the sleeping strategy,}\\ \kappa = r \text{ because the minimal distance to the interferer is the distance to the serving BS.}\end{cases}$$

■

Proof of Proposition 8

In the proof of Proposition 4, the distribution of the area A of the typical cell was approximated by equation A.46. Since the typical cell is approximated by a disc of radius R_c, the distribution of this radius is obtained using the change of variable $R_c = \sqrt{\frac{A}{\pi}}$:

$$f_{R_c}(r) = 2\frac{(\pi\lambda_{\mathrm{B}})^c}{\Gamma(c)} c^c r^{2c-1} \exp(-\pi\lambda_{\mathrm{B}} c r^2). \tag{A.56}$$

This expression is exactly the pdf of a Nakagami distribution with parameters $m = c$ and $\Omega = \frac{1}{\pi\lambda_{\mathrm{B}}}$. Hence $R_c \sim \text{Nakagami}\left(c, \frac{1}{\pi\lambda_{\mathrm{B}}}\right)$.
The next step is to derive the probability generating function of $\Psi_{\mathrm{U}}(\mathcal{C}_0)$ conditioned on R_c. Note that $\Psi_{\mathrm{U}}(\mathcal{C}_0)$ is denoted Ψ_0 in the rest of the proof. From its definition, the probability generating function can be developed as follows:

$$\begin{aligned} G_{\Psi_0}(\theta|R_c) &= \mathbb{E}\left[\theta^{\Psi_0}\right] \\ &\overset{(a)}{=} \mathbb{E}\left[\theta^{\sum_{\mathbf{x}\in\Phi_{\mathrm{U}}} \mathbb{1}(\|\mathbf{x}\|\leq R_c)}\right] \\ &= \mathbb{E}\left[\prod_{\mathbf{x}\in\Phi_{\mathrm{U}}} \theta^{\mathbb{1}(\|\mathbf{x}\|\leq R_c)}\right]. \end{aligned} \tag{A.57}$$

(a) is obtained from the definition of the random counting measure defined in equation 2.1. Using the PGFL for a PCP given in equation 2.15, $G_{\Psi_0}(\theta|R_c)$ can be written as follows:

$$G_{\Psi_0}(\theta|R_c) = \exp\left(-\lambda_{\mathrm{U}}^p \int_{\mathbb{R}^2} \left[1 - \exp\left(\overline{m}\left[\int_{\mathbb{R}^2} \theta^{\mathbb{1}(\|\mathbf{x}+\mathbf{y}\|\leq R_c)} f(\mathbf{x})d\mathbf{x} - 1\right]\right)\right] d\mathbf{y}\right), \tag{A.58}$$

where f is the pdf associated with the PCP (given by equation 2.13 for a TCP and equation 2.14 for a MCP). Equation A.58 can be further developed using polar coordinates such that $v = \|\mathbf{x}\|$ and $w = \|\mathbf{y}\|$:

$$\begin{aligned} G_{\Psi_0}(\theta|R_c) &= \exp\left(-2\pi\lambda_{\mathrm{U}}^p \int_{\mathbb{R}^2} \left[1 - \exp\left(\overline{m}\left[\int_0^{R_c} \theta f_d(v|w)dv + \int_{R_c}^{\infty} f_d(v|w)dv - 1\right]\right)\right] wdw\right) \\ &= \exp\left(-2\pi\lambda_{\mathrm{U}}^p \int_{\mathbb{R}^2} \left[1 - \exp\left(\overline{m}\left[\int_0^{R_c} (\theta-1)\theta f_d(v|w)dv\right]\right)\right] wdw\right), \end{aligned} \tag{A.59}$$

where $f_d(v|w)$ is the pdf of the distance to the origin for a point of the PCP, knowing the distance between the corresponding cluster center and the origin. The expression of $f_d(v|w)$ respectively for a TCP and a MCP is given by [27]:

$$f_d^{\mathrm{TCP}}(v|w) = \frac{v}{\sigma_{\mathrm{U}}^2} \exp\left(-\frac{(v^2+w^2)}{2\sigma_{\mathrm{U}}^2}\right) I_0\left(\frac{vw}{\sigma^2}\right), \quad \text{for } v \geq 0, w \geq 0, \tag{A.60}$$

$$f_d^{\mathrm{MCP}}(v|w) = \begin{cases} \frac{2v}{r_m^2}, & \text{for } 0 \leq v \leq r_m - w, 0 \leq w \leq r_m, \\ \frac{2v}{\pi r_m^2} \arccos\left(\frac{v^2+w^2-r_m^2}{2vw}\right), & \text{for } |r_m - w| < v \leq r_m + w. \end{cases} \tag{A.61}$$

After some simplifications in equation A.59 and an integration over the distribution of R_c, the expression of the $G_{\Psi_0}(\theta)$ is given by:

$$G_{\Psi_0}(\theta) = \int_0^{\infty} \exp\left\{-2\pi\lambda_{\mathrm{U}}^p \int_0^{\infty} \left(1 - \exp\left[-\overline{m}(1-\theta)\xi(r,w)\right]\right) wdw\right\} f_{R_c}(r)dr, \tag{A.62}$$

where $\xi(r,w)$ is given for the two types of PCP by:

$$\xi^{\mathrm{TCP}}(r,w) = 1 - \mathcal{Q}_1(w\sigma_{\mathrm{U}}^{-1}, r\sigma_{\mathrm{U}}^{-1}), \tag{A.63}$$

$$\xi^{\mathrm{MCP}}(r,w) = \frac{1}{r_m^2}\left(\left[\min\left(r, \max(r_m - w, 0)\right)\right]^2 + \frac{2}{\pi}\int_{\min(r,|r_m-w|)}^{\min(r,r_m+w)} u \arccos\left(\frac{u^2+w^2-r_m^2}{2uw}\right) du\right), \tag{A.64}$$

where $\mathcal{Q}_1(\cdot)$ is the Marcum Q-function.
The pmf of the load is finally obtained by performing the inverse z-transform of the probability generating function, which for numerical computation is approximated by a IDFT:

$$f_{\mathcal{A}}(n) = \mathrm{IDFT}\left\{ G_{\Phi_{u_0}}\left(e^{j2\pi n/N}\right)\right\}. \tag{A.65}$$

■

Proof of Proposition 9

Let us recall the expression of the succes probability given in equation 5.13 when the typical UE is served by a BS of tier j located $\mathbf{x_j}$:

$$\mathbb{P}_{suc}(\tau, \mathbf{x}_j) = \sum_{n=0}^{M-1} \frac{(-\tau M r_j^{\alpha})^n}{n!(P_j\beta)^n} \mathcal{L}^{(n)}_{N,\mathcal{I}_j^{tot}}\left(\frac{\tau M r_j^{\alpha}}{\beta P_j}; r_j\right),$$

where $r_j = \|\mathbf{x}_j\|$.
The LT transform of the noise and interference term is given by Corollary 5 with $\mathcal{L}_{\mathcal{I}_0}(s) = 1$:

$$\mathcal{L}_{N,\mathcal{I}_j^{tot}}(s; r_j) = \exp[\zeta_{exp}(s)]. \tag{A.66}$$

The LT transform is thus given by an exponential as it was the case in the derivation of the coverage probability in Proposition 5. Following the same step,s and by identifying $\eta(s)$ with $\zeta_{exp}(s)$ and using the expression of the l^{th} derivative of $\zeta_{exp}(s)$ given in Lemma 11, finishes the proof.

■

Proof of Proposition 10

In this situation, the LT of the noise and interference term cannot be written as an exponential. The success probability is thus not given by the one norm of an exponential matrix. The l^{th} derivative of $\mathcal{L}_{N,\mathcal{I}_j^{tot}}$ must therefore be computed using Leibniz's general derivation rule:

$$\mathcal{L}^{(l)}_{N,\mathcal{I}_j^{tot}}(s) = \sum_{n=0}^{l} \binom{n}{k} \mathcal{L}^{(l-n)}_{\mathcal{I}_0}(s) \mathcal{L}^{(n)}_{\mathcal{I}_{exp}}(s). \tag{A.67}$$

The n^{th} derivative of $\mathcal{L}_{\mathcal{I}_0}(s)$ and $\mathcal{L}_{\mathcal{I}_{exp}}(s)$ are respectively given by equation 5.26 of Lemma 12 and by equation 5.24 of Corollary 6. Putting all this together and evaluating the expressions for $s = \frac{\tau M r_j^{\alpha}}{\beta P_j}$ finishes the proof.

■

Proof of Proposition 11

Recall the expression of the coverage probability stated in equation 5.30:

$$\mathbb{P}_{cov}\left(\tau|r_{k,1};k^*=k;s_k(a_{k,1})=0\right)=\mathbb{P}_{cov,k^*}\left(\tau|r_{k,1};k^*=k;s_k(a_{k,1})=0\right)+\sum_{j\in\mathcal{K}_0\setminus\{k^*\}}\mathbb{P}_{cov,j}\left(\tau|r_{k,1};k^*=k;s_k(a_{k,1})=0\right) \quad \text{(A.68)}$$

As seen in Propositions 9 and 10, the probability of success does not depend on the particular index of the serving BS. It only depends on the distance to this serving BS. This distance however has a different distribution for each BS of a tier. Furthermore, knowing that the typical UE is served by the j^{th}, the probability to be connected to the i^{th} BS of this tier is linked to the sleeping probability of all closer BSs. Taking all these aspects into account allows to write the coverage probability of tier $j\in\mathcal{K}_0\setminus\{k^*\}$ as:

$$\mathbb{P}_{cov,j}\left(\tau|r_{k,1};k^*=k;s_k(a_{k,1})=0\right)=\int_{\overline{P}_{k,j}r_{k,1}}^{R_{max}}\mathbb{P}(S_{\Phi_j}|r_c;r_{k,1};k^*=k;s_k(a_{k,1})=0)\mathbb{P}_{suc}(\tau,r_c|S_{\Phi_j})\sum_{i=1}^{|\hat{I}_j|}\left(1-\mathbb{E}\{s_j\}\right)^{i-1}f_{R_{j,i}}(r_c|\overline{P}_{k,j}r_{k,1})\,dr_c, \quad \text{(A.69)}$$

where $|\hat{I}_j|$ is the cardinality of the set of index of the BSs from tier j.
The term $\sum_{i=1}^{|\hat{I}_j|}\left(1-\mathbb{E}\{s_j\}\right)^{i-1}f_{R_{j,i}}(r_c|\overline{P}_{k,j}r_{k,1})$ is thus the sum of the pdfs for each BS distance to the typical UE, weighted by the probability to be connected to each specific BS.

A big difference for $j=k^*$ is that it is known that the closest BS of this tier is sleeping. Taking this into account, the expression is given by:

$$\mathbb{P}_{cov,k^*}\left(\tau|r_{k,1};k^*=k;s_k(a_{k,1})=0\right)=\int_{r_{k,1}}^{R_{max}}\mathbb{P}(S_{\Phi_{k^*}}|r_c;r_{k,1};k^*=k;s_k(a_{k,1})=0)\mathbb{P}_{suc}(\tau,r_c|S_{\Phi_{k^*}})\sum_{i=2}^{|\hat{I}_{k^*}|}\left(1-\mathbb{E}\{s_{k^*}\}\right)^{i-2}f_{R_{k^*,i}}(r_c|r_{k,1})\,dr_c. \quad \text{(A.70)}$$

■

Proof of Proposition 12

The difference with the development performed in Proposition 8 is that the position of the cluster center is constrained. Indeed, in equation 4.23, an integral over the distance w to the cluster center is performed from 0 to infinity. This is not the case anymore since the radius of the circular Voronoï region R_c is known. Therefore, there cannot be any BS within a distance of $2R_c$. Since the characterisation of load C is performed for a PCP of UEs having BSs as cluster centers, the integral on w must be performed from $2R_c$ to infinity.

■

Proof of Proposition 13

The difference with the development performed in Proposition 8, is that the position of the cluster center is known to be at the origin of the euclidean plane. In that case, there is no integral to perform on the position of the cluster center of the UEs. Thanks to Slivnyak's theorem, the distribution of the PPP to which the typical BS belongs does not change when it is thinned by this BS at the origin. The HPPP formed by all BSs is thus a HPPP of intensity

$\lambda_{tot}^{\mathrm{BS}}$. Following the steps of the proof of Proposition 8, and knowing that the cluster center is at the origin, finishes the proof.

■

A.3 Proofs of the Corollaries

Proof of Corollary 1

The expression of $\mathbb{P}_{cov}^{RS}$ given in Proposition 1 is evaluated for $\sigma^2 = 0$:

$$\begin{aligned}
\mathbb{P}_{cov,\sigma^2=0}^{RS}(\tau) &= 2\pi q\lambda_{\mathrm{B}} \int_{R_{\min}}^{\infty} r \exp\left(-\pi q\lambda_{\mathrm{B}}\left(r^2(1+\rho(\tau,\alpha)) - R_{\min}^2\right)\right) dr \\
&= 2\pi q\lambda_{\mathrm{B}} \exp\left(\pi q\lambda_{\mathrm{B}} R_{\min}^2\right) \int_{R_{\min}}^{\infty} r \exp\left(-\pi q\lambda_{\mathrm{B}} r^2(1+\rho(\tau,\alpha))\right) dr \\
&= \frac{\exp\left(\pi q\lambda_{\mathrm{B}} R_{\min}^2\right)}{(1+\rho(\tau,\alpha))} \exp\left(-\pi q\lambda_{\mathrm{B}} R_{\min}^2(1+\rho(\tau,\alpha))\right) \\
&= \frac{\exp\left(-\pi q\lambda_{\mathrm{B}} R_{\min}^2\rho(\tau,\alpha)\right)}{(1+\rho(\tau,\alpha))}.
\end{aligned}$$

■

Proof of Corollary 2

The expression of $\mathbb{P}_{WCP}^{SS}$, given in Proposition 3, is evaluated for $\sigma^2 = 0$:

$$\begin{aligned}
\mathbb{P}_{WCP,\sigma^2=0}^{SS}(\tau) =& \frac{\mathbb{E}\{as(a)\}}{\mathbb{E}\{a\}} \int_{R_{\min}}^{\infty} \exp\left(-\pi\mathbb{E}\{s\}\lambda_B\ r^2\rho(\tau,\alpha)\right) f_{R_1}(r;\lambda_B)dr \\
&+ \frac{(\mathbb{E}\{a\} - \mathbb{E}\{as(a)\})}{\mathbb{E}\{a\}} \sum_{i=2}^{\infty} \mathbb{E}\{s\}(1-\mathbb{E}\{s\})^{i-2} \\
&\int_{R_{\min}}^{\infty} \exp\left(-\pi\mathbb{E}\{s\}\lambda_B\ r^2\rho(\tau,\alpha)\right) f_{R_i}(r;\lambda_B)dr \\
\overset{(a)}{=}& \frac{\mathbb{E}\{as(a)\}}{\mathbb{E}\{a\}} I_1 + \frac{(\mathbb{E}\{a\} - \mathbb{E}\{as(a)\})}{\mathbb{E}\{a\}} \sum_{i=2}^{\infty} \mathbb{E}\{s\}(1-\mathbb{E}\{s\})^{i-2} I_i. \qquad \text{(A.71)}
\end{aligned}$$

(a) follows by defining $I_i = \int_{R_{\min}}^{\infty} \exp\left(-\pi\mathbb{E}\{s\}\lambda_B\ r^2\rho(\tau,\alpha)\right) f_{R_i}(r;\lambda_B)dr$. This integral can be developed independently as follows:

$$\begin{aligned}
I_i =& \frac{2(\pi\lambda_{\mathrm{B}})^i}{(i-1)!} \int_{R_{\min}}^{\infty} r(r^2 - R_{\min}^2)^{i-1} \exp\left(-\pi\mathbb{E}\{s\}\lambda_B\ r^2\rho(\tau,\alpha)\right) \exp\left(-\pi\lambda_{\mathrm{B}}(r^2 - R_{\min}^2)\right) dr \\
\overset{(b)}{=}& \frac{(\pi\lambda_{\mathrm{B}})^i}{(i-1)!} \exp\left(-\lambda_B R_{\min}^2\rho(\tau,\alpha)\right) \int_0^{\infty} u^{i-1} \exp\left(-\pi\lambda_B u\left(1+\mathbb{E}\{s\}\rho(\tau,\alpha)\right)\right) du \\
\overset{(c)}{=}& \frac{\exp\left(-\pi\mathbb{E}\{s\}\lambda_{\mathrm{B}} R_{\min}^2\rho(\tau,\alpha)\right)}{(1+\mathbb{E}\{s\}\rho(\tau,\alpha))^i}. \qquad \text{(A.72)}
\end{aligned}$$

(b) is obtained by applying the variable change $u = r^2 - R_{\min}^2$ and (c) by solving the integral. Before including equation A.72 into A.71, the following identity is derived for $0 < a < 1$ and $b > 0$:

$$\begin{aligned}
\sum_{i=2}^{\infty} \frac{a(1-a)^{i-2}}{(1+ab)^i} =& \frac{a}{(1+ab)^2} \sum_{j=0}^{\infty} \left(\frac{1-a}{1+ab}\right)^j \\
\overset{(d)}{=}& \frac{a}{(1+ab)^2} \frac{(1+ab)}{a(1+b)} \\
=& \frac{1}{(1+b)(1+ab)}.
\end{aligned}$$

(d) ks obtained by using the geometric sum identity for $\frac{1-a}{1+ab} < 1$. By using equation A.72 and this identity with $a = \mathbb{E}\{s\}$ and $b = \rho(\tau, \alpha)$, equation A.71 becomes:

$$\begin{aligned}\mathbb{P}^{SS}_{WCP,\sigma^2=0}(\tau) =& \frac{\mathbb{E}\{as(a)\}}{\mathbb{E}\{a\}} \frac{\exp\left(-\pi\mathbb{E}\{s\}\lambda_{\mathrm{B}}R^2_{\min}\rho(\tau,\alpha)\right)}{(1+\mathbb{E}\{s\}\rho(\tau,\alpha))} \\ &+ \frac{(\mathbb{E}\{a\} - \mathbb{E}\{as(a)\})}{\mathbb{E}\{a\}} \frac{\exp\left(-\pi\mathbb{E}\{s\}\lambda_{\mathrm{B}}R^2_{\min}\rho(\tau,\alpha)\right)}{(1+\rho(\tau,\alpha))(1+\mathbb{E}\{s\}\rho(\tau,\alpha))} \\ =& \exp\left(-\pi\mathbb{E}\{s\}\lambda_{\mathrm{B}}R^2_{\min}\rho(\tau,\alpha)\right) \frac{1+(\rho(\tau,\alpha)\mathbb{E}\{as(a)\}/\mathbb{E}\{a\})}{(1+\mathbb{E}\{s\}\rho(\tau,\alpha))\,(1+\rho(\tau,\alpha))}.\end{aligned}$$

■

Proof of Corollary 3

The expression of $\mathbb{E}\{a\}$ directly follows from the expectation of a negative binomial distribution. The two other expectations can be developed as:

$$\mathbb{E}\{s(a)\} = \sum_{k=0}^{\infty} s(k) f_{\mathcal{A}}(k) = \sum_{k=\lceil\mu\rceil}^{\infty} f_{\mathcal{A}}(k) = 1 - \sum_{k=0}^{\lceil\mu-1\rceil} f_{\mathcal{A}}(k) = \bar{F}_{\mathcal{A}}(\lceil\mu-1\rceil).$$

$$\mathbb{E}\{as(a)\} = \sum_{k=0}^{\infty} ks(k) f_{\mathcal{A}}(k) = \sum_{k=\lceil\mu\rceil}^{\infty} k f_{\mathcal{A}}(k) = \mathbb{E}\{a\} - \sum_{k=0}^{\lceil\mu-1\rceil} k f_{\mathcal{A}}(k).$$

■

Proof of Corollary 4

The LT transform of the sum of two independent random variables is given by the product of their LT transform. The LT transform of the interference and of the noise are respectively given by Lemma 6 and by $\exp(-s\sigma^2)$.

■

Proof of Corollary 5

The LT transform of the sum of two independent random variables is given by the product of their LT transform. The LT transform of the interference and of the noise are respectively given by Lemma 10 and by $\exp(-s\sigma^2)$.

■

Proof of Corollary 6

The first derivative of $\mathcal{L}_{\mathcal{I}_{exp}}$ is given by:

$$\mathcal{L}^{(1)}_{\mathcal{I}_{exp}}(s) = \zeta^{(1)}_{exp}(s)\mathcal{L}_{\mathcal{I}_{exp}}(s). \tag{A.73}$$

The next derivatives can be computed by recursion using Leibniz's formula as follows:

$$\mathcal{L}^{(l)}_{exp}(s) = \sum_{n=0}^{l-1} \binom{l-1}{n} \zeta^{l-n}_{exp}(s)\mathcal{L}^{i}_{exp}(s). \tag{A.74}$$

■

Proof of Corollary 7

From equation 5.42, the expression of $f_{Load\ A}$ can be further developed by identifying equations 5.41 and 4.26 as follows:

$$\begin{aligned}
f_{Load\ A}(n) &\overset{(a)}{=} \int_0^\infty \frac{(\lambda^{\mathrm{UE}}\pi r^2)^n}{n!}\exp(-\lambda^{\mathrm{UE}}\pi r^2)2\frac{(\pi\lambda^{\mathrm{BS}})^c}{\Gamma(c)}c^c r^{2c-1}\exp(-\pi\lambda^{\mathrm{BS}}cr^2)dr \\
&= \frac{2c^c}{\Gamma(c)\Omega^c}\frac{(\lambda^{\mathrm{UE}}\pi)^n}{\Gamma(n+1)}\int_0^\infty r r^{2(n+c-1)}\exp\left[-r^2\left(\lambda^{\mathrm{UE}}\pi+\frac{c}{\Omega}\right)\right]dr \\
&\overset{(b)}{=} \frac{2c^c}{\Gamma(c)\Omega^c}\frac{(\lambda^{\mathrm{UE}}\pi)^n}{\Gamma(n+1)}\int_0^\infty \frac{t^{n+c-1}}{(\lambda^{\mathrm{UE}}\pi+\frac{c}{\Omega})^{n+c}}\exp(-t)dt \\
&\overset{(c)}{=} \frac{2c^c}{\Gamma(c)\Omega^c}\frac{(\lambda^{\mathrm{UE}}\pi)^n}{\Gamma(n+1)}\frac{1}{(\lambda^{\mathrm{UE}}\pi+\frac{c}{\Omega})^{n+c}}\Gamma(n+c) \\
&= \frac{\Gamma(n+c)}{\Gamma(n+1)\Gamma(c)}\left(\frac{1}{1+c\lambda^{\mathrm{BS}}/\lambda^{\mathrm{UE}}}\right)^n\left(\frac{c\lambda^{\mathrm{BS}}/\lambda^{\mathrm{UE}}}{1+c\lambda^{\mathrm{BS}}/\lambda^{\mathrm{UE}}}\right)^c. \qquad \text{(A.75)}
\end{aligned}$$

(a) is obtained by defining $\Omega = \frac{1}{\pi\lambda^{\mathrm{BS}}}$. (b) is obtained by the change of variable $t = r^2\left(\lambda^{\mathrm{UE}}\pi + \frac{c}{\Omega}\right)$.
(c) is obtained by identification of the definition of the Gamma function.
Equation A.75 is exactly the definition of a NB distribution.

■

UNIVERSITÉ CATHOLIQUE DE LOUVAIN
École polytechnique de Louvain
Rue Archimède, 1 bte L6.11.01, 1348 Louvain-la-Neuve, Belgique | **www.uclouvain.be/epl**